Traian-Nicolae Preda

Modelling of Active Distribution Grids for Stability Analysis

Thesis for the Degree of Philosophiae Doctor

Trondheim, February 2016

Norwegian University of Science and Technology
Faculty of Information Technology,
Mathematics and Electrical Engineering
Department of Electric Power Engineering

NTNU
Norwegian University of
Science and Technology

NTNU
Norwegian University of Science and Technology

Thesis for the Degree of Philosophiae Doctor

Faculty of Information Technology, Mathematics and Electrical Engineering
Department of Electric Power Engineering

ISBN 978-82-326-1422-6 (printed ver.)
ISBN 978-82-326-1423-3 (electronic ver.)
ISSN 1503-8181

Doctoral theses at NTNU, 2016:41

Printed by NTNU Grafisk senter

Preface

This thesis is submitted to the Norwegian University of Science and Technology (NTNU) for partial fulfilment of the requirements for the degree of philosophiae doctor (PhD).

This work has been financed by the research project ″Optimal infrastructure for seamless integration of distributed generation″ (OiDG), supported by the Research Council of Norway and 15 companies within electricity distribution in Norway.

I would like to thank my supervisors Professor Kjetil Uhlen, NTNU and Dr. Dag Eirik Nordgård from SINTEF Energy Research for their guidance and support.
Furthermore, I would like to thank Professor Nouredine Hadjsaid from G2elab–Grenoble Institute of Technology, France for giving me the opportunity for a research exchange in his group.

I would also like to thank to Associate Professor Trond Toftevaag for our valuable discussions and cooperation.

Last but not least I would like to thank to Manager Flavio Fernandez and to the Support team from DIgSILENT GmbH, Gomaringen, Germany for making possible my research stay with the group and for their entire help with PowerFactory.

Trondheim, February 2016
Traian Nicolae Preda

To my family

Summary

In the last years the share of distributed generation connected into distribution grids has increased considerably. As their number increases, distribution and transmission network operators are becoming aware on the risks DG can represent on the stable operation of national power systems.

To cope with this, the grid code requirements are becoming more and more demanding in order to ensure the secure and reliable supply of energy to the end users. Early grid code requirements were asking Distributed Generation units to disconnect from the grid when disturbances occurred. This was sufficient because the DG penetration was not so high. Nowadays, when most of the European power systems must handle a large share of DG units, more complex and stringent requirements must be fulfilled by the DG units. By reviewing different grid codes this thesis, shows that the technical connection guidelines are varying from country to country. Moreover as the grid connection of DG units with power electronics interface become more widespread, new requirements have found their place in these grid codes. Some of the new capabilities which non−synchronous DG units have to handle during fault occurrence in the grid are: fault ride−through capabilities, reactive current injection or absorption, power oscillations damping and synthetic inertia. In Europe and North America, a regulatory harmonization approach is seen by the introduction of standards and grid codes for large interconnected power systems, for example the ENTSO−E grid code and the IEEE 1547 standard. In Norway investments in small scale hydro units and wind turbines are numerous and expected to increase also as a result of incentives as the green certificates market. Approximatively 98.5 % of the electricity production originates from large hydro power plants. But there is also a large potential for small scale hydro generation. As the distribution grids in the regions where all this potential lies, are in general an ageing infrastructure, the DSOs are concerned about the technical issues they will have to handle to integrate all DG units.

The focus of this PhD work is to investigate the technical grid code requirements related to the integration of small scale hydro generators in the future Norwegian active distribution grids.

To narrow the research of this work, two main research topics were chosen.

I. The first was to investigate the Low Voltage−Fault Ride Through requirement and to identify potential shortcomings of it. Two specific topics were studied:
   1. The adequacy of the external power systems modelling for assessing the LV−FRT capabilities of DG units
   2. The impact of voltage phase angle variation on the LV−FRT capabilities of DG units

II. The second research topic deals with the development of reduced order models of Active Distribution grids (ADG). The aim is to develop practical methods for establishing model equivalents of ADGs that can be applied by TSOs, when performing systems studies. Also here two specific research areas were chosen:

1. The development of dynamic equivalents of ADGs for rotor angle transient stability analysis
2. The development of dynamic equivalents of ADGs for rotor angle small signal stability analysis

Within these research areas the PhD work contributes with understanding on how the dynamic equivalents for transient stability can be obtained for a test ADG. Moreover, it was studied how the characteristics of a disturbances impact the identification of coherent generators. For the case of small signal dynamic equivalents the work contributes to the slow coherency theory, related to the identification of slow coherent groups of generators when the modelling of synchronous generators are increased and when the excitation system is included.

This research shows that for ADGs with large penetration of small scale hydro units, the oscillation modes similar with the inter−area modes as for TPSs are the inter−machines modes within ADGs. This is because of a good damping of these low frequency oscillation modes. The thesis shows that for ADGs coherency among the DG units some show up within different local plant modes. Linear analysis with simple models for generators fails to identify correctly the groups of coherent DGs as the groups which can be recognized by running a time domain analysis.

A method is proposed which uses time domain decomposition of the state variables within inter−machines modes to determine the coherent groups. Having this method available, the computation of phase and magnitude from the time response for a certain oscillation mode can be done easily. For an ADG the complex Euclidean Distance can be then used to cluster the units in coherent groups. The proposed method is later used to obtain the parameters of equivalent groups of coherent generators. In the last part of this work this method is combined with a model parameter identification algorithm to determine the parameter of aggregated generators.

The thesis can be summarised as in the following:

1. First, an overview of different national grid codes for DG integration is presented and some topics which were not covered in the LV−FRT requirement were identified and investigated. These topics are the inadequacy of external power system modeling and the absence of voltage phase angle variation. The study of these two research topics (the inadequacy of external power system modeling and the absence of voltage phase angle variation) are representing the main contributions of this PhD research to the LV−FRT requirement.

2. In the second part of the thesis practical methods for establishing model equivalents of ADGs were developed for the purpose of TPS studies. Dynamic equivalents for transient and small signal stability were considered.

   2.1 When computing the dynamic equivalents for transient stability it was observed that they are dependent of the characteristics of a disturbance (e.g. location,

duration and type. Although these equivalents are disturbance dependent, they provide a good basis for estimation of the Critical Clearing Time (CCT) as well as of the transient stability limits with respect to the original model.

2.2 For the case of dynamic equivalents for small signal stability, the classical method of slow coherency was studied. Further it was shown how the level of modeling accuracy of the synchronous generator and of the excitation system impacts the identification of slow coherent generators. It was shown that the use of linear analysis for simple models of synchronous generators fails to identify correctly the groups of coherent DGs as seen by running a small disturbance time domain analysis. To cope with this problem, a method is proposed which uses the time domain decomposition of state variables to determine the coherent groups and to obtain the parameters of equivalent generators.

List of Abbreviations

AC8B	–	Alternator – supplied controlled rectifier excitation system
ADG	–	Active Distribution Grid
AG	–	Aggregated Generator
AVR	–	Automatic Voltage Regulator
CCT	–	Critical Clearing Time
CIGRE	–	Conseil International des Grands Réseaux Électriques
DAE	–	Differential – Algebraic Equations
DG	–	Distributed Generation
DPL	–	DIgSILENT Programming Language
DR	–	Distributed Resources
DSO	–	Distribution System Operator
ED	–	Euclidean Distance
ENTSO–E	–	European Network of Transmission System Operators of Electricity
EU	–	European Union
EXNEBB	–	Bus or Solid Fed SCR Bridge Excitation System Model Type NEBB
EW	–	Extended Ward
EXNI	–	Bus or Solid Fed SCR Bridge Excitation System Model Type NI
FACTS	–	Flexible Alternating Current Transmission System
GT	–	Generator – Transformer
G20	–	The Group of Twenty
HV	–	High Voltage
IEEE	–	Institute of Electrical and Electronics Engineers
HYGOV	–	Hydro Governor
LV	–	Low Voltage
LV–FRT	–	Low Voltage Fault Ride Through
MV	–	Medium Voltage
OiDG	–	Optimal infrastructure for seamless integration of distributed generation
PCC	–	Point of Common Coupling
PST	–	Power System Toolbox
RMS	–	Root Mean Square
SMIB	–	Single Machine Infinite Bus
ST1A	–	A potential – source controlled – rectifier excitation system
TPS	–	Transmission Power System
TSO	–	Transmission System Operator
WAG	–	Wind Aggregated Generator
WG	–	Wind Generator

List of Symbols

Phasors or complex quantities are underlined (e.g. $\underline{U}$)
Boldface symbols denote a matrix or a vector (e.g. $\mathbf{A}$)

a_{ij}, b_{ij}	–	Linearization coefficients
a_P, b_P, c_P	–	Weights of the ZIP (impedance–current–power) load model in the absorbed active power
a_Q, b_Q, c_Q	–	Weights of the ZIP (impedance–current–power) load model in the absorbed reactive power
c_k	–	Magnitude of the excitation of the k^{th} mode
$\cos\varphi$	–	Power Factor
$d_{i,j}$	–	Metric Euclidean Distance between the rotor angles of the i^{th} generator and the j^{th} generator
d_{ij}^{w}	–	Metric Euclidean Distance between the rotor angles of the i^{th} generator and the j^{th} generator
$\mathbf{A}$	–	State matrix
$\mathbf{A}_{\omega}$	–	Sub– matrix of the state matrix $\mathbf{A}$
$\overline{\mathbf{A}}$	–	State matrix with damping
$\mathbf{A}_{ij}, \mathbf{B}_{ij}$	–	Matrices of the linearization coefficients
$\mathbf{B}$	–	Input matrix
$\mathbf{C}$	–	Output matrix
D	–	Damping coefficient
$\mathbf{D}$	–	Feed–forward matrix
$\underline{E}$	–	Fault location in % of the total length of the transmission line
E_d, E_q	–	Direct– and quadrature–axis component of the steady state internal emf
E_{fd}	–	Excitation emf proportional to the excitation voltage V_{fd}
$E_{F,MAX}, E_{F,MIN}$	–	Maximum and minimum output of the exciter
$\underline{E}'$	–	Transient internal emf proportional to the flux linkages of the field winding and solid steel rotor body (includes armature reaction)
E'	–	Magnitude of the transient internal emf
E'_d, E'_q	–	Direct– and quadrature–axis component of the transient internal emf
E''_d, E''_q	–	Subransient emf induced in the fictitious d– and q–axis armature coil
f	–	Damped frequency
I_B	–	Reactive current magnitude during fault

I_N	–	Rated current
I_d, I_q	–	Direct– and quadrature–axis component of the armature current
I_{fd}	–	Field current of the generator
I_r	–	Instantaneous reactive current
$I_{r,\max}$	–	Instantaneous reactive current maximum limit
$I_{r,\min}$	–	Instantaneous reactive current minimum limit
$\underline{I}$	–	Armature current phasor
$\underline{I}_R, \underline{I}_B, \underline{I}_I$	–	Vector of complex currents of the boundary buses (B), remote buses (R) and internal (I)
$\underline{I}'_B$	–	Equivalent injections of currents
$\mathbf{I}$	–	Unit matrix
J_i	–	Moment of inertia
$k_{i,a}$	–	Coefficient measuring the electrical distance of node *i*
K_A	–	Amplifier gain
K_E	–	Exciter gain
K_P	–	Scaling factor with respect to active power
K_Q	–	Scaling factor with respect to reactive power
K_T	–	Transient stability limit
$K_1, K_2, K_3, K_4\ K_5, K_6$	–	Linearization constants
$\mathbf{K}_1, \mathbf{K}_2, \mathbf{K}_3, \mathbf{K}_4, \mathbf{K}_5, \mathbf{K}_6$	–	Matrices of the linearization constants
L_{ads}	–	Direct–axis armature to rotor mutual saturated inductance
L_{aqs}	–	Quadrature–axis armature to rotor mutual saturated inductance
L_d	–	Dichotomic matrix solution of Ricatti equation *R(L)*=0.
L_{fd}	–	Self – inductance of the excitation winding *fd*
L_g	–	Grouping matrix
L_l	–	Armature leakage inductance
L_{1d}	–	Direct–axis rotor equivalent leakage inductance
L_{1q}	–	1st Quadrature–axis rotor equivalent leakage inductance
L_{2q}	–	2nd Quadrature–axis rotor equivalent leakage inductance
M	–	Coefficient of inertia

P	–	Active power
P_{acc}	–	Accelerating power
P_e	–	Electromagnetic air–gap active power of the generator
$P_{e,D}$	–	Fault electromagnetic air–gap active power of the generator
$P_{e,P}$	–	Post–fault electromagnetic air–gap active power of the generator
$P_{e,0}$	–	Pre–fault electromagnetic air–gap active power of the generator
P_G	–	Active power supplied to the grid by a generator
P_L	–	Active power absorbed by a load
P_m	–	Mechanical power supplied by a prime mover to the generator
P_n	–	Nominal active power
P_0	–	Reference active power
Q	–	Reactive power
Q_G	–	Reactive power supplied/absorbed to the grid by a generator
Q_L	–	Reactive power absorbed by a load
Q_0	–	Reference reactive power
R_a	–	Resistance of the armature winding of a generator
R_{fd}	–	Resistance of the excitation winding *fd*
R_{grid}	–	Resistance of external grid
R_{1d}	–	Direct–axis rotor equivalent leakage resistance
R_{1q}	–	1st Quadrature –axis rotor equivalent leakage resistance
R_{2q}	–	2nd Quadrature –axis rotor equivalent leakage resistance
s	–	Laplace operator
S_k	–	Short–circuit apparent power
S_n	–	Nominal apparent power
t_a	–	Duration of the disturbance
$t_{actual,CCT}$	–	Actual critical clearing time
t_n	–	Starting time
t_{CCT}	–	Critical clearing time
t_0	–	Starting time
T_A	–	Amplifier time constant of the excitation system
T_D	–	Damping torque component
T_e	–	Electromagnetic air–gap torque of the generator
T_E	–	Exciter time constant

T_m	–	Mechanical torque provided by a prime mover to the generator
T_R	–	Voltage transducer time constant
T_S	–	Synchronizing torque component
u	–	Input variables
U	–	Line to line voltage magnitude during fault
U_C	–	Controlled voltage magnitude
U_{EH}	–	Extra high voltage
U_{EL}	–	Extra low voltage
U_g	–	Voltage magnitude at the generator terminals
U_H	–	Upper voltage
U_{HF}	–	Upper full – load voltage
U_l	–	Line to line terminal voltage
U_L	–	Lower voltage
U_{LF}	–	Lower full – load voltage
U_n	–	Nominal voltage
U_N	–	Line to line rated voltage
U_{rated}	–	Rated voltage
U_{TYP}	–	Typical operating voltage
$\underline{U}$	–	Terminal voltage phasor
$\underline{U}_R, \underline{U}_B, \underline{U}_I$	–	Vector of complex voltages of the boundary buses (B), remote buses (R) and internal (I)
U_0	–	Pre–fault /Initial line to line voltage magnitude
ΔU_r	–	Line to line voltage deviation
V	–	Modal matrix of right eigenvectors
V_1	–	Eigensubspace corresponding to the slow modes of A for the reference generators
V_2	–	Eigensubspace corresponding to the slow modes of A for the non–reference generators
v	–	Row of the right – eigenvectors subspace
x	–	State variables
X_d, X'_d, X''_d	–	d–axis synchronous, transient and subtransient reactance
X_{grid}	–	Reactance of external grid
$x_i(t)$	–	Instantaneous value for a general signal x of the i^{th} generator
$\boldsymbol{X}_i(t)$	–	Instantaneous magnitude value for a general signal x of the i^{th} generator

X_l	–	Reactance of the transmission line
X_q, X_q', X_q''	–	q−axis synchronous, transient and subtransient reactance
X_t	–	Reactance of the transformer
Δx_i	–	Coefficient measuring the effect of disturbance at node i
y	–	Algebraic variables
$y_i(t)$	–	Instantaneous value for a general signal y of the i^{th} generator
$\mathbf{Y}_i(t)$	–	Instantaneous magnitude value for a general signal y of the i^{th} generator
$Y_{i,a}$	–	The admittance value between the i^{th} bus and the location of disturbance ε
$\underline{Y}_{ij} = G_{ij} + jB_{ij}$	–	Element of the admittance matrix
$\underline{Y}_{ij}^{red} = G_{ij}^{red} + jB_{ij}^{red}$	–	Element of the reduced admittance matrix
$\underline{Y}_{BB}, \underline{Y}_{BR}, \underline{Y}_{RR}, \underline{Y}_{RB}, \underline{Y}_{IB}, \underline{Y}_{BI}, \underline{Y}_{II}$	–	Admittance sub−matrices where subscript (B) refers to the boundary buses ,(R) to the remote buses and (I) to the internal buses
$\underline{Y}'_{BB}$	–	Equivalent admittance matrix
Z	–	Impedance magnitude
α	–	Real part of λ
α_P	–	Sensitivity coefficient of voltage with respect to the active power
α_Q	–	Sensitivity coefficient of voltage with respect to the reactive power
α_V	–	Line to neutral voltage magnitude error between i^{th} bus and the j^{th} bus
$\underline{\alpha}_V$	–	Line to neutral voltage phasor error between i^{th} bus and the j^{th} bus
γ	–	Tolerance coefficient
γ_i	–	Disturbance impact index
δ	–	Rotor angle with respect to an infinite busbar
δ_c	–	critical rotor angle on the $P-\delta$ curve
$\delta_{ij,0}$	–	Rotor angles error between the i^{th} generator and the j^{th} generator
δ_m	–	Unstable equilibrium point of the rotor angle on the $P-\delta$ curve
δ_P	–	Post−fault steady –state equilibrium point of the rotor angle on the $P-\delta$ curve
δ_0	–	initial rotor angle on the $P-\delta$ curve
ε	–	Fault location in % of the total length of the transmission line
ε_m	–	Error of the signals' magnitudes
ε_δ	–	Rotor angle error

ε_{ϕ} – Error of the signals' phases
ζ – Damping ratio
η – ″Fast″ states
θ – Voltage angle
λ – Eigenvalue of $\mathbf{A}$
υ – State variable of the exciter
ξ – ″Slow″ states
ψ_{ad}, ψ_{aq} – Air–gap mutual flux linkages rotor equivalent leakage resistance
ψ_{d} – Total flux linkage of damper winding in d–axis
ψ_{fd} – Total flux linkage of the field winding
ψ_{1q} – Total flux linkage of the 1st damper winding in q–axis
ψ_{2q} – Total flux linkage of the 2nd damper winding in q–axis
ω – Rotor speed
ω_0 – Synchronous rotor speed
$\phi_{i,k}(t)$ – Instantaneous phase
$\phi_{i,x}(t)$ – Instantaneous phase value for a general signal x of the i^{th} generator
$\phi_{i,y}(t)$ – Instantaneous phase value for a general signal y of the i^{th} generator
$\boldsymbol{\Phi}$ – Right eigenvector of state variable x for the corresponding λ
$\mathbf{\Phi}$ – Right eigensubspace
$\boldsymbol{\Psi}$ – Left eigenvector of state variable x for the corresponding λ
$\mathbf{\Psi}$ – Left eigensubspace
Ω – Imaginary part of λ

Table of Contents

Chapter 1

Introduction

Transmission power systems (TPS) have evolved during last century to large interconnected systems comprising thousands of buses covering long distances [1], [2]. Also the distribution grids have evolved from only supplying load (consuming power from the transmission grid) into active networks with increasing amounts of small scale generation integrated at this level, named distributed generation (DG). The increasing share of DG units is a result of the efforts to increase the share of renewable power generation and to reduce carbon emissions. Favorable regulatory frameworks together with the corresponding incentives create favorable conditions for the growth of DG units based on renewable sources of energy [3].

In this new context, operational problems have been reported by both DG units' developers and Distribution System Operators (DSOs). These problems are mainly related to overvoltages, bidirectional power flows and intermittent power. In addition to this, DG had to disconnect when disturbances occurred in the distribution grids [3].

The increased integration of DG causes new challenges to the existing power system, to which transmission (TSO) and distribution system operators (DSO) are paying special attention.

1.1. Background and Motivation

DG based on renewable energy resources are considered to play a key role in the future energy system by reducing the dependence of the conventional, fossil fuel based, power plants and creating the path towards a more sustainable and environmentally friendly energy supply.

This aspect is very important within the Smart Grids concept, [4]. This idea is highlighted as:

"The Smart grid will require extensive interaction between various actors in the electric energy system e.g. centralized and distributed generation, transmission and distribution networks, active end-users, market solutions and communication technologies, and holds a significant benefit with regards to obtain a sustainable energy supply ." [4]

This PhD work was part of the research project "Optimal infrastructure for seamless integration of distributed generation" (OiDG) supported by the Research Council of Norway and 15 companies within electricity distribution in Norway.

The PhD thesis addresses some technical challenges which potential DG developers and system operators must tackle from the power systems' stability perspective.

The concept of Distributed Generation (DG) as defined by the CIGRE and IEEE, is:

According to [5], DG units are defined as units which are: *"not centrally planned, today not centrally dispatched, usually connected to the distribution network and smaller than 50-100MW. (Not centrally planned or dispatched means that major influences such as unit commitment or reactive power generation are out of control of the system operator)"*, [5].

The Institute of Electrical and Electronics Engineers (IEEE) defines DG or DR (distributed resources) in the Standard 1547−2003, as: ″Sources of electric power that are not directly connected to a bulk power transmission system. DR includes generators and energy storage technologies″, [6].

A) Challenges regarding integration of DG units in Europe

In Europe as the energy sector represents the main source of greenhouse gases, the energy policy problems and the desired solutions were presented in the 20/20/20 plan. The 20/20/20 plan is proposing an increase of energy use efficiency with 20% and an increase of the renewable energy resources share at the EU level with 20% by 2020. Ambitious plans with respect to this goal are presented also in other national energy policies of the G20 [7]. The increased interest in distributed generation is also due to the fact that the cost of electricity production of small distributed generation compared to the large conventional units has been reduced by 30% to 60% in the time interval ranging from 1960−2000 [8] Figure 1.1 presents the share of electricity generation having as primary source both fossil fuel and renewable energy in the total electricity generation share in Europe in the last years. It can be observed a growth of renewables from 13.4% in 1998 to 18% in 2008 and 27.4% in 2010.

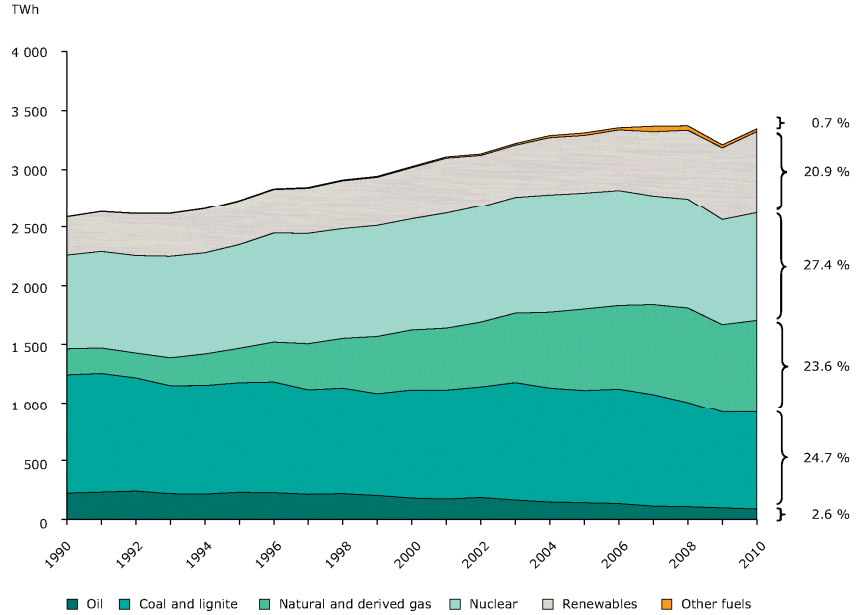

Figure 1.1. Gross electricity production by fuel, EU-27 [7]

Moreover, as presented in [4] the main challenges regarding the integration of DG units in different national distribution grids are the bidirectional power flows in MV and LV grids and the need for new control and protection solutions.

B) Challenges regarding integration of DG units in Norway

As presented in [3], Norway has to reach the goals of the EU 20/20/20 directive and it is expected to increase the share of renewable energy generation to 67.5% in 2020 from 58% in 2005. Norway joined Sweden in 2012 in a common green certificate market. This is expected to give an increase of 26.4 TWh of renewable in the two countries. But as presented in [4] most of the Norwegian distribution grids are an ageing infrastructure and are operated by approximatively 135 DSOs. As Norway is a mountains country rich in precipitation, 98.5% of the electricity production to come from large hydroelectric power plants [9].

According to [4], in Norway DG is defined as generation or energy storage units up to 10MW. But the majority of DG units are small scale hydro units, divided into 3 categories of generators:

- Micro units: smaller than 100kW
- Mini units: 100−1000kW
- Small units: 1−10MW

The research papers: [3] and [4] (are part of the same project as the PhD work: OiDG) investigated the status of DG integration in Norway and the challenges which DSOs have to tackle. According to [4] in 2008 there were approximately 800 small scale hydro units installed in Norway, but this large number of units covered only 5% of the total installed capacity.

[9] presents the estimated potential for DG integration in Norway to 18.5 TWh.

Figure 1.2 shows how this potential is distributed across Norway:

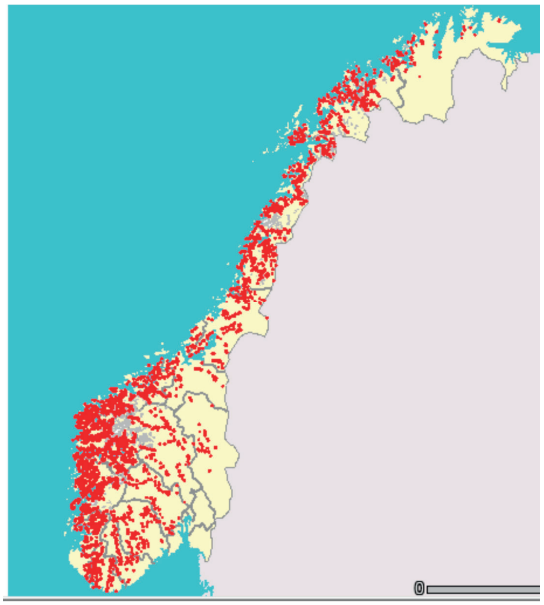

Figure 1.2. Potential for hydro energy DG in Norway with development cost < 3 NOK/kWh (approx. < 0,4 € /kWh) [9]

Most of the possible DG units are located in sparsely populated areas where generally the distribution grids are weak [4].

In the same study [4] a survey was presented in order to establish what are the main problems and the main analyses performed by DSOs in order to tackle the DG penetration. Figure 1.3 present the results of this survey.

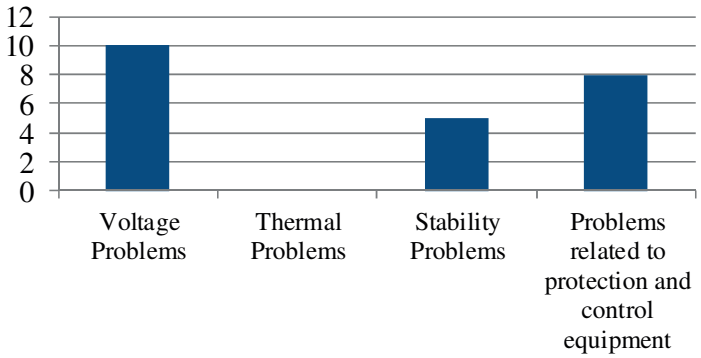

Figure 1.3. Type of operational problems experienced with existing DG units [4]

The survey [4] concluded that in Norway the DG developers are already facing different type of problems from the integration of DG units. Therefore, this PhD work addresses the stability problems and investigates what are the gaps of the nowadays grid code requirements related to DG.

1.2. Problem Statement

The existing power systems are challenged as the share of DG at MV distribution level is increasing. In order to ensure the security of operation and power quality in these grids, transmission and distribution power system operators have issued connection and operation guidelines related to integration of distributed generation.

Grid codes are not new topics in the power systems literature. They started to appear more than 15 years ago, for transmission systems, as a set of technical guidelines and operation specifications which large conventional power plants needed to comply with. The grid codes differed from country to country due to different regulations and different characteristics of their national power systems. At distribution grid level, grid codes were mainly used to specify and design the guidelines which the DSOs will apply in the planning and development of distribution grids, with the compliance of end users (loads).

In today's context, when generation has moved, also to lowest levels of the power systems (medium and low voltage levels), some loads have transformed from passive components into active ones and power systems into entities with a bidirectional energy and information flow. When this change occurred in the distribution grids, the DSOs normally assessed the DG integration by conducting simple integration studies (load flow, basic power quality studies) because the amount of DG integration was small and the stipulated technical guidelines were simple or even absent [10]. Currently, when the share of DG is increasing, there is an awareness for the need to revise and upgrade the DG connection guidelines, in order to achieve a stable and proper operation of the overall power systems.

As presented earlier, large amounts of DG at distribution level will likely have an impact on transmission systems as well, and in order to study this impacts distribution system cannot longer be modeled as simple load buses in stability transmission system studies. Instead a more adequate representation is needed [11] [12].

This will greatly simplify the representation of ADGs in power system stability studies, as it reduces the number of power systems elements that will have to be modeled. This type of representation will allow different DSOs to exchange the models of these grids without worrying about confidently issues.

In the last years, a harmonization work of grid codes related to DG has been carried out at international level and the results are being shaped into a set of standards and recommendations.

This PhD work addresses some of the key issues related to grid code requirements for DG units.

1.3. Research Objectives

As mentioned in the previous Section, grid code requirements for DG units are of interest for DSOs and TSOs, as well for DG developers. The overall objective of this PhD work is to investigate different national grid codes related to DG and find the topics which are not well covered and possible solutions to these. Namely, the objectives of this research are as follows:

Part I of this PhD work addresses to the topics which are not well covered in Low Voltage Fault−Ride Through (LV−FRT) grid code requirement related to power systems analysis and modeling from a DSO perspective, which in detail means:

1. To survey and observe the new trends of national grid codes related to DG integration. And to identify the topics which are not well covered in Low Voltage Fault−Ride Through (LV−FRT) grid code requirement.
2. To investigate the adequacy of the external grid modeling when LV−FRT is assessed for dynamic studies related to DG integration.
3. To investigate the impact of voltage phase angle changes on LV−FRT performance of DG units.

Part II of this PhD work addresses the increased complexity of modelling of active distribution grids (ADGs) for TSO studies. As the classical passive lumped load model cannot be used to represent these grids under dynamic conditions, aggregated models as dynamic equivalents of power systems can be an approach to model these grids for future TSOs studies. Specifically, the research objectives tackled in the second part of this work are classified depending on the nature of rotor angle stability investigated:

A. Dynamic equivalents of ADGs for rotor angle transient stability

1. To investigate dynamic equivalents theory used for the assessment of transient stability into power systems.

2. To implement a model reduction algorithm into a simulation platform for a test ADG.
3. To study the impact of disturbance duration, location and type on the coherency identification of generators.
4. To assess the adequacy of the reduce model by validating against the original model using different criteria.

B. Dynamic equivalents of ADGs for rotor angle small signal stability

1. To investigate dynamic equivalents theory used for assessment of small signal stability into power systems.
2. To investigate the slow coherency concept for small scale hydro units into a test ADG.
3. To study the impact of increasing generator modeling on the identification of slow coherent small scale hydro units into a test ADG.
4. To investigate the impact of excitation systems on the identification of slow coherent of small scale hydro units into a test ADG.
5. To propose a new method to cluster small scale hydro units which takes into consideration both the magnitude and phase of time domain decomposition of units' signals. This method will allow observing how the non−linearity of a real power system impacts the coherency phenomenon.
6. To propose an aggregation algorithm of the small scale hydro units and of their controllers based on the state variables' time domain responses and a parameter model identification algorithm.

The analyses are done considering that a power system can be decomposed into 3 main areas for model reduction:

- An area representing the power system under study (internal power system),
- An external power system
- A remote power system

Figure 1.4 summarizes the research directions related to the model reduction considered in this work.

a) The adequacy of the external power system modelling (TPS) for assessing the LV−FRT capabilities of DG units

   a.1) DG unit is representing the internal area
   a.2) TPS represent the external and remote power system

b) The model reduction of ADGs for transmission power systems studies

   b.1) TPS represent the internal area
   b.2) ADGs represents the external and remote power systems

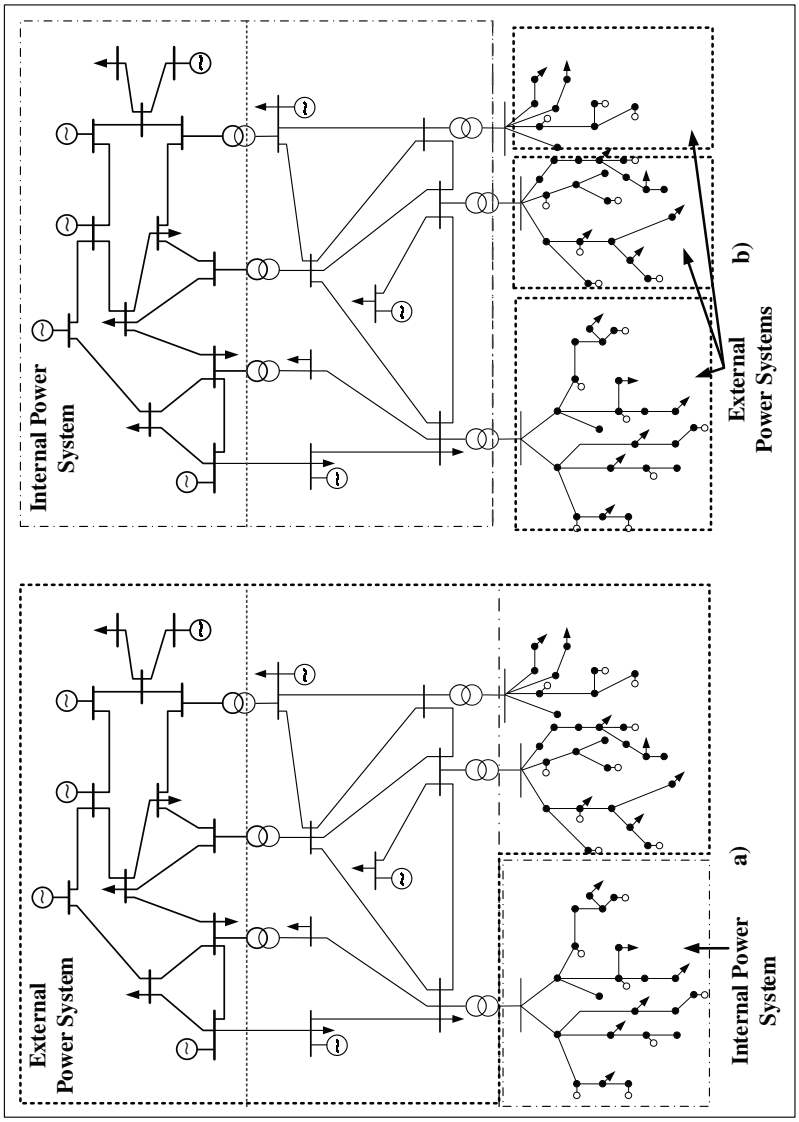

Figure 1.4. PhD work in model reduction for power systems analysis with different voltage level

1.4. Scope and Limitations

The main scopes and limitations of this PhD work are as follows:

1. Only power systems analyses were carried out to investigate the considered contributions to the grid code requirements related to Distributed Generators.
2. DG units were limited to small scale hydro units specific to the Norwegian power grids.
3. In the test transmission power system, only fixed speed wind turbines and hydro power plants were considered as these are the primary energy resources in Norway.
4. DIgSILENT PowerFactory and Power System Toolbox – PST and standard models available in PowerFactory have been used, as simulation platform

1.5. Main Contributions

The main contributions of this PhD work are as following:

1. An overview of different national grid codes related to the integration of DG units is presented in Chapter 2. Topics which were not covered in the Low Voltage–Fault Ride Through requirement were identified and investigated further in Chapter 3. These topics are:

   1.1 The inadequacy of external power system modeling in the LV–FRT requirement

   - The investigation has shown that by using a Thévenin equivalent to study a DG unit integration, overall inaccurate LV–FRT results are obtained for the main responses of DG unit (as rotor angle, voltage magnitude and angle variation, active and reactive power). This is mainly due to the fact that a Thévenin equivalent does not represent the electromechanical dynamics as a complete model representation of power system would do. Therefore dynamic equivalents based on Ward and Extended Ward were proposed as possible solutions to represent the external TPS when this type of study must be done by TSOs.

   1.2 The absence of voltage phase angle variation in the LV–FRT requirement

   - An analysis taking into account only the voltage change as the perturbation will lead in many cases most likely to erroneous conclusions regarding the transient stability of the unit and of critical clearing time value. In addition, the study shows that the type (and parameterization) of the unit's automatic voltage controller in this case have a significant impact on the unit's CCT.

2. The modelling of Active Distribution Grids (ADGs) for rotor angle stability assessment. The contributions are:

   2.1 The investigation of adequacy of the ADGs modeling using dynamic equivalents for rotor angle transient stability analysis

   - In Chapter 4, these types of equivalents were proposed in order to reduce the order model of ADGs and to preserve the dynamics and the transient stability limits of the original model. It was observed that these equivalents are very much dependent by the characteristics of disturbance (as location, duration and type) for which they are computed.

   2.2 The investigation of adequacy of the ADGs modeling using dynamic equivalents for rotor angle small signal stability analysis

   - In the first part of Chapter 5 the main contributions relates to the slow coherency theory. This theory was considered to produce these equivalents and further it was investigated how the increased modelling of the synchronous generator impacts the identification of slow coherent generators. It was observed that by using the electro−mechanical and transient models the same groups of generators were obtained. But by using simple models of synchronous generators the algorithm fails to identify correctly the groups of coherent generators as the one produced by running a time domain simulation for a small disturbance. A contribution in this field is to include the excitation system model; with this a similar grouping is obtained with the ones resulting from running the time domain simulation.
   - In the second part of Chapter 5 the main contribution is related to investigation of why linear analyses cannot identify correctly the groups of coherent into an ADG as the one produced by running a time domain simulation. This investigation is related to ADGs connected to strong TPSs. This assumption was confirmed by observing that for ADGs there are not unique modes in which the same grouping of the coherent generators can be observed as by running a time domain simulation for a small disturbance. It was shown that groups of coherent generators, similar with the one identified in the time domain simulation, are recognizable in several inter−machine modes. This conclusion is true as the time domain simulation is the result of a mix of multiple oscillation modes. Now, as the identification of coherent generators using linear analysis is not any longer straightforward, the small signal time response decomposition is chosen in order to obtain the groups of generators and further to identify the parameters of equivalent generators. The contribution of this Chapter is related to the mathematical manipulation of the

time response decomposition which allows the computation of magnitude and phase angle of a particular mode. The results of this mathematical manipulation are further used to cluster the generators in the most observable modes of the time domain simulation, by using the Euclidean Distance in polar coordinates between each of the generators. In the end of Chapter 5, a method based on the same time response decomposition is proposed to obtain the parameters of equivalent generators. For each group of coherent generators, the equivalent time responses of signals (within a selected range of modes) are computed as the summation of time responses of each generator, but rescaled with the participation factors corresponding to each selected mode. Further, the equivalent time responses are used in a model parameter identification algorithm, to obtain the parameters of equivalent generators.

1.6. Outline of the Thesis

The PhD thesis contains seven Chapters and six Appendixes. Each Chapter is divided in Sections and Sub−Sections. The content it is organized as follows:

Chapter 1: Introduction

This Chapter introduces the reader to the status of DG integration in EU and in Norway. Also, presents the main challenges of integrating DGs in Europe with a special attention on the Norwegian case. It further presents the research objectives, scopes, limitations and the main contributions of the PhD work.

Chapter 2: Grid Codes Requirements for Distributed Generation for Integration into Power Systems

This Chapter presents the common grid codes requirements which are found in different national grid codes. The overview of these requirements is done for both steady state and dynamic conditions. A special attention is given to the review of the IEEE 1547 and the ENTSO−E guidelines. The scope of this overview is for a complete treatment of the subject. The main scope of this Chapter is to study LV−FRT grid code requirement and to identify those topics which are not well covered by this requirement.

Chapter 3: New Contributions to the Grid Codes Requirements for Integration of Distributed Generation into Power Systems

This Chapter presents proposed contributions of this PhD work related to the LV−FRT grid code requirements. These main contributions are related to the modeling of the external power systems and to the impact of the voltage phase angle variation on the assessment of the LV−FRT requirements.

Chapter 4: Dynamic Equivalents of Active Distribution Grids for Rotor Angle Transient Stability Studies

Chapter 4 presents the contributions of this PhD work regarding the model reduction of ADG for rotor angle transient stability. The first part of Chapter 4 introduces a test ADG and presents a method to produce dynamic equivalents of ADG for investigating transient stability in main transmission system. In second part the impact of disturbance duration, location and type on the coherency identification of generators is investigated, quantify by the disturbance impact index.

Chapter 5: Dynamic Equivalents of Active Distribution Grids for Rotor Angle Small Signal Stability Studies

Chapter 5 contributes to the small signal equivalents methods to reduce ADGs. In the first part of the Chapter, the classical method of slow coherency is investigated for the introduced test ADG. This method of grouping the generators it is studied for different models of synchronous generators and it is compared against a time domain simulation for a small signal perturbation. In the second part, the problems which results from using the linear analysis to cluster the DG units into an ADG are studied. And a new method based on the time domain decomposition of DG's signals is proposed to identify the coherent generators in the test ADG. Based on this method a dynamic equivalent for the ADG is produced for which the parameters of equivalent generators are obtained using a parameter identification algorithm.

Chapter 6: Discussions

In Chapter 6 the main research contributions are discussed.

Chapter 7: Conclusions and Future Work

Some concluding remarks and suggestions for future work are presented in this Chapter.

Appendix 1: Test Transmission Power System

Appendix 2: Test Radial Distribution Grid

Appendix 3: Test Active Distribution Grid

Appendix 4: The Impact of Generator and Excitation System Modeling on the Slow Coherency Identification– Computed Eigenvalues

Appendix 5: Dynamic Equivalents of Active Distribution Grids using a Model Parameter Identification Method

Appendix 6: Magnitude and Phase Calculation Using the Time Decomposition of the State Variables

1.7. List of publications

During the PhD work the following publications were written and submitted to different international conferences. The chapters of this PhD thesis are based on the following selected papers, which the author was main or co-author for. In chronological order the research publications are:

Main author:

- **Publication A: Preda, Traian Nicolae**; Uhlen, Kjetil; Nordgård, Dag Eirik. (2012) *"An overview of the present grid codes for integration of distributed generation"*, CIRED 2012 Workshop: Integration of Renewables into the Distribution Grid, Lisbon, Portugal, 29–30 May 2012**.** [13]

- **Publication B: Preda, Traian Nicolae**; Uhlen, Kjetil; Nordgård, Dag Eirik; Toftevaag, Trond. (2012) *"External Grid Representation for Assessing Fault Ride Through Capabilities of Distributed Generation Units"*, 2012 3rd IEEE PES Innovative Smart Grid Technologies Europe (ISGT Europe). [14]

- **Publication C: Preda, Traian Nicolae**; Uhlen, Kjetil; Nordgård, Dag Eirik; Toftevaag, Trond. (2013) *"Dynamic equivalents of active distribution power systems for investigation of transient stability"*, CIRED 2013 Electricity Distribution Systems for a Sustainable Future. [15]

- **Publication D: Preda, Traian Nicolae**; Uhlen, Kjetil; Nordgård, Dag Eirik. (2013) *"Clustering Distributed Generation Using the Instantaneous Euclidean Distance in Polar Coordinates",* 2013 4th IEEE PES Innovative Smart Grid Technologies Europe (ISGT Europe, Lyngby, 6–9 Oct. 2013. [16]

- **Publication E: Preda, Traian Nicolae**; Uhlen, Kjetil; Hadjsaid, Nouredine. (2014) *"Dynamic Equivalents of Active Distribution Grids Based on Model Parameters Identification"*, IEEE PES General Meeting 2014, National Harbor, Washington D.C., USA, 27–31 July 2014.

- **Publication F: Preda, Traian Nicolae**; Uhlen, Kjetil; *"A Test Distribution Grid for Study of Slow Coherency Concept "*, IEEE PowerTech 2015, Eindhoven, Netherlands, June 29 –July 2, 2015.

Co–author:

- **Publication G:** Toftevaag, Trond; Marvik, Jorun Irene; **Preda, Traian Nicolae**. (2012) *"Impact of voltage phase angle changes on low-voltage ride-through performance of DG-units"*, CIRED 2012 Workshop: Integration of Renewables into the Distribution Grid, Lisbon, Portugal, 29–30 May 2012.

● **Publication H:** Toftevaag, Trond; **Preda, Traian Nicolae**; Uhlen, Kjetil. (2013) *"Impact of voltage phase angle changes on low-voltage ride-through performance of small scale hydro DG units"*, CIRED 2013 Electricity Distribution Systems for a Sustainable Future, Stockholm, Sweden, 10–13 June 2013.

These results are the basis for the chapters of this thesis.

During the PhD work other publications where written as part of the PhD study. **Publication I** was written in addition to the PhD course: TET 8340–*"Instantaneous Power Theories and Compensation with Power Electronics"*

Other publications not included in the PhD thesis:

● **Publication I: Preda, Traian Nicolae**; Uhlen, Kjetil; Nordgård, Dag Eirik. (2012) *"Instantaneous Harmonics Compensation using Shunt Active Filters in a Norwegian Distribution Power System with Large Amount of Distributed Generation"*, PEDG 2012: 3rd IEEE International Symposium on Power Electronics for Distributed Generation Systems.

Chapter 2

Grid Codes Requirements for Integration of Distributed Generation into Power Systems

This Chapter presents a review of the common grid codes requirements of different countries. The overview of these requirements is done for both steady state and dynamic conditions. A special attention is given to the review of the IEEE 1547 and the ENTSO−E guidelines. The focus is both steady state and dynamic conditions and the main is to study the current Low Voltage−Fault Ride Through grid code requirements and to identify those topics which are not well covered by these. This Chapter is based on ***Publication A****.*

2.1. Introduction

This Chapter provides an overview of the most recent and comprehensive grid codes regarding DG integration at distribution level. First a list of the reviewed grid codes regarding DG integration at distribution level is presented. In Section 2.3 and 2.4 the grid code requirements are divided by the type of studies they address: steady state and dynamic operations, and examples are given for specific national grid codes. These examples are presented for a complete cover of the subject. The main focus is to present existing LV−FRT requirements and to identify topics which are currently not well covered by these. These topics will be thoroughly investigated throughout the PhD work and are representing the main contributions of this thesis.

2.2. Common Requirements for Grid Codes Related to Distributed Generation

This Section reviews the following set of common technical connection requirements, based on the operation states of an Active Distribution Grid (ADG):

a) Requirements for steady state operation (ch. 2.3):

– Frequency and voltage ranges
– Active power output control
  Reactive power output control

b) Requirements for dynamic operation during grid disturbances:

– Low Voltage Fault Ride Through
– Grid voltage support during disturbances

– Reactive current injection or absorption for fast acting voltage control
– Synthetic inertial capability or inertia emulation
– Oscillations damping in ADGs
– Frequency control support

The grid codes reviewed are listed in the Table 2.1.

Table 2.1. Grid codes related to DG reviewed in paper A [13].

Country		**Grid Codes related to DG**
Canada	Hydro–Québec (February 2009)	″Requirements for the Interconnection of Distributed Generation to the Hydro–Québec Medium–Voltage Distribution System″ [17]
	Manitoba Hydro (January 2003)	″Interconnection Guideline for Connecting Distributed Resources to the Manitoba Hydro Distribution System″ [18]
Denmark (October 2008)		″Technical Regulation for Thermal Power Station Units larger than 11 kW and smaller than 1.5MW″ [19]
Germany (June 2008)		″Guideline for generating plants' connection to and parallel operation with the medium–voltage network″ [20]
Ireland (March 2011)		″EirGrid Grid Code″ [21]
Norway (October 2006)		″Network Code for Requirements for Grid Connection Applicable to generators with maximum active power production less than 10 MW in (the) distribution grid.″ [22]
Spain (October 2008)		″Technical requirements for wind power and photovoltaic installations and any generating facilities whose technology does not consist on a synchronous generator directly connected to the grid″ [23]
United Kingdom (June 2009)		″The Grid Code″ [24] ″The Distribution Code″ [25]

In addition, two international publications – on the technical requirements for DG integration are also surveyed– see Table 2.

Table 2.2. International grid codes related to DG integration.

ENTSO–E (January 2012)	″Requirements for Grid Connection Applicable to all Generators″ [26]
IEEE–1547 (July 2003)	″Standard for Interconnecting Distributed Resources with Electric Power Systems″ [27]

2.3. Requirements for Steady State Operation

In steady state operation of a distribution grid, DG units are required to operate within a defined range around the nominal voltage at the point of common coupling (PCC).

The steady state frequency–voltage operation ranges are presented in most surveyed grid codes for the following four operating conditions:

- A range where a continuous operation is required
- A range where DG can operate but with output reduction (the restrictiveness and scale limits of these operation areas differ from country to country)

- A range where it is possible to operate but for which no output reduction or no requirements are defined
- A range where immediate disconnection is required

The most demanding grid codes regarding frequency ranges are those from the UK [24], Ireland [21] and Denmark [19]. The span of operation areas are between 47 Hz and 52.0–53.0 Hz. In terms of voltage limitations during normal steady state operation the most comprehensive grid code is that of Hydro-Québec, where the requirements cover a range between 0–140 percent of nominal line voltage.

The ENTSO–E code is one of the most comprehensive grid codes in respect to steady state frequency ranges requirements for DG units connected below 110 kV. This grid code covers almost the entire European synchronous area, stating voltage and frequency limits. The ENTSO–E draft grid code from 2012 also states that DG units must disconnect for specified voltages. Figure 2.1 depicts an example for voltage-frequency ranges related to steady state operation of DG units, as defined by Denmark's TSO, Energinet.dk. [19]

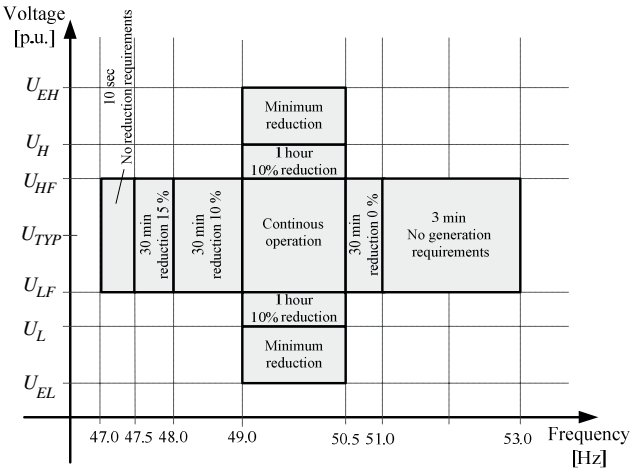

Figure 2.1. Voltage-frequency steady state operation areas defined by Energinet.dk (for thermal generation units between 11 kW and 1.5 MW), [19].

Active power-frequency control in steady state operation can be defined in case of ADGs with DG integration as the capacity of units to control the active power production in order to keep the frequency within rated limits and to maintain the regulatory obligations commissioned from the DSO [24]. This requirement is meant to ensure a stable operation during islanding and is also related to the possibility of DG units to provide ancillary services.

Table 2.3 shows the requirement on active power ramp ranges requirements from different grid codes.

Table 2.3. Active power ramp ranges.

Country		Active power ramp range
Canada	Hydro-Québec	Ramp up or down in an adjustable 2 to 60 minutes, from minimum 0 MW (stopped) to maximum power plant output, [17].
Denmark		For voltages representing 0.9 pu and 1.1 pu of nominal voltage, the reduction of maximum power must not be greater than 10 %, [19]
Germany		Must be able to reduce active power in steps of 10 % of the agreed capacity with the network operator [20]
Ireland		Requires from DG units to ramp up and down a capacity of not less than 1.5 % of the registered capacity per minute when the unit is in normal dispatch condition, [21].
Spain		The ramp up rate value is maintained at 10 % and the duration of this action is 250 ms, [23].
ENTSO–E draft code		Requires from the DG units ramp ranges between 2-10 % with a full activation time frame 6-30 sec, [26].

Regarding the control strategy related to the steady state operation: reactive power–voltage (Q–U) can be defined as property of the DG units to maintain the voltage level within limits at the PCC by injection or absorption of reactive power as long as the voltage control equipment is not saturated [24]. In Table 2.4 some reactive power control requirements which DG units need to comply with are summarized.

Table 2.4. Reactive power control requirements for DG.

Country		Reactive power control requirements for DG
Canada	Hydro-Québec	Must have the capability to exchange reactive power with ADG at an over-excited or under-excited power factor less or equal with 0.95 [17]
	Manitoba Hydro	- DG based on synchronous generator, must control the PCC voltage in the ranges within 95–105 % of the rated voltage [18] - DG based on induction generators or a power electronics interface must to correct the power factor to ±0.95 or better [18]
Denmark		DG unit must ensure a reactive power production with power factor (related to tan φ) within the range –0.20 and 0.40 with respect to the rated active power and within the rated limits for voltage [19]
Germany		DG unit can be operated with reactive power output corresponding to a power factor (related to cos φ) in the PCC between 0.95 underexcited and 0.95 overexcited [20]
Ireland		DG unit must to ensure at the maximum active power production a reactive power of 30 % with respect to the rated one, in both leading and lagging mode, power factor between 0.85 underexcited and 0.85 overexcited [21]
Norway		DG unit must be dimensioned to ensure a power factor of 0.95–1.0 at maximum active power production [22]
Spain		DG unit must exchange reactive power with ADG at any active power production up to 20 % from the rated value. Lower than 20 % the capacity for reactive power exchange can decrease in a linear dependency down to zero [23]
UK		DG units must ensure a transfer of reactive power in the PCC at rated active power output at a power factor between 0.95-leading and 0.95–lagging. This reactive power limits applies for active power production of DG units up to 20% of the rated active power [24]

The ENTSO–E draft code [26] presents a survey of the aforementioned requirements related to reactive power control requirements in steady state operation. In IEEE standard 1547 [6] there are no such specifications on this topic.

2.4. Requirements for Dynamic Operation During Disturbances

An ADG is a dynamic system and is affected continuously by disturbances. In order to remain stable after being subject to disturbances some requirements (during a fault occurrence and post fault state) are imposed to DG units connected in distribution grids. Most of the reviewed grid codes require that the operation of the unit continues during the fault even if the voltage is dropping to inadmissible values or even to zero.

The LV–FRT is defined as voltage–time profiles presenting the course of grid voltage as function of time in the PCC with the DG unit. This grid voltage in the PCC is considered for the phase which sustains the largest voltage drop during the fault [26].This curve shows the overall fault time range: before, during and after the fault occurs. Table 2.5 presents a summary of LV–FRT capabilities is presented (including LV–FRT capabilities for wind generators). Spain, Germany and ENTSO–E require DG units to support the grid during fault by injecting a specified amount of reactive current.

Table 2.5. FRT requirements for DG in different national grid codes.

Country	**Low Voltage Fault ride-through capability**			
	Duration of fault	**Voltage drop level**	**Post fault time recovery**	**Reactive current injection**
Canada Hydro–Québec	150 msec	$0\%U_{rated}$	0.18 sec	–
Denmark	50 msec	$20\%U_{rated}$	1 sec	–
Germany	150 msec	$0\%U_{rated}$	3 sec	Up to 100%
Ireland	600 msec	$50\%U_{rated}$	–	–
Spain	500 msec	$20\%U_{rated}$	0.5 sec	Up to 100%
UK	140 msec	$15\%U_{rated}$	1.2 sec	–
ENTSO-E	40 msec	$15\%U_{rated}$	1.5-3 sec	Up to 100%
IEEE 1547	–	–	–	–

By conducting the survey related to the LV–FRT requirements it was observed that the investigated grid codes do not cover topics as:

- External grid modeling
- Impact of voltage angle variation
- ADG modeling for TSO studies

These topics will be treated thoroughly in this PhD work.

As the current injection must be done fast, with the rapid increase of the reactive power generation, the amount of active power must be reduced. Immediately after the fault is cleared, the unit will restore the active power production prior to the fault in a ramp manner within predefined values [20], [23], [26]. In the Spanish grid code the process of reactive

current injection or absorption during a disturbance (when the voltage drops below 0.85 [p.u.]) is similar with the process of automatic voltage regulator for conventional synchronous generation. In this case the controller is designed as a PI control, as presented in Figure 2.2. The controller has as output the instantaneous reactive current I_r limited by the saturation values (dependent of voltage) $I_{r,max}$ and $I_{r,min}$, U_c is the voltage set point, V is the voltage in the PCC (all parameters are RMS values), [23].

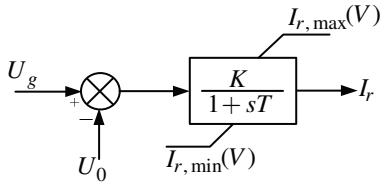

Figure 2.2. Simplified block diagram of an error proportional regulator for reactive current injection or absorption as defined in the Spain's grid code [23].

The ENTSO–E draft grid code defines the reactive current injection or absorption as fast acting voltage control. According to this requirement the control is activated if the voltage is deviating from the steady state value between 0 and ±10 % [26]. By activating the fast acting voltage control, a contribution of reactive current will be supplied at the low voltage side of the first step up transformer. This contribution must be of a least 2 % of the rated current per percent of voltage deviation and the DG unit must be capable of providing this reactive current in 40 ms after the occurrence of disturbance. The ENTSO–E draft grid code requires that, the supplied reactive current during the fault duration should not be less than 1 p.u. of the short term dynamic rating of equipment, delivered when the voltage drops below 40 % of steady state value at PCC. The principle of fast acting voltage control or fast reactive current injection or absorption, is depicted in Figure 2.3.

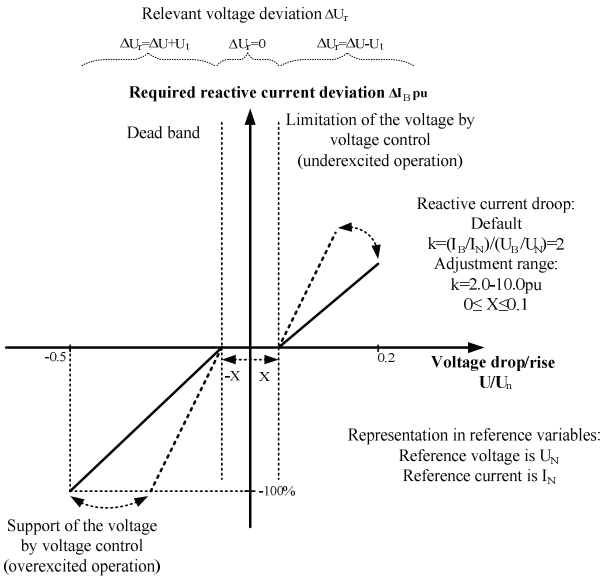

Figure 2.3. Voltage support principle as defined in ENTSO−E draft grid code. [26]

Some new features are starting to appear in the recent grid codes, like inertia emulation and oscillations damping in ADG [23] [26].

The **inertia emulation** is referring to capability of DG units (connected via frequency converters) to generate active power variations with respect to the derivative of frequency in the PCC or in the form of some predefined curves; reference [26] presents an example of such a curve.

Regarding **damping of oscillations** in distribution grids, some grid codes state that the DG units can be required to be equipped with power system stabilizers in order to damp power oscillations in frequency range between 0.15−2 Hz, as reference [23] requires.

2.5. Summary

This Chapter reviews different national grid codes related to the integration of DG units. The surveyed grid codes were from both transmission and distribution level of the power system, as some of the countries introduce requirements for DG connection in their national transmission grid codes. The national grid codes vary between countries and this is because of the different degree of DG penetration into the national power systems. In the early versions of the grid codes, DG units were requested to disconnect from the grid during perturbed conditions, indifferent of the generation technology. This request has been replaced with more complex specifications in the newer codes, which also makes a clear distinction between

synchronously and non−synchronously generation units. Within EU, the ENTSO-E is trying to level all the specifications into a common grid code already in action.

This review focuses on the Low Voltage Fault Ride−Through (LV−FRT) requirement for DG units, and identified the following topics that are not well covered by this requirement:

1. External power system modeling when the LV−FRT requirements are investigated.
2. The impact of voltage phase variation on the synchronously DG units FRT capabilities.
3. Adequate modeling of the distribution grids with large penetration of DG units for rotor angle stability studies, from a TSO perspective.

These topics are the main research topics for the next Chapters.

Chapter 3

New Contributions to the Low Voltage Fault Ride − Through Requirements for Integration of Distributed Generation into Power Systems

The chapter is based on **Publication B**, **D**, **G** and **H** *and presents the contributions of this PhD work regarding Low Voltage Fault Ride Through (LV−FRT) grid code requirements. In Section 3.2 different external power system models, used to investigate LV−FRT capabilities of small scale hydro units are investigated by comparison with the Thevenin source proposed by the grid codes. These models are proposed to replicate the dynamics associated with the bulk transmission grid. In Section 3.3, the concept of LV−FRT is extended by taking into consideration the impact of voltage phase angle variation on the dynamic behavior of small generators.*

3.1. Introduction

As presented in Chapter 2, the existing power systems are challenged as the share of distributed generation (DG) at MV distribution level is increasing. In order to ensure the security of operation and power quality in these grids, transmission and distribution power system operators have issued guidelines for connection and operation of distributed generation. Some of these guidelines are designed to assess LV−FRT capabilities when dynamic studies are performed for distributed generation units. While most of the ongoing research has addressed the LV−FRT capabilities of the DG unit when the most severe fault occurs close to the point of common coupling, some research questions remain related to the adequacy of the representation of the external grid and of the impact of the voltage phase angle on the LV−FRT requirements. Therefore, Section 3.2 will compare several representations of external grid proposed by different authors for achieving more accurate results of fault ride–through capabilities of small scale hydro units versus the model proposed by the grid code requirement (Thevenin source). And in Section 3.3, the concept of LV−FRT is being extended by taking into consideration the impact of the voltage phase variation on the capabilities of small scale hydro units. These two research topics represent the main contributions of this PhD work to the LV−FRT requirement.

3.2. External Grid Representation for Assessing Low Voltage Fault Ride−Through Capabilities of Distributed Generation Units

3.2.1. Low Voltage Fault Ride – Through Capabilities

In the distribution grid code [20], LV−FRT capabilities are related to the capacity of a DG unit to maintain the rated values of the active power production and voltage at PCC in pre− and post− fault conditions. Maintaining the rated voltage at PCC is done by injecting an amount of a reactive current during the fault, [20] [26]. With respect to the voltage dip during fault, a LV−FRT profile can be defined. According to [26], the LV−FRT capability is defined as a voltage–time magnitude presenting the course of external power system voltage as function of time for the point of common coupling (PCC) where the DG unit is connected, when a fault emerges. Also, this refers to the phase which sustains the largest voltage dip during the fault, [26].

In this work, the voltage dip profile for achieving the LV−FRT capability of a small scale hydro unit is defined according to the distribution grid code in [20]. The voltage source connected at the DG unit bus−bar emulates a voltage against time profile as illustrated in Figure 3.1. The grid code requires that for voltages above the curve the DG must not be disconnected, [20].

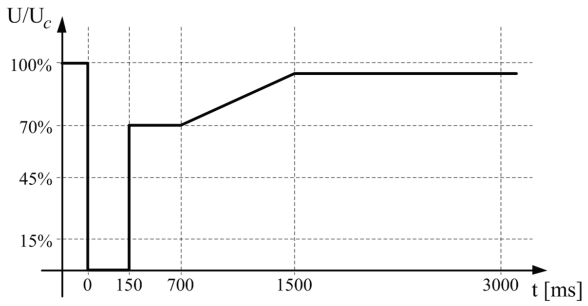

Figure 3.1. Voltage magnitude against time profile for assessing LV−FRT_capability, [20]

3.2.2. Modelling of External Power System

In this Sub−Section, four modeling approaches of the external grid, proposed by [28], are described and applied for investigating the impact on LV−FRT capabilities of a small scale hydro unit. The results are shown in Sub−Section 3.2.3. These modeling approaches are:

1.Thévenin equivalent

2.Multi-machine power system

3.Dynamic equivalents based on **Ward** reduction technique
4. Dynamic equivalents based on **Extended Ward** power system reduction techniques

A common approach for representing the external grid in LV−FRT studies is by using a *Thévenin* equivalent [29] [30], for which a short−circuit power and an equivalent impedance are specified. This modeling approach is used when the DG dynamic behavior is achieved locally (around the PCC) with a simplified external grid representation [31]. However, in order to reproduce the transient behavior associated with all generation units (including DG) from the external grid and to obtain realistic information about stability margins, the infinite bus−bar or single machine representation can be inappropriate [28] [31] [32]. Under these conditions, a multi-machine power system and dynamic models for external grid (based on *Ward* and *Extended Ward* power system reduction techniques) are considered, in other studies [28] − [33]. The methods for obtaining these equivalents for steady state and dynamic studies are investigated and described in detail in [28], [33] − [34], and are applied for a benchmark power system, as detailed in Sub−Section 3.2.2 B.1).

3.2.2. A) Thévenin equivalent

According to the grid codes presented in [29] and [30] the external grid can be modeled as a *Thévenin* equivalent consisting of a voltage source behind grid impedance. According to [29] the voltage source shall emulate the LV−FRT profile as a certain voltage against time curve, specified by the DSO or TSO. Moreover, the voltage source needs to provide at the initial time of simulation a voltage equal to 1 p.u. in the PCC. The same reference states that the grid impedance ratio R_{grid}/X_{grid} should be 0.1 corresponding to a grid voltage angle of 84.3 degrees. Regarding the short circuit power, S_k, defined for the grid impedance, reference [29] states that it should be ten times larger compared to the rated apparent power P_n of the DG unit, but according to the reference [30] this ratio should span between 20 and 50. A model for the *Thévenin* equivalent used as representation of the external grid can be depicted as in Figure 3.2 [29]:

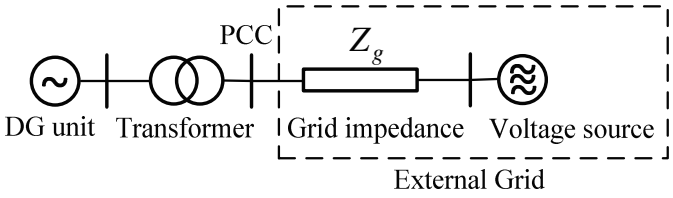

Figure 3.2. Thévenin equivalent for the representation of external grid in LV−FRT studies. [29]

The dynamic analysis of the DG unit connected at bus 7100 in the benchmark power system (shown in Figure 3.3) was first investigated when the external grid was modeled using a *Thévenin* equivalent represented according to [30] (R_{grid}/X_{grid}=0.1, S_k/S_n=20). The results from this model is shown in Section 3.2.4.

3.2.2. B) Multi-machine power system

According to [28] and [31] the representation of the external grid as a multi-machine power system can offer a better representation of the dynamics associated with the external grid, and also between the generation unit or FACTS [31] and the rest of the power system under both steady state and dynamic conditions. Reference [28] presents a variation of the test power system for integration of wind power into TPSs, proposed by [28] for integration of FACTS devices in TPSs. In this Sub−Section the LV−FRT capability of a small scale hydro unit will be assessed by connecting the DG unit into a benchmark power system (consisting of both distribution and transmission) with mixed generation: wind and hydro power. This is representing the full power system model.

However, in systems with a large number of buses and large amount of generation units (including DG), the modeling complexity can be a drawback, [34] [35]. Therefore, dynamic equivalents can be a better approach, [2] [36] [32] as will be discussed in Sub−Section 3.2.2. B.2).The topology of this benchmark grid is presented in Sub−Section 3.2.2. B.1).

- **Benchmark multi-machine power system for representation of the external grid**

The topology of the benchmark power system is depicted in Figure 3.3 and is based on a research model developed in [37]. The generation units consists of four hydro units with high installed capacity connected at 300 kV voltage level (buses 7114-300 kV, 7124-300 kV and 7130-300 kV), and two fixed speed based wind farms with medium installed capacities (WG1–66 kV and WG2–66 kV).

In addition, two small scale hydro units are connected at 22 kV (buses 7110–22 kV and 7120–22 kV). The distribution power system is represented by the 22 and 66 kV voltage levels, as the transmission power system is represented by the 300 kV voltage level. The line data is given in Table A1.1 in Appendix A. All the hydro units are synchronous generators based and their data is given in Tables A1.2 and A1.3.

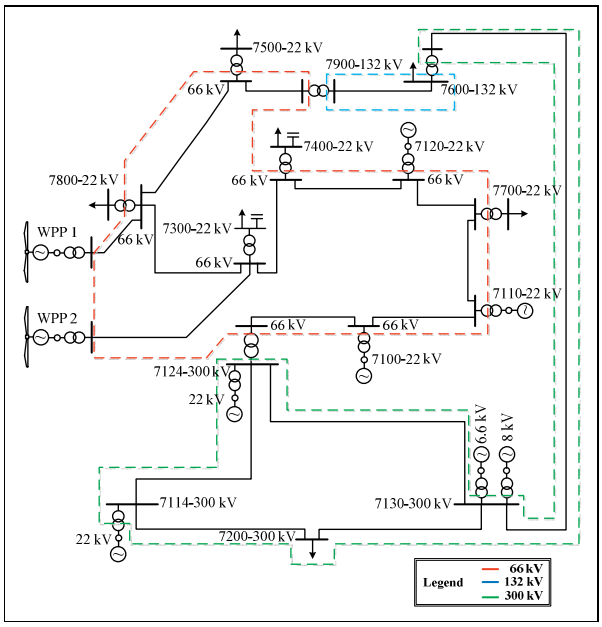

Figure 3.3. Benchmark power system for multi-machine representation of external grid [37].

Fixed−speed based wind farms were implemented from the template examples of DIgSILENT Power Factory© and modeled according to [38].

According to [39], the fixed−speed based wind turbines are modeled using a squirrel cage induction generator, for which the active power production is controlled by using a pitch−angle controller. According to the same source, capacitors banks are installed to compensate for the reactive power consumption of the induction generator. The data for the wind power plant is presented in Table A1.4.

The distribution power system (at 66 kV) is connected with the bulk transmission system via a transformer between buses 7124−66 kV and 7124−300 kV. The data for the transformers is presented in the Appendix A1.5. The benchmark power system was simulated using DIgSILENT Power Factory 14.0© platform. In the distribution power system two capacitors banks are connected at the nodes 7300−22 kV and 7400−22 kV. This is done in order to improve the voltage levels in these two load areas. The data of the two compensating systems is provided in Table A1.6.

All synchronous generators units are modelled using the standard model of the synchronous generator available in DIgSILENT Power Factory 14.0© platform. The hydro units are equipped with automatic voltage regulators modeled as an AVR−EXNEBB and hydro turbines and governors−based on HYGOV model, which are basic models implemented from DIgSILENT Power Factory© *Standard Models* library [38]. The macro−blocks and data

for the HYGOV is presented in Table A1.8. As for the EXNEBB and EXNI AVRs system is given in Table A1.9 and A1.10.

The loads are modelled as constant power loads. Their corresponding data is given in Table A1.6. In the next paragraph an introduction is provided regarding load modelling in power systems modeling and analysis.

- **Load characteristics and modelling**

In general, modeling of load areas in power systems is a complex problem as their representation as aggregate models must be done and updated correctly. The dependencies of load's active and reactive power with the voltage and frequency of connection bus, add complexity to the problem.

As presented in [40] and [41] the static approaches are the most used techniques to model the loads in power systems studies. In the static models, the load P and Q are depended of bus–bar voltage and scales factors K_P and K_Q, and can expressed as:

$$P = P\left(K_P, U\right) \tag{3.1}$$

$$Q = Q\left(K_Q, U\right) \tag{3.2}$$

Generally, in the power systems literature two classical static approaches are used to model the loads [40].

a) Exponential model

defined by the next expressions:

$$P = K_P P_0 \left(\frac{U}{U_0}\right)^{\alpha_P} \tag{3.3}$$

$$Q = K_Q Q_0 \left(\frac{U}{U_0}\right)^{\alpha_Q} \tag{3.4}$$

Where: – K_P and K_Q are scaling coefficients (equal with 1 in the base case)

– P_0, Q_0 and U_0 are the reference active and reactive power, respectively the reference voltage

– α_P and α_Q are coefficients which describe the type of load and determine the sensitivity of active and reactive power with the voltage

Depending of the values these coefficients, three types of load models can results (the *ZIP* model), presented in Table 3.1.

Table 3.1. Exponential load model.

Load Model	α_P	α_Q
Constant Impedance (**Z**)	2	2
Constant Current (**I**)	1	1
Constant Power (**P**)	0	2

b) Polynomial model

In practice, the representation of complex loads is done by summating the aforementioned characteristics with the same α_P and α_Q coefficients. In this case, the expressions of P and Q become:

$$P = K_P P_0 \left[a_P \left(\frac{U}{U_0} \right)^2 + b_P \left(\frac{U}{U_0} \right) + c_P \right] \tag{3.5}$$

$$Q = K_Q Q_0 \left[a_Q \left(\frac{U}{U_0} \right)^2 + b_Q \left(\frac{U}{U_0} \right) + c_Q \right] \tag{3.6}$$

$a_P, b_P, c_P, a_Q, b_Q, c_Q$ – represents the weights of each of the component from the **ZIP** model and satisfies the next conditions:

$$a_P + b_P + c_P = 1 \tag{3.7}$$

$$a_Q + b_Q + c_Q = 1 \tag{3.8}$$

3.2.2. C) Dynamic Equivalents for Power Systems

Due to the high number of bus–bars and generation units, the complete representation of the power systems is sometimes difficult to model [1] [2] [33]. So, different studies propose or investigate steady state or dynamic reduced equivalents of wide area power systems. According to [1], [33] [36], [42] and [43] these power system equivalents will consist of three main areas: an area representing the power system under study (internal power system), an external power system and a remote power system, as illustrated Figure 3.4. In Figure 3.4, the set DG unit–transformer and correspondent PCC (7100-66 kV), represent the internal power system. The remote power system represented by the bus 7200–300 kV is modeled as TPS.

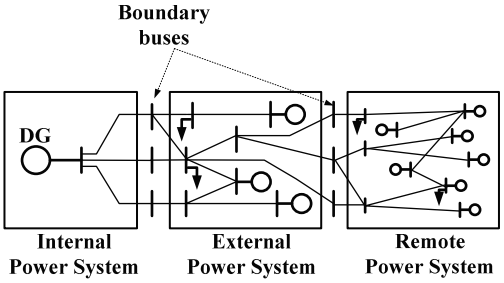

Figure 3.4. Differentiation of a power system
in areas of interest, [44]

The boundary buses are defined according to the objectives of the power system analysis. For dynamic equivalency of the external grid (considered outside of the boundary bus 7100), the steps proposed in [43] and [45] are used. This method mainly consists in three steps [45]:

a) Identification of the coherent generators from external power system
b) Reduction of the topology of the external power system
c) Dynamic aggregation of the coherent generators

In the next paragraphs some generalities regarding methods of coherency identification, network reduction and synchronous generators aggregation are presented.

As presented above a wide area power system can be split in three zones (as presented in Figure 3.4) and retaken in Figure 3.5:

1. Internal power system (area under study)
2. External power system
3. Remote power system

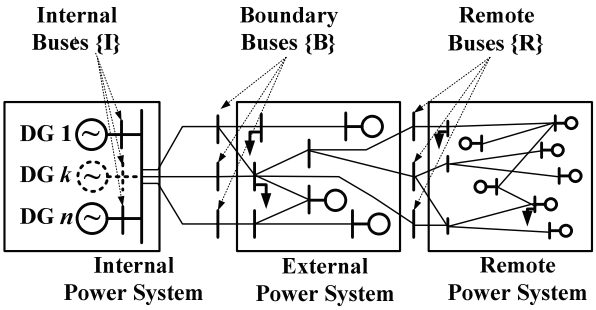

Figure 3.5. Power systems decomposition
in areas of interest.

Where: {I} –internal buses, {B} – the boundary buses and {R} –remote buses

– Coherency Identification

As presented in the power systems literature, two generators are considered coherent if their rotor angle difference is constant and small enough after a disturbance or multiple disturbances emerged in the internal area, [40]. According to [40]: ″an equivalent network obtained for an initial state (pre–fault) is only valid for other states (transient or steady state) if the transformation ratio (defined by (3.9)) can be assumed to remain constant for all nodes in a given group″. Considering two nodes i and $j \in \{A\}$, as presented in [40]:

$$\frac{\underline{U}_i(t)}{\underline{U}_j(t)} = \frac{\hat{U}_i}{\hat{U}_j} = \underline{\alpha}_V \tag{3.9}$$

With $\hat{}$ denoting the initial state.
(3.9) can rewritten in a phasor manner as:

$$\frac{\underline{U}_i(t)}{\underline{U}_j(t)} = \frac{U_i(t)}{U_j(t)} e^{j[\delta_i(t)-\delta_j(t)]} = \alpha_V \tag{3.10}$$

If the voltage magnitude is assumed to be constant (PV buses) [40], then (3.10) translates to:

$$\delta_i(t) - \delta_j(t) = \varepsilon_\delta \tag{3.11}$$

For the generators represented using the classical model $\underline{E}_i'$, $\delta_i(t)$ and $\delta_j(t)$ represents the rotor angles in the transient state.

But as the concept of coherency was revised by the author in **Publication D** the following practices to address this concept mainly were found, [16]:

Considering two general recorded signals from the i^{th} and j^{th} generators for which the coherency needs to be investigated these signals, can be represented in polar coordinates as in (3.12) and (3.13):

$$x_i(t) = \boldsymbol{X}_i(t) e^{\phi_{i,x}(t)} \tag{3.12}$$

$$y_j(t) = \boldsymbol{Y}_j(t) e^{\phi_{i,y}(t)} \tag{3.13}$$

where:

– $\boldsymbol{X}_i(t)$ and $\boldsymbol{Y}_j(t)$ are the instantaneous magnitudes of the rotor angle signals $x_i(t)$ and $y_j(t)$

– $\phi_{i,x}(t)$ and $\phi_{i,y}(t)$ are the instantaneous phases of the rotor angle signals $x_i(t)$ and $y_j(t)$

Generally, the coherency concept is tackled in literature ((3.12) and (3.13)) by three main groups of methods:

- **Coherency of magnitude** [40]

$$\left|\boldsymbol{X}_i(t)-\boldsymbol{Y}_j(t)\right|<\varepsilon_m \quad t=[t_0,t_n] \tag{3.14}$$

As presented above, two generators can be recognized as electromechanically coherent if the spatial positions of their rotors remain in synchronism over a time interval. This can be mathematically expressed for the rotor angles as:

$$\left|\delta_i(t)-\delta_j(t)\right|=\delta_{ij,0} \tag{3.15}$$

or in the ideal case

$$\left|\delta_i(t)-\delta_j(t)\right|=0 \tag{3.16}$$

The electromechanical coherency is presented in Figure 3.6 for three generators: *i*, *j* and *k*, where generator *i* is coherent with *j*, as the rotor angle difference is small and constant. Generator *k* is not coherent with the group of the other two. [40]

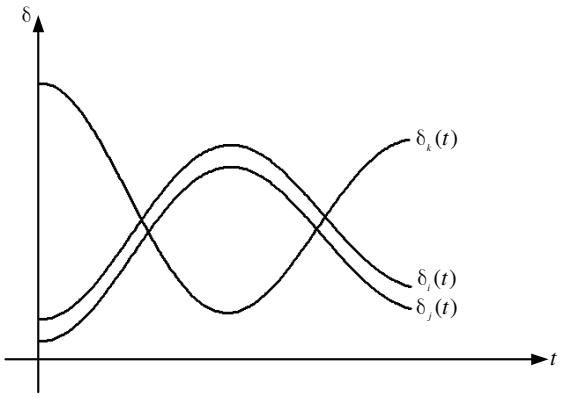

Figure 3.6. Rotor angle variations in time of three generators
(generators *i* coherent wiht *j* and generator *k* in phase opposition) [40]

This approach is mainly used to identify the electromechanical coherency together with the computation of the metric Euclidean Distance between the i^{th} and j^{th} units, over a time interval, as proposed in [46], by (3.17):

$$d_{i,j}=\sqrt{\sum_{t=t_1}^{T}\left(\delta_i(t)-\delta_j(t)\right)^2} \tag{3.17}$$

- **Coherency of phase**

References [33] and [47] are proposing that two generators can be considered coherent if the difference of their phases given in (3.12) and (3.13) must respect the condition:

$$\left|\phi_{x,i}(t)-\phi_{y,i}(t)\right|<\varepsilon_{\phi}\ t=[t_0,t_n] \tag{3.18}$$

- **Coherency of magnitude and phase**

For which both (3.14) and (3.18) need to be validated over a time interval $t=[t_0,t_n]$, were t_0 and t_n represents the starting and ending time of the signal recording [47] [48].

Then, the definition of each of electromechanical coherency concept can be summarized as shown in Figure 3.7.

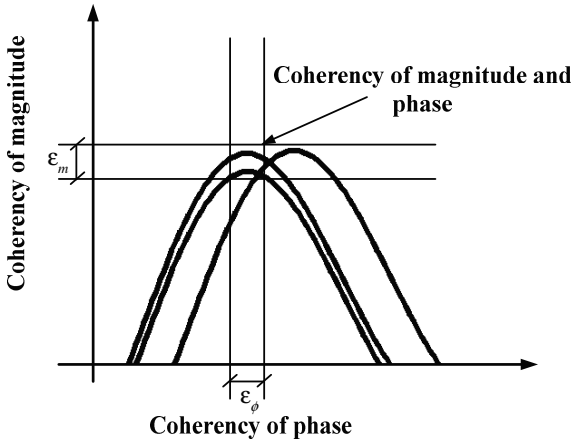

Figure 3.7. Coherency concept: 1−of magnitude, 2−of phase and 3−of magnitude and phase

– Network Reduction

Two methods are investigated in Section 3.2.3 for reducing the distribution network, specifically a Ward equivalent with current injections and an Extended Ward or Ward−PV as known in the common literature. An extended comparison of the two methods was produced in **publication B** for interconnected power systems. [14]

- **Ward Equivalent with current injections**

For a given separation of a power system (as presented in Figure 3.8) the Ward equivalent with current injections can be computed as follows and as presented in [49] With the general separation of the buses of a wide area power system into Figure 3.5: internal buses {I}, boundary buses {B} and remote buses {R} the admittance matrix can be written [49]:

$$\begin{bmatrix} \underline{Y}_{RR} & \underline{Y}_{RB} & 0 \\ \underline{Y}_{BR} & \underline{Y}_{BB} & \underline{Y}_{BI} \\ 0 & \underline{Y}_{IB} & \underline{Y}_{II} \end{bmatrix} \begin{bmatrix} \underline{U}_R \\ \underline{U}_B \\ \underline{U}_I \end{bmatrix} = \begin{bmatrix} \underline{I}_R \\ \underline{I}_B \\ \underline{I}_I \end{bmatrix} \tag{3.19}$$

Considering just the boundary and remote buses, (3.19) becomes:

$$\begin{bmatrix} \underline{Y}_{RR} & \underline{Y}_{RB} \\ \underline{Y}_{BR} & \underline{Y}_{BB} \end{bmatrix} \begin{bmatrix} \underline{U}_R \\ \underline{U}_B \end{bmatrix} = \begin{bmatrix} \underline{I}_R \\ \underline{I}_B \end{bmatrix} \tag{3.20}$$

With a Gauss mathematical manipulation on $[\underline{Y}_{BB}]$ and $[\underline{I}_B]$ matrices an equivalent admittance matrix can be obtained:

$$[\underline{Y}'_{BB}] = [\underline{Y}_{BB}] - [\underline{Y}_{BR}][\underline{Y}_{RR}]^{-1}[\underline{Y}_{RB}] \tag{3.21}$$

With an equivalent injection of currents in the boundary buses:

$$[\underline{I}'_B] = [\underline{I}_B] - [\underline{Y}_{BR}][\underline{Y}_{RR}]^{-1}[\underline{I}_R] \tag{3.22}$$

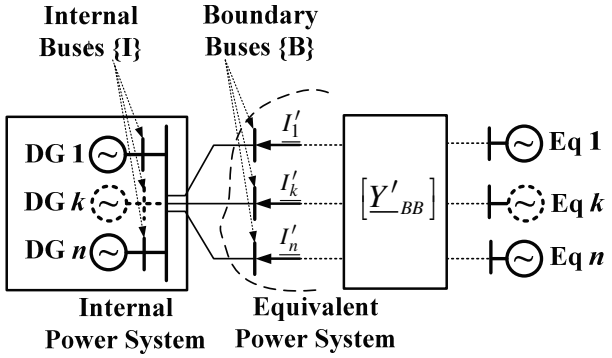

Figure 3.8. Ward Equivalent representation with current injections [49].

- **Extended Ward Equivalent (Ward PV Equivalent)**

As presented in [49] a Ward equivalent do not preserve the PV buses, therefore errors in the reactive power control and voltage magnitude can show up. Therefore, the classical Ward equivalent is extended in order to improve the reactive power flow. This is done, as explained in [44], by attaching to each *i* boundary bus defined as PQ bus (load bus), a fictitious admittance branch [$\underline{y}_i$] (which is the short-circuit admittance between the i^{th} boundary bus and each generator from external grid) and voltage controlled bus (PV) (as presented in Figure 3.9). Initially, $P=0$ and $U=U_{i,0}$, so the fictitious generator bus does not contribute with any

active and reactive power. When the operating conditions of the study power system changes then these buses will contribute with an absorption or generation of reactive power [33] [44].

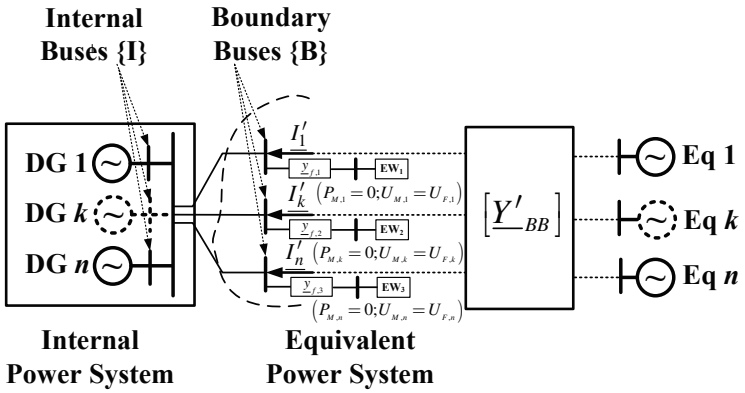

Figure 3.9. Extended Ward Equivalent representation [49].

The *Network Reduction* tool provided by DIgSILENT Power Factory© produces a power system equivalent of the external area, which contains only the boundary buses. After the power system reduction process is finished the equivalent of the external grid will be represented by using equivalent transfer impedances between all buses and voltage sources connected at all boundary buses (voltage sources specified in the dynamic equivalents diagrams as EW (Extended Ward equivalent)) [38].

– Aggregation of DG Synchronous Generator Units and Controllers

For reducing the order of the distribution grid model the aggregation of the DG units and their correspondent controllers represent an important step. This is due to the high number of differential equations which must be represented in the original model. The technique used to reduce the generators from one coherent area is developed in [50] and is presented in the following.

- **Synchronous generator modelling and aggregation**

Using a sixth−order representation of the synchronous generator, the differential equations describing the operation of the i^{th} generator, are (3.23−3.24) [40]:

The differential equations which describes the mechanical operation:

$$\begin{cases} M_i \dot{\omega}_i = P_{m,i} - P_{e,i} \\ \dot{\delta}_i = \omega_0 \omega_i \end{cases} \tag{3.23}$$

The differential equations which describes the electrical operation are:

$$\begin{cases} T'_{d0,i}\dot{E}'_{q,i} = E_{f,i} - E'_{q0,i} - I_{d,i}\left(X_{d,i} - X'_{d,i}\right) \\ T'_{q0,i}\dot{E}'_{d,i} = -E'_{d0,i} + I_{q,i}\left(X_{q,i} - X'_{q,i}\right) \\ T''_{d0,i}\dot{E}''_{q,i} = E'_{q0,i} - E''_{q0,i} - I_{d,i}\left(X'_{d,i} - X''_{d,i}\right) \\ T''_{q0,i}\dot{E}''_{d,i} = E'_{d0,i} - E''_{d0,i} + I_{q,i}\left(X'_{q,i} - X''_{q,i}\right) \end{cases} \tag{3.24}$$

Assuming that R_a=0, the algebraic equations are:

$$\begin{cases} U_{d,i} = E'_{d,i} + X'_{q,i}I_{q,i} \\ U_{q,i} = E'_{q,i} - X'_{d,i}I_{d,i} \end{cases} \tag{3.25}$$

a.1) Equivalent parameters of the mechanical differential equations

Considering that a coherent area is formed by a number of m of coherent generators, as presented in [50] the aggregated inertia parameter is given by following equation:

$$M^{eq} = \sum_{i=1}^{m} \frac{M_i}{m} \tag{3.26}$$

$$P_m^{eq} = \sum_{i=1}^{m} \frac{P_{m,i}}{m} \tag{3.27}$$

a.2.) Equivalent parameters of the electrical differential equations. Synchronous (d,q) reactances

In order to determine the equivalent parameters of the differential equations which describe the electrical operation of generators, (3.25) is written in terms of d–q currents in [50] as:

$$\begin{bmatrix} I_{d,i} \\ I_{q,i} \end{bmatrix} = \begin{bmatrix} 0 & -\frac{1}{X_{d,i}} \\ \frac{1}{X_{q,i}} & 0 \end{bmatrix} \begin{bmatrix} U_{d,i} \\ U_{q,i} \end{bmatrix} - \begin{bmatrix} 0 & -\frac{1}{X_{d,i}} \\ \frac{1}{X_{q,i}} & 0 \end{bmatrix} \begin{bmatrix} E_{d,i} \\ E_{q,i} \end{bmatrix} \tag{3.28}$$

Or rewritten in a compact form:

$$I_i = A_i U_i - A_k U_k \tag{3.29}$$

The equivalent current model as presented in [50]is:

$$I^* = \left(\sum_{i=1}^{m} T_i A_i T_i^{-1}\right) U - \left[T_1 A_1 \cdots T_m A_m\right]\left[E_1 \cdots E_m\right] \tag{3.30}$$

With:

$$I^* = \begin{bmatrix} I_D^* \\ I_Q^* \end{bmatrix} \tag{3.31}$$

$$T_i = \begin{bmatrix} \cos\phi_i & -\sin\phi_i \\ \sin\phi_i & \cos\phi_i \end{bmatrix} \tag{3.32}$$

$$\phi_i = \delta_i - \theta_i \tag{3.33}$$

Where θ_i the rotor angle of the equivalent machine is defined as [50]:

$$\tan(2\theta_i) = \frac{\sum_{i=1}^{m}\left(\frac{1}{X_{q,i}} - \frac{1}{X_{d,i}}\right)\sin(2\delta_i)}{\sum_{i=1}^{m}\left(\frac{1}{X_{q,i}} - \frac{1}{X_{d,i}}\right)\cos(2\delta_i)} \tag{3.34}$$

The A^* coefficient matrices are defined in [50] as:

$$A^* = \begin{bmatrix} A_{11}^* & A_{12}^* \\ A_{21}^* & A_{22}^* \end{bmatrix} = \sum_{i=1}^{m} T_i A_i T_i^{-1} \tag{3.35}$$

$$A_{11}^* = -A_{22}^* = -\frac{1}{2}\sum_{i=1}^{m}\left(\frac{1}{X_{q,i}} - \frac{1}{X_{d,i}}\right)\sin(2\phi_i) \tag{3.36}$$

$$A_{12}^* = -\sum_{i=1}^{m}\left(\frac{1}{X_{q,i}}\sin^2(\phi_i) + \frac{1}{X_{d,i}}\cos^2(\phi_i)\right) \tag{3.37}$$

$$A_{21}^* = \sum_{i=1}^{m}\left(\frac{1}{X_{q,i}}\cos^2(\phi_i) + \frac{1}{X_{d,i}}\sin^2(\phi_i)\right) \tag{3.38}$$

With these A^* coefficient matrices the equivalent synchronous reactances are computed in [50]as:

$$X_D^* = -\frac{1}{A_{12}^*} \tag{3.39}$$

$$X_Q^* = -\frac{1}{A_{21}^*} \tag{3.40}$$

The transient and subtransient reactances are computed in the same manner using the X_d', X_q', X_d'' and X_q''.

- **Excitation system aggregation**

In this part a simplified the excitation system was used. This excitation system consists just of one block which describes the transfer function of the voltage controller with the input the error of the voltage (ΔU) and output the field excitation voltage (E_{fd}).Figure 3.10 presents the simplified control scheme [49].

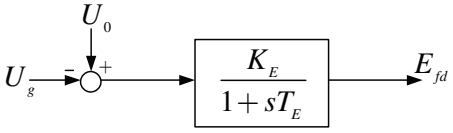

Figure 3.10. A simplified excitation system model.

The differential equation describing the operation of the excitation system is [49]:

$$\frac{dE_{fd}}{dt} = \frac{1}{T_e}\left[K_e\left(U_0 - U_g\right) - E_{fd}\right] \tag{3.41}$$

With d_k coefficient defined in [50]:

$$d_i = T_{d0}'^* X_d'^* \frac{\cos\phi_i}{X_{d,i}' T_{d0,i}'} \tag{3.42}$$

$$K_E^* = \sum_{i=1}^{m} \frac{K_{E,i}}{m} \tag{3.43}$$

$$T_E^* = \frac{1}{\sum_{i=1}^{m} \frac{d_i}{T_{E,i}}} \tag{3.44}$$

The governor and turbine model were not considered in this case as it was assumed that their dynamics are much slower comparing with the electromagnetic ones. These steps are applied for the benchmark power system illustrated in Figure 3.3 as described in the following:

3.2.3. Study Case

3.2.3. A) Identification and dynamic aggregation of the coherent generators from external power system

According to [35] and [46] this method consists of building coherent groups in which generators swing together after a fault occurred in the area of study. In this study case a bolted three phase symmetrical short-circuit cleared after 150 ms, as presented in [20] was considered. This fault was applied at the boundary bus of internal power system (PCC of DG unit). The identification of coherent generators and their corresponding areas was conducted by using the concept of Euclidean distances, as described in [46]. According to [46], the identification of the coherent generators from the external power system was based on comparing the rotor angle signals between each two generators, except for the DG unit for which the LV–FRT capabilities are investigated. The generators' rotor angles were registered as time series: $\delta_i(t)$ for the i^{th} generator and $\delta_j(t)$ for the j^{th} generator. The time series were used to compute the Euclidean distance (ED in radians) between the i^{th} and j^{th} generators as given in (3.45) [46]:

$$d_{i,j} = \sqrt{\sum_{t=t_1}^{T} \left(\delta_i(t) - \delta_j(t)\right)} \tag{3.45}$$

Where:

$\delta_i(t)$ – represents the rotor variation of the i^{th} generator registered for each time instant t

$\delta_j(t)$ – represents the rotor variation of the j^{th} generator registered for each time instant t.

A time step of 10 ms was used for the simulation. To obtain the Euclidean distances between generator units a Dynamic Programming Language (DPL) [38] script was developed in DIgSILENT Power Factory 14.0©. This script is an iterative process which identifies the minimum Euclidean distances between generators. The different steps of the *DPL* identification and aggregation of the coherent groups of generators are depicted in the flow chart in Figure 3.1.

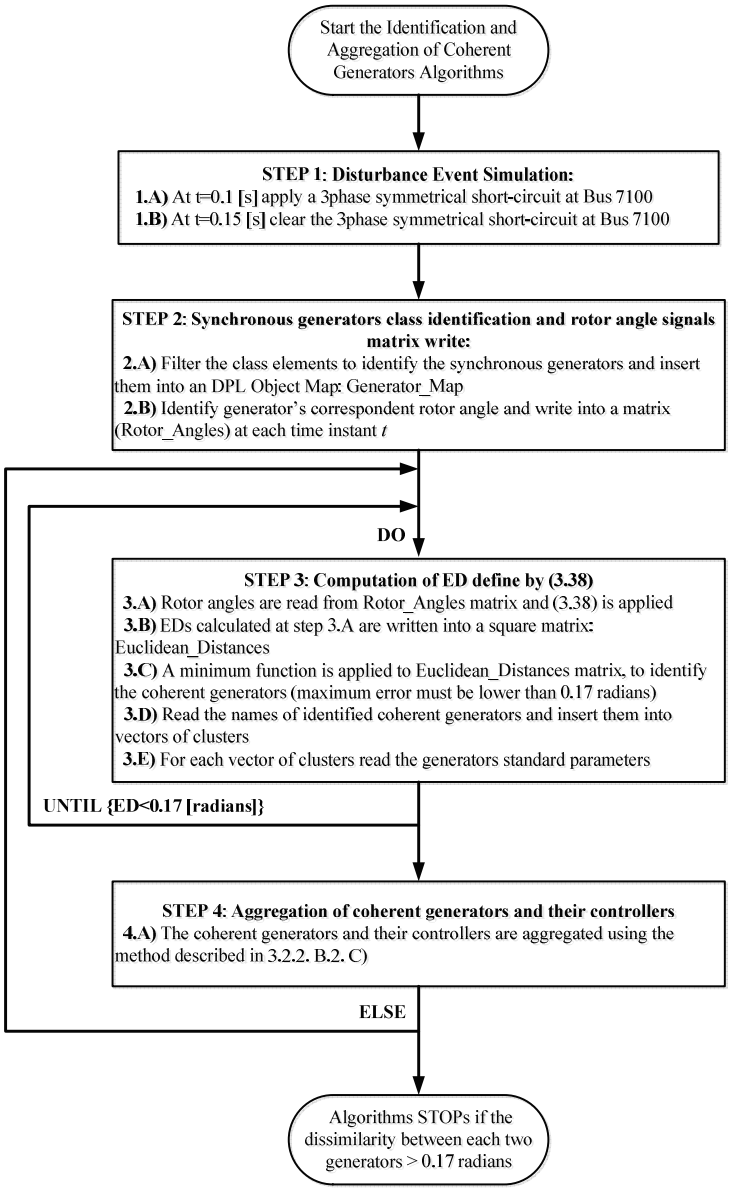

Figure 3.11. Flow chart depicting the steps of identification and aggregation of coherent generators.

In Figure 3.12 the rotor angles signals of both units from ADG and from TPS side are plotted after the fault occurred at bus 7100-66 kV. The plots illustrate that generators 7114 and 7124 from ADG are coherent, resulting in the first coherent group of generators. The second coherent group is represented by generators 7130-8 kV and 6.6 kV. For generators 7110 and 7120 the Euclidean distance in all three iterations was computed as 0.279 radians which is larger than 0.17 radians, and indicate that the two generators are not coherent. The coherent groups of generators in the areas of the benchmark power system are represented in Figure 3.13.

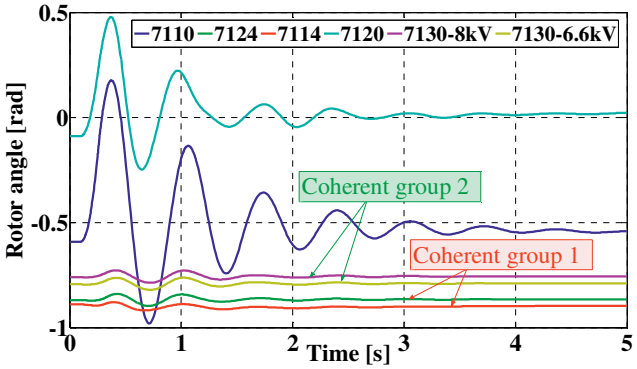

Figure 3.12. Rotor angles of generators from 1st iteration of *DPL* script.

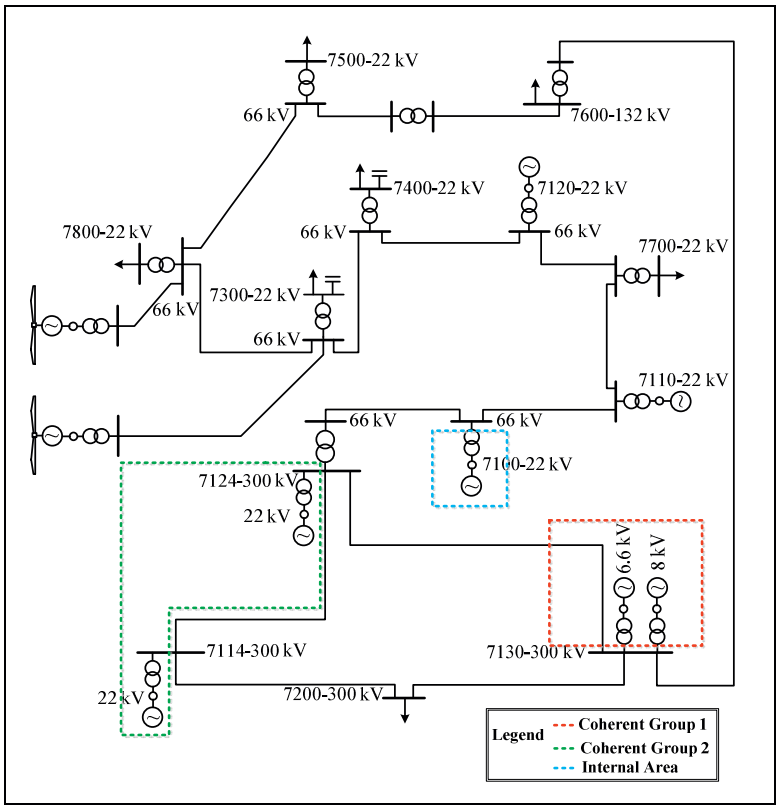

Figure 3.13. Coherent groups of generators in the benchmark power system after 1st iteration.

These coherent groups are validated by the first iteration of *DPL* script. By running the second iteration with the same location of the fault, the script identifies that the new generators corresponding to the aggregation of coherent groups 1 and 2 (AG1 and AG2) are coherent. This is validated by plotting the rotor angles corresponding to the new aggregated generators, as depicted in Figure 3.14. After computing the new aggregated generator corresponding to coherent groups 1 and 2 (AG3), in the third iteration the script stops meaning that no coherency is identified any longer in the external grid. This can be observed by analyzing the rotor angles plots of the aggregated generator AG3, units 7110 and 7120, as depicted in Figure 3.15.

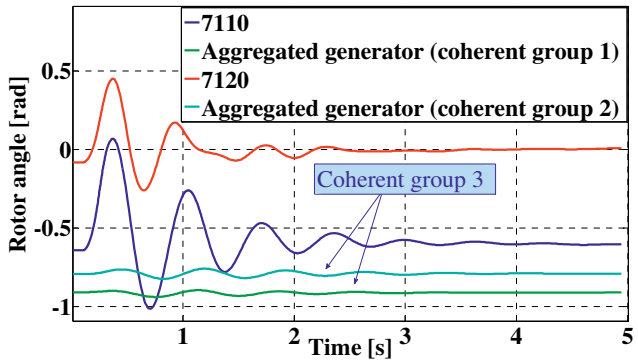

Figure 3.14. Rotor angles of generators from 2nd iteration of *DPL* script.

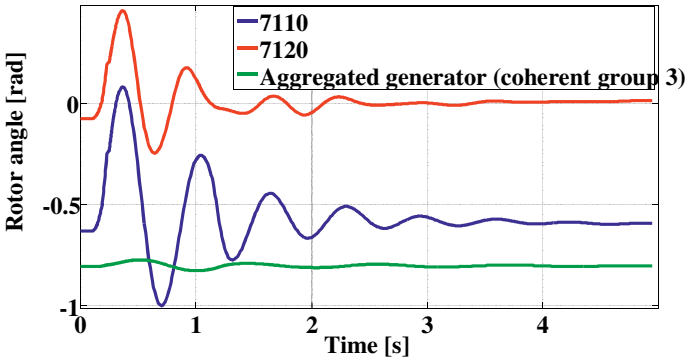

Figure 3.15. Rotor angles of generators from 3rd iteration of *DPL* script.

The coherency clustering process of the generating units in the benchmark power system (other than the DG unit under study) is schematically represented in Figure 3.16.

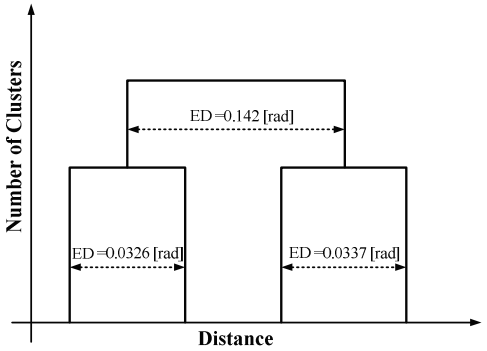

Figure 3.16. Coherency clustering of generation units from benchmark power system.

The two wind farms were modeled as fixed speed wind turbine generators equipped with squirrel cage induction generators. For dynamic aggregation of wind farms the concept of single equivalent machine was used as described in [51], for which the equivalent apparent power rating represents the sum of individual wind farms ratings. Likewise, the equivalent compensating capacitor banks size will represent the sum of the individual wind farm capacitor banks [51]. For the sake of simplicity, the controllers related to the operation of synchronous units were selected identical, so no dynamic aggregation was needed. As for wind farms the same models were used for aero-dynamic and mechanical turbine representation, so also in this case no aggregation was needed. It is obvious that in distribution grids where different types of generation and their corresponding controllers will be added, the issue of dynamical aggregation of controllers must be rigorously considered.

3.2.3. B) Reduction of the topology of the external power system

In this part, *Ward* and *Extended Ward* methods for power system reduction equivalents were investigated.

A complete presentation related to network reduction was introduced in Sub–Chapter 3.2.2. Some of the methods to reduce the grid model for Load Flow studies it will be summarized again. This is done in order to make the literature of this work more approachable to the readers with no experience in power systems model reduction.

According to [33] and [44], these methods of power systems equivalence are based on reduction techniques of the nodal admittance matrix of the external power system and the boundary buses. Also the same references states that the equivalent of the external power system will be represented by a fixed admittance equivalent network and equivalent current injections with respect to the original one at the boundary buses [44] [33]. The power system reduction results from a Gauss elimination technique of the admittance matrix of the power system to be reduced between the boundaries buses, by considering the representation of loads as constant impedances, [46]. According to [44] and extensively detailed further, the difference between these two methods is that an Extended Ward equivalent model takes into consideration a more accurate reactive power control in the external power system, while a

Ward equivalent does not. This is realized, as explain in [44] by attaching to each *i* boundary bus defined as load bus, a fictitious admittance branch (which is the short-circuit admittance between the i^{th} boundary bus and each generator from external grid) and voltage controlled bus (PV). Initially, $P=0$ and $V=V_{i,0}$, so the fictitious PV bus do not contribute with any active and reactive power. When the operating conditions of the study power system changes then these buses will contribute with an absorption or generation of reactive power. [44] [51]

In this study case, these equivalence approaches were applied for the benchmark power system presented in Sub–Chapter 3.2.2. B.1). Figure 3.17 presents the resulting wide area dynamic equivalent based on a Ward network reduction of the original benchmark power system. In this case for the boundary buses were selected next buses: the PCC of the DG unit, the equivalent buses where the resulted aggregated synchronous and wind generators (AG3 and WAG-22 kV) were connected and the connection buses of the synchronous generators 7110-66 kV and 7120-66 kV. The equivalent buses correspond to the connection buses of the largest generators to be aggregated. This equivalent was obtained by using the *Network reduction* function of DIgSILENT Power Factory 14.0© platform [38]. According to [38], this power system reduction tool is based on a method which ensures that all the sensitivities (first order derivative of voltage magnitude and angle with respect to active and reactive power) of the equivalent grid measured in each boundary bus will be equal with the sensitivities of the original external area to be reduced. The *Network Reduction* tool provided by DIgSILENT Power Factory© produces a power system equivalent of the external area, which contains only the boundary buses. After the power system reduction process is finished the equivalent of the external grid will be represented by using equivalent transfer impedances between all buses and voltage sources connected at all boundary buses [38]. Moreover, a validation of the benchmark power system equivalents is needed to be studied after the process of power system reduction is complete. [32] The validation of benchmark power system equivalents with respect to the original one was investigated by taking in consideration the following two constraints:

1. *The rotor angle of the DG unit under investigation must have the same swinging pattern, under both original and reduced model (with rotor angle errors smaller than 10 degrees or 0.17 rad)* [34]
2. *Equivalent load flow calculations must provide errors smaller than 0.1% (user-defined)* [38]

To validate the first constraint, the considered short circuit at DG interconnection bus 7100-66 kV was applied for the detailed four cases of external grid representation: *Thévenin* equivalent, benchmark power system, wide area dynamic equivalents based on *Ward* and *Extended Wa*rd power system reduction techniques. In all four cases the rotor angle of DG unit connected at bus 7100 was registered and plotted as shown in Figure 3.18. It can be observed that the rotor angle curves in the cases when power system equivalents were used overlap the case when the complete power system is modeled. The maximum error is of 0.0041 rad.

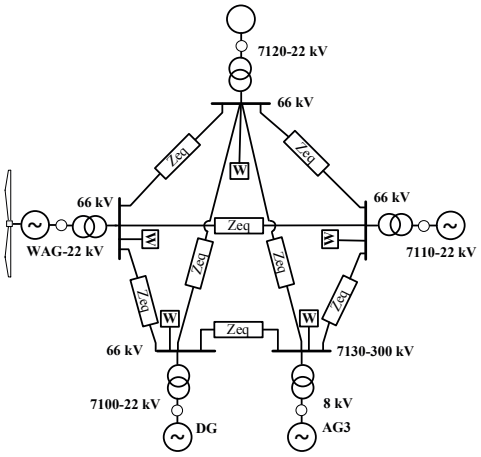

Figure 3.17. Ward equivalent of original benchmark power system for DG unit LV−FRT capabilities assessment.

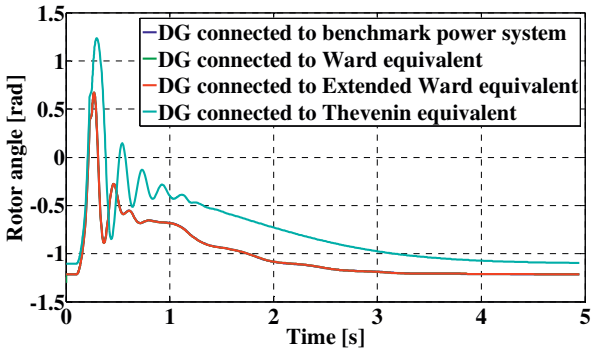

Figure 3.18. Rotor angles of DG connected to different external grid representations.

For rotor angle variation response in the case when external grid is modeled using a *Thévenin* equivalent, it can be observed that even the curve variation has a pattern close to the curves obtained for detailed models of external grid, the initial value and then the entire range of variation values for this parameter are erroneous. The maximum error with respect to the original case is of 0.52 rad.

This can validate the assumption that the connection of a small scale generator unit to a relatively strong power system equivalent cannot model properly the real dynamics, especially the ones associated with the rotor angle swings of other generation units when LV−FRT is investigated. The second constraint was also validated, as no error stating that the

violation of constraint was produced after running the function for power system reduction in the simulation platform.

3.2.4. Discussions

In this part the LV–FRT capabilities of DG unit will be discussed, considering all four aforementioned approaches for modeling of the external grid are considered.

In this case the considered DG is a synchronous generator small scale hydro unit with an installed capacity of 1.6 MVA, equipped with the same automatic voltage regulator and hydro governor models as presented in Sub–Chapter 3.2.2. B.1). In terms of LV–FRT capabilities, Figure 3.19 presents the voltage variation profiles at PCC when the same short circuit event used in previous sections, emerged at bus 7100-66 kV (DG connection bus). The LV–FRT capabilities are investigated when all four cases of external grid representation were considered (*Thévenin* equivalent, benchmark power system, dynamic models based on Ward and Extended Ward power system reduction techniques). These voltage profiles are compared with the LV–FRT curve defined by the distribution grid code [3.1] as presented in Sub–Chapter 3.2.1. As can be observed, the voltage profile corresponding to the case when the DG unit is connected with a *Thévenin* equivalent crosses the LV–FRT profile defined in [20] immediately after the fault is cleared, meaning that the unit cannot sustain a stable post fault operating condition and must be disconnected. In the case when the external grid is represented by a wide area dynamic equivalent based on a Ward power system reduction method it is observed that the voltage rises above the LV–FRT profile define by the grid code [20] defined profile, in the third stage of post fault recovery. The reason why a Ward power system equivalent cannot achieve a LV–FRT curve close to the one produced by the representation of the detailed model of power system is the non-accuracy of the reactive power control of the equivalent grid.

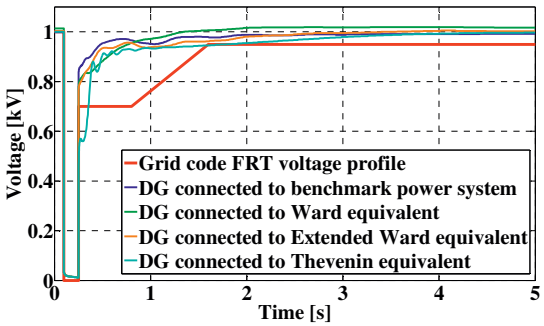

Figure 3.19. Voltage magnitude variation curves of DG unit connected to different external grid representations.

By considering the reactive power change with the change of state of internal power system [33] [44] a more accurate voltage variation curve can be obtained. This curve is in the area where no disconnection of DG unit is required and is associated with the representation of external power system by a dynamic equivalent based on an Extended Ward power system

reduction technique. As can be observed in Figure 3.19 this curve do not track rigorously the curve obtained when DG unit is simulated in the real power system. This is due to the combined effect of aggregation and power system reduction errors. Figures 3.20 and 3.21 present the variations of the DG unit's active and reactive power after the fault is cleared. For both power variations it can be observed that by modeling the external grid using a *Thévenin* equivalent the actual dynamic behavior of small scale hydro power plant cannot be achieved. Moreover, it can be observed that significant differences appear for the variations of active and reactive power, when the external grid is modeled by using a *Thévenin* equivalent with respect to the original or equivalents of benchmark power system. These variations are far smaller compared with cases when external grid is modeled by using the complete model or equivalents of the benchmark power system and not suitable to allow the DG unit to withstand the fault. The smaller magnitudes registered for the oscillations associated with the representation of the external grid by using a *Thévenin* equivalent can further result in erroneous ratings of the generation unit and wrongly tuned controllers. In the case when large numbers of DG units are integrated these combined effects can have a negative impact on the overall stable operation of the ADG. It can be also observed that the time scales for which new steady state values of critical parameters are obtained, differs from the case when a *Thévenin* equivalent of the power system is considered with respect to the complete model or equivalents.

When dynamic equivalent models of the external grid were used it can be observed that in the first oscillation of the active power variation track very well the variation described by the original power system. However, for the next two oscillations the magnitudes of the variations related to the equivalent models are lower compared to the variation produce by the original power system. This is due to the fact that the dynamic equivalents do not have the capability of computing rigorously the active power losses as also presented in [35] [36]. For the reactive power variations a large difference as observed between the peaks of the first oscillations associated with the connection in the real power system of the DG unit and the one associated with the *Thévenin* equivalent. This difference is of approximately 7.11 MVAr.

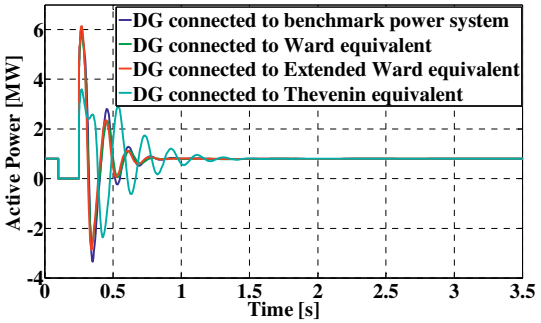

Figure 3.20. Active power variation curves of DG unit connected to different external grid representations.

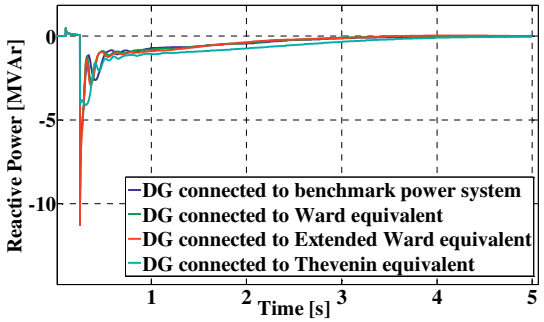

Figure 3.21. Reactive power variation curves of DG unit connected to different external grid representations.

As **Publications G** and **H** presents, when LV–FRT capabilities of a DG unit are investigated, just by taking into account only the variation of voltage magnitude erroneous results can occur, and the research proposes that a careful analysis of the impact of voltage angle variation when a fault emerged in the grid must be also considered, [52] [53]. Especially, that large excursion of the voltage angle will have a significant impact on the active power flow in the power system. This investigation will be detailed further in Sub-Chapter 3.3.In Figure 3.22 the voltage angle variations at the PCC of DG unit are presented with different models for external grid representation. It can be observed that by using an Extended Ward equivalent model of the external grid will track rigorously the curve produced when the DG unit is connected in the benchmark power system. Also, it can be observed that by using a *Ward* equivalent the same pattern as the one related to the benchmark power system is tracked. By using the *Ward* equivalent some oscillations are observed. This is due to the inaccuracies in the reactive power flow introduced by this model. When a *Thévenin* equivalent is used, a large error (of approximately 3 degrees) is produced after the fault is cleared. For the first swing in the time span between the fault is applied and cleared, the dynamic equivalent models of external grid give a very good representation of the peak value of voltage angle.

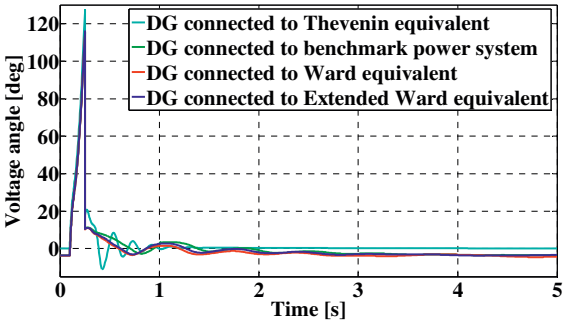

Figure 3.22. Voltage angle variation curves of DG unit connected to different external grid representations.

3.3. Impact of Voltage Phase Angle Variation on the Low−Voltage Fault Ride−Through Studies

3.3.1. General Introduction

The LV−FRT requirements are mainly addressed by the national grid codes as the capability of the generation units to withstand to one or more voltage drops for certain durations of time [29].

In Sub−Section 3.2.1 the LV−FRT requirement was introduced by defining a voltage borderline for the voltage variation versus time. When faults occur in the grid, they create both changes in the magnitude and phase of bus−bar voltages. This is the main contribution of Publications **G** and **H** which investigated the possible impact of decoupling the voltage phase angle variation from the voltage magnitude in the DG response and to present the consequences of neglecting this impact in the LV−FRT curves.

3.3.2. The Impact of Voltage Phase Angle Variation on Low Voltage−Fault Ride−Thorough Requirement

Using the test system presented in this Sub−Section, the following steps where considered in order to observe the impact of both the voltage magnitude and phase angle on the LV−FRT capabilities of the DG unit.

Step 1. Simulation of disturbance event. A three phase resistive short circuit is applied at different bus−bars of the test grid.

Step 2. Recording of separate time series for the voltage magnitude and phase angle variations at the DG bus−bar.

Step 3. The swing machine is replaced with a controlled voltage source for which the input will be the time series of the voltage magnitude and, respectively, phase angle variations.

Step 4. Investigation of the DG unit capabilities during simulations of voltage magnitude and angle at the PCC are observed, together with the active and reactive power variations as well the rotor angle.

3.3.2.1. Test Distribution Grid

The system model used in this research is presented in Figure 3.23. The system model consists of a simple 132 and 66 kV radial regional grid, a 22 kV distribution grid and a 300 kV (swing bus). Two loads are connected in the system, at BUS22_1 and BUS66_1, respectively. The loads are modeled as *Z=constant*. The synchronous generator is connected to the 22 kV grid via a 0.69/22 kV transformer. Data for lines, transformers, loads and generator are given in Appendices A2.1−A2.4.

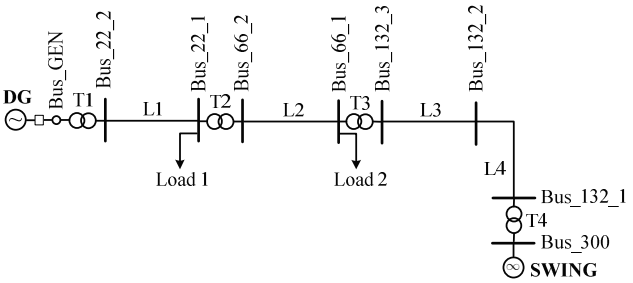

Figure 3.23. Single line diagram of system under study.

The synchronous generator model is equipped with a brushless excitation and an automatic voltage regulator. This excitation system model corresponds to model Type AC8B in [54]. Data for the excitation system are given in Appendix A2.5. The generator is operated with constant mechanical torque; therefore no turbine/governor model is included.

3.3.2.2. Study Cases

The following study cases were considered to approach the problem:

Study Case 1. A three−phase resistive symmetrical fault applied to bus−bar Bus_66_1. The value of resistive characteristic is established to 1.9 Ω.

Study Case 2. A three−phase resistive symmetrical fault applied to bus−bar Bus_22_1. The same resistive value for the fault is applied.

The instant considered for the fault inception is 1 s. In both cases, the fault clearing time is 250 ms. The DG unit has the following setpoints: $P_{setpoint}$=4 MW and $V_{setpoint}$=1 p.u..

3.3.2.3. Results

Applying the fault events presented in Study Cases 1 and 2 the following variation of the voltage magnitude at buses Bus_66_1 and Bus_22_1 are obtained, as shown in Figure 3.24. The correspondent voltage angle variations are presented in Figure 3.25.

Figure 3.24 shows large excursions in both variations of voltage magnitude and angle.

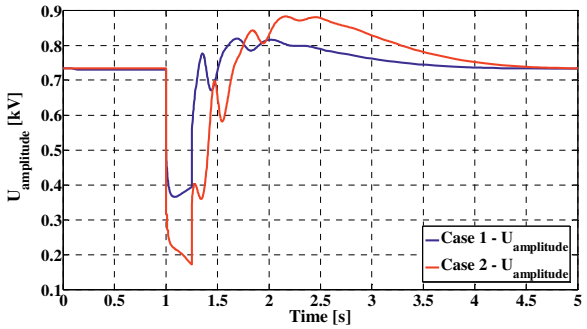

Figure 3.24. Voltage amplitude on generator bus, Bus_GEN, in Cases 1 and 2. Temporary 3-phase fault at Bus66_1 and Bus22_2, respectively. [52]

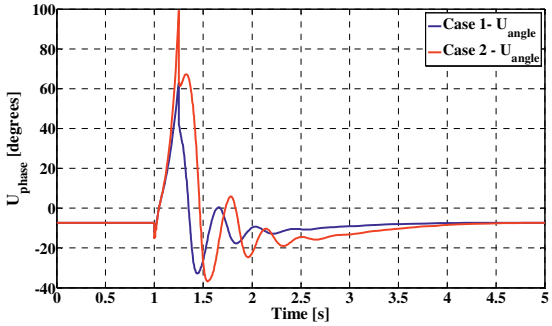

Figure 3.25. Voltage phase angle on generator bus, Bus_GEN, in Cases 1 and 2. Temporary 3-phase fault at Bus66_1 and Bus22_2. [52]

Figures 3.26 a), b) and 3.27 a), b) show the transient response of the DG unit in terms of active and reactive powers.

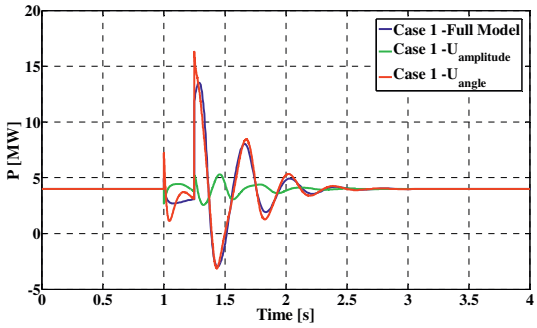

Figure 3.26.a). Response in generator's active power for Case 1 (3-phase fault om Bus22_2). [52]

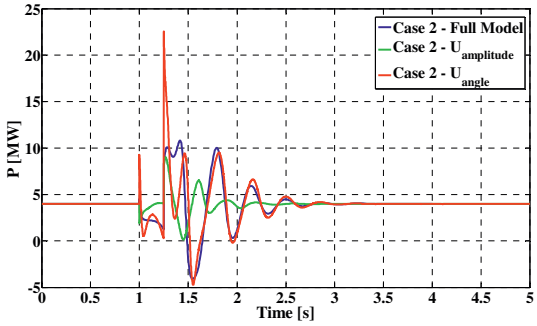

Figure 3.26.b). Response in generator's active power for Case 2 (3-phase fault om Bus22_2). [52]

These responses are compared for the basic case (when the DG unit is connected to the full model) with respect to the cases where the changes in voltage amplitude (depicted in the plots as $U_{amplitude}$) and phase angle (depicted in the plots as U_{phase}) are applied.

The inputs for the voltage magnitude and angle variations used to control the voltage source are presented in Figures 3.24 and 3.25.

From Figures 3.26 a significant difference can be observed between the full model response in active power and the response obtained when only change in voltage amplitude makes the perturbation can be observed, as to the fault in question. This pattern is not observed between ″full model″ case and ″voltage phase angle″ case.

As for Case 2, the significant difference show up between the responses obtained when only change in voltage angle makes the perturbation with respect to the full model and voltage amplitude.

This happens during the second swing of the simulation. After this, the third and fourth swings show the same pattern for the ″full model″ and ″phase angle″ cases. This is not the same situation for ″voltage magnitude″ case swings, which are lower in magnitude and damps much faster.

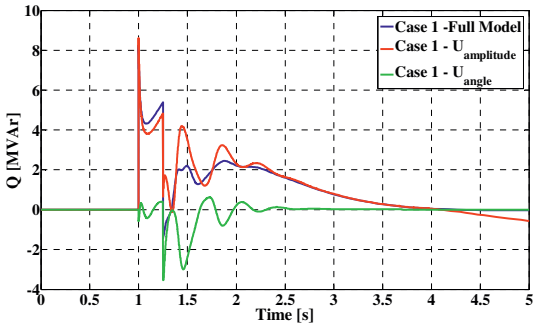

Figure 3.27.a). Response in generator's reactive power for Case 1 (3-phase fault om Bus22_2). [52]

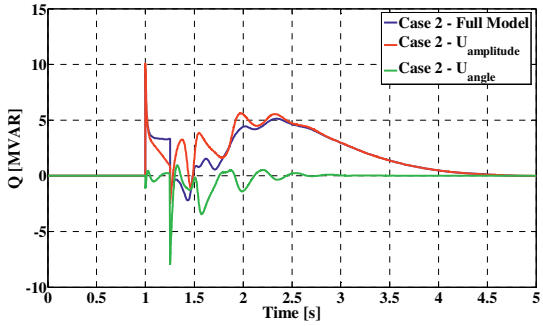

Figure 3.27.b). Response in generator's reactive power for Case 2 (3-phase fault om Bus22_2). [52]

As presented in the above Figures, a significant difference between the full model response in reactive power and the response was obtained when only change in voltage phase angle is applied, for both Cases. Approximately identical responses it are observed between ″full model″ case and ″amplitude″ case, except for the initial 600-700 ms after the fault inception.

3.3.3. The Impact of Voltage Phase Angle Variation on Critical Clearing Time

Considering the same simulation model as presented in Figure 3.16, the impact of the voltage magnitude and phase angle variations on the Critical Clearing Time for different study cases were investigated.

To observe in addition how different types of excitation and AVR models impacts the results, two types of excitation systems were chosen. A detailed presentation these two types of exciter and AVR models are presented in [54] and [55] . Simulations for the next study cases were performed using SIMPOW® [55].

Table 3.2. Exciter and AVR models [54].

Model 1	IEEE AC8B
Model 2	Variation of the brushless excitation system with DC commutator

The macro–blocks and data of these two excitations systems are presented in Appendices A2.5 and A2.6.

To conduct the investigation, the following steps are applied:

Step 1. Computation of the CCT when fault occurs at different locations in the grid, using the two excitation systems for the small hydro unit.

Step 2. Simulation of disturbance event with the same duration as the CCT computed at **Step 1**.

A three phase resistive short circuit event is applied at different bus–bars of the test grid.

Step 3. Recording of the separate time series for the voltage magnitude and phase angle at the DG bus–bar variations.

Step 4. The swing machine is replaced with a controlled voltage source for which the input will be separately the time series of the voltage magnitude and, respectively, phase angle variations.

Step 5. Investigating of the DG unit capabilities during simulations Voltage magnitude and angle at the PCC are observed, together with the active and reactive power variations as well the rotor angle.

3.3.3.1. Study Cases

The following study cases where considered:

Study Case 1. The same as in Study Case 1 of Sub–Chapter 3.3.2.1. In this case the fault resistance is R_f= 1.9 Ω.

Study Case 2. A three–phase resistive symmetrical fault applied to bus–bar Bus_22_2. The same resistive value for the fault is applied.

The instant considered for the fault inception is considered 1s. The study cases will be investigated for both situations of the excitation systems as summarized in the Table 3.2.

Table 3.3. Study cases.

Study cases	Fault applied at Bus:	Excitation System Model
Case 1A	Bus66_1	Model 1
Case 1B	Bus66_1	Model 2
Case 2A	Bus22_2	Model 1
Case 2B	Bus22_2	Model 2

3.3.3.2. Results

The following values for the CCT was obtained from the simulation of the above study cases:

Table 3.4. Critical clearing time [*ms*] for considered study cases.

Study cases	CCT [ms]
Case 1A	623
Case 1B	366
Case 2A	313
Case 2B	272

Appyling the faults described in the Cases 1A and 1B, the change in voltage amplitude as function of time on the generator bus (Bus_GEN) as a result of is shown in Figure 3.28.

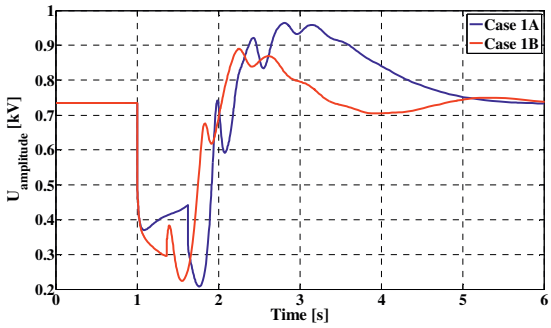

Figure 3.28. Voltage amplitude on generator bus (Bus_GEN) for Case 1A and Case 1B [53].

The corresponding change in voltage phase angle is given in Figure 3.29.

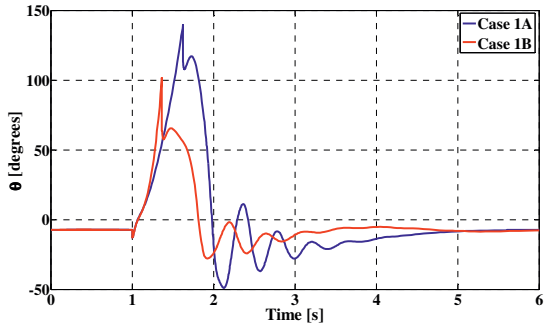

Figure 3.29. Voltage phase angle on generator bus (Bus_GEN) for Case 1A and Case 1B [53].

In Figure 3.30 and 3.31 the variations in voltage amplitude and phase angle, are shown for Case 2A and Case 2B.

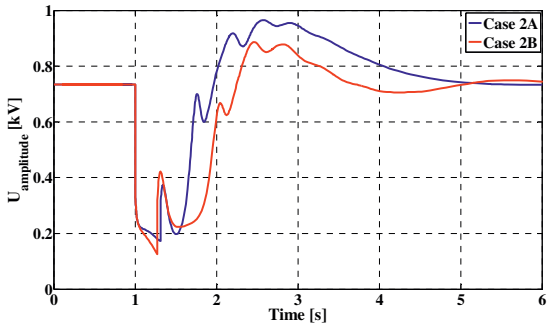

Figure 3.30. Voltage amplitude on generator bus (Bus_GEN) for Case 2A and Case 2B [53].

Figure 3.31 show that large difference of the voltage phase angle appears when the fault take place at different locations in the grid: Bus_22_2 and Bus_66_1.

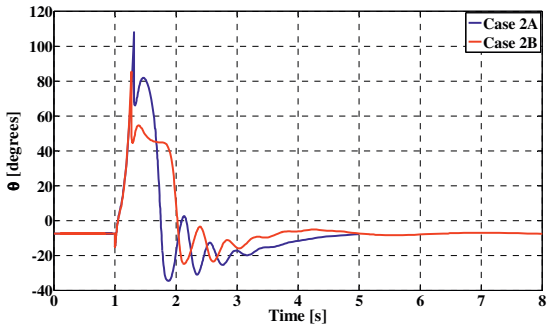

Figure 3.31. Voltage phase angle on generator bus (Bus_GEN) for Case 2A and Case 2B [53].

Figure 3.32 shows the DG unit rotor angle variation for the cases when a fault is simulated in the distribution grid compared to the case of controlled voltage source. As presented above, this voltage source has the input of the voltage magnitude variation obtained for the fault with the duration of the CCT in the ″full model″ case.

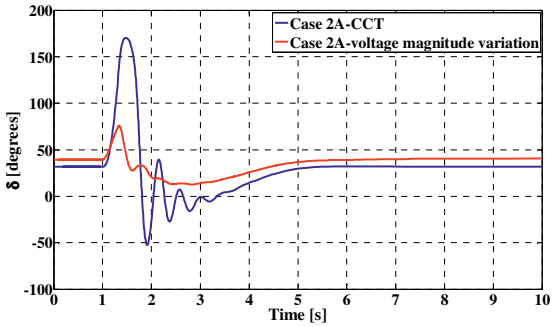

Figure 3.32. Rotor angle variations for Case 2A – full model and defined voltage magnitude vs time profile [53].

3.3.3.3. Discussion

In Section 3.3, results which investigate the LV–FRT capabilities of a DG unit clearly show that the expected transient response strongly depends on both changes in amplitude and phase angle of the terminal voltage caused by a fault which occurs in the grid. The largest error shows up in the active power response.

Therefore it can be concluded that an analysis taking into consideration only the voltage change of the perturbation, will in many cases most likely lead to erroneous conclusions regarding transient stability of the unit and critical clearing time.

The results also show that the type of AVR poses a great impact on the computed CCT. A depreciation of the transient stability is also observed in the case when a decoupling of the voltage magnitude to the phase angle is considered.

3.4. Summary

In this Chapter, new contributions to the LV–FRT requirements were introduced.

These contributions addresses to the adequacy of the external power system modeling by comparison to the model proposed by the grid codes (Thevenin source) and to the impact of voltage phase angle variation on the LV–FRT requirement. It is observed that by using a controlled voltage source to assess the LV–FRT capabilities of a small scale hydro unit, erroneous results can be achieved. Better results were achieved by assessing the capabilities of the DG unit by using a benchmark or a reduced order model dynamic equivalent. In the second part, the impact of considering the voltage angle variation it was investigated when the LV–FRT requirement is studied. It was observed that by using a voltage magnitude against time variation profile, the capabilities and the transient limits are also erroneous. More accurate results can be achieved when using a unified voltage magnitude–angle variation against time.

Chapter 4

Dynamic Equivalents of Active Distribution Grids for Rotor Angle Transient Stability Studies

The chapter is based on **Publication C** *and presents the investigations of this PhD work regarding the model reduction of ADG for rotor angle transient stability. In Section 4.2 the method to produce dynamic equivalents of ADG for transient stability analysis in main transmission systems is presented. Section 4.2.3 investigates the impact of disturbance duration, location and type on the coherency identification of generators, quantify by the disturbance impact index. In the end of this Chapter the steps to produce a dynamic equivalent for test ADG is studied and two criteria to validate this type of equivalents are considered.*

4.1. Problem statement

Distribution networks had evolved from passive systems, (meaning transferring the electrical energy from main bulk system to the end users) into active systems with an increased share of distributed generation. As most of this distributed generation is based on synchronous generator technology, the dynamic response of these small scale generation units and their controllers on the bulk transmission power system cannot be any longer neglected.

The transient stability study investigates if the reduced model preserves the voltage magnitude and phase angle variation in the Point of Common Coupling (PCC) with the bulk system. As the Critical Clearing Time (CCT) and transient stability limits are of interest when transient stability analyses are performed, these criterions are used to validate this method for the use of large transmission power systems studies.

The general idea of the work presented in this Chapter is to show that adequate modeling of active distribution grids in transmission system transient analysis can be done by use of reduced order dynamic equivalents.

4.1.1. The Concept of Rotor Angle Transient Stability

The study of transient stability relates to the analysis of the power system regarding how it behaves when exposed to large disturbances as: outage of a line and/or generator, large excursions of the load areas or emerging of severe disturbances (as short− circuits). In order to solve the nonlinear set of differential equations an integration method with fixed or variable steps are used. The most used numerical integration as described in [41] are:

1. Euler Methods
2. Runge−Kutta Methods

The purpose for computing the transient state (or states) of a power system is to observe if the transition from the original steady–state (x_0, y_0) to a new steady–state is stable (x_1, y_1). In order to observe if a power system is stable or not, a time-domain simulation is used.

The ***first scope*** of this time-domain simulation is to observe the oscillation curves of the generator's corresponding relative rotor angle. For this, three possible characteristics can be observed [41]:

1. The stable case– in which the rotor angle after some damped swings recover to a new steady state value
2. The unstable case–or the ″first swing unstable case″ in which after the first oscillation the rotor angle continues to increase steadily until the loss of synchronism.
3. The first swing is stable but the next ones are of increased magnitude.

The ***second scope*** is to compute the Critical Clearing Time.

Critical Clearing Time is defined in [49] as the maximum time interval between the instant of time when the disturbance occurs and the instant of clearing, with the ability of the power system to recover to a stable operation point.

A simplified method to compute the CCT can be done by using the Equal–Area Criterion, which is an approximation of the time domain simulation way to obtain the CCT. Considering A_{acc} and A_{dec} as the accelerating area, respectively deceleration area, the transient stability of the power system is ensured if $A_{acc} < A_{dec}$, as shown in Figure 4.1.

The case when $A_{acc} = A_{dec}$ is called the ***transient stability limit***. Figure 4.1 shows depicted the $P=f(\delta)$ curves characteristics to obtain the Equal–Area Criterion.

As presented in [56], the rotor angle points used in Figure 4.1 are:

1. δ_m is the unstable equilibrium point or $(\pi - \delta_P)$
2. δ_P is the post–fault steady –state equilibrium point
3. δ_m is the same with the unstable $(\pi - \delta_0)$equilibrium point, if the pre– and post– fault topologies coincide.

In the next lines, δ_c (corresponding to the critical rotor angle value) is calculated for the Single–Machine Infinite Bus (SMIB). The topology of the SMIB case is presented in Figure 4.2 and consists of a machine connected to an infinite bus via a double circuit transmission line with fault occurring on one of the circuits [40] [41]. The generator is modelled using the classical model (a constant e.m.f E' behind the transient reactance) defined as (4.1):

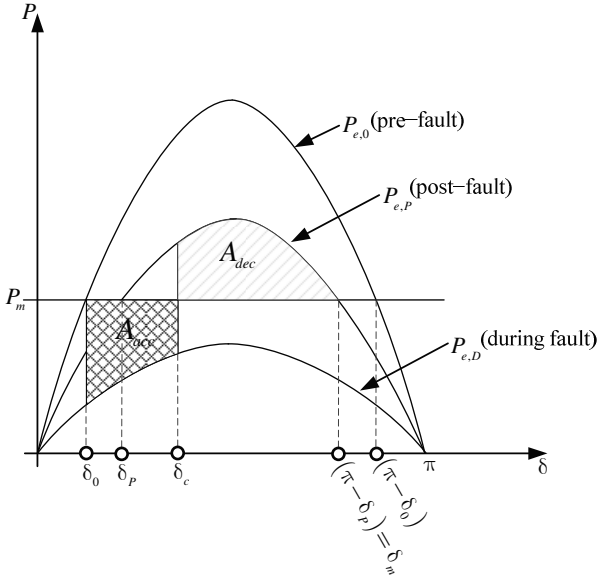

Figure 4.1. Equal−Area Criterion for obtaining the Critical Clearing Angle. [56]

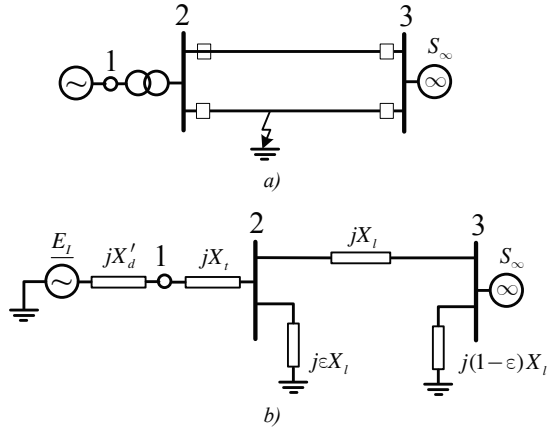

Figure 4.2. Single Machine Infinite Bus (SMIB) to assess transient stability in power systems. a) Single line diagram. b) Faulted SMIB. [49]

$$\underline{E'} = E' e^{j\delta'} \tag{4.1}$$

Figure 4.3 is presents the phasor diagram corresponding to the transient operation of the SMIB system.

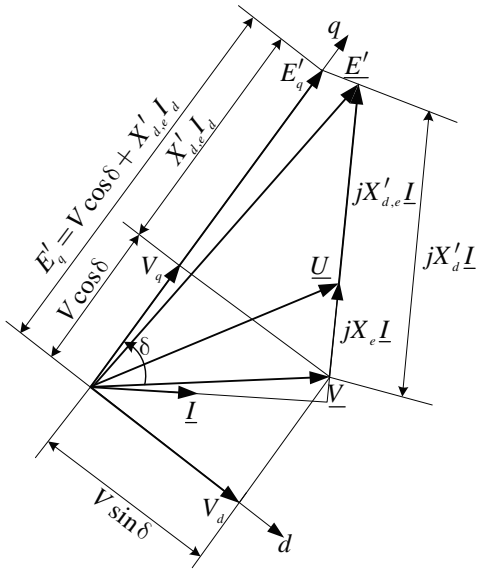

Figure 4.3. Phasor diagram of the SMIB in transient state. [49]

Considering D=0 and:

$$\frac{d^2\delta}{dt^2} = \frac{d\omega}{dt} \tag{4.2}$$

The swing equation can be written:

$$\frac{2H}{\omega_0}\frac{d^2\delta}{dt^2} = P_m - P_e = P_a \tag{4.3}$$

Doing the mathematical manipulation described, as described in [56] the stability condition is:

$$\int_{\delta_0}^{\delta_m} P_a\, d\delta = \int_{\delta_0}^{\delta_m} \left(P_m - P_e\right) d\delta = 0 \text{ with } P_a\left(\delta_m\right) \leq 0 \tag{4.4}$$

In order to calculate the *Critical Clearing Angle* the two formulas related to the A_{acc} and A_{dec} areas are equaled A_{acc}= A_{dec}, as presented in (4.5) and (4.6):

$$A_{acc} = \int_{\delta_0}^{\delta_c} \left\{ P_m - P_{eD}(\delta) \right\} d\delta \tag{4.5}$$

$$A_{dec} = \int_{\delta_c}^{(\pi-\delta_P)} \left\{ P_{eP}(\delta) - P_m \right\} d\delta \tag{4.6}$$

$$\int_{\delta_0}^{\delta_c} \left\{ P_m - P_{eD}(\delta) \right\} d\delta = \int_{\delta_c}^{(\pi-\delta_P)} \left\{ P_{eP}(\delta) - P_m \right\} d\delta \tag{4.7}$$

Thus the *Critical Clearing Angle* (δ_c) becomes:

$$\delta_c = \arccos\left[(\delta_m - \delta_0)\sin(\delta_0) + \cos(\delta_m) \right] \tag{4.8}$$

Using δ_c equation (4.8), the Critical Clearing Time (t_c or CCT) can be computed, as detailed in [49]:

$$t_c = \sqrt{\frac{H}{\omega_0 P_m}(\delta_c - \delta_0)} \tag{4.9}$$

Using (4.9) one of the transient stability margin (based on different time constants) formula can be expressed as in [40]:

$$K_{time} = \frac{t_c - t}{t_c} \tag{4.10}$$

Where:

t_c – is the CCT

t – is the Actual Clearing Time, which takes into consideration the time constants of the protection, of breakers and signals transmission.

The other formulas for the stability margin can be written [49]:

- Based on available deceleration area:

$$K' = \frac{A_{dec}}{A_{dec,available}} \tag{4.11}$$

– Based on the difference between the deceleration and acceleration areas [49]:

$$K'' = \frac{A_{dec} - A_{acc}}{A_{acc}} \tag{4.12}$$

4.2. Dynamic Equivalents of Active Distribution Grids for Investigation of Transient Stability

Dynamic equivalents for power systems are very well established theories especially for large interconnected power systems, but it can also be applied to active distribution power systems as these systems are generally sparse and starting to accommodate an increasing amount of small scale generation units. The basic idea is to separate the power system into three main areas depending on the impact after a disturbance occurs, [2].

According to [40] these main areas are: the internal area, the external area and a remote area. Figure 4.4 illustrates this differentiation.

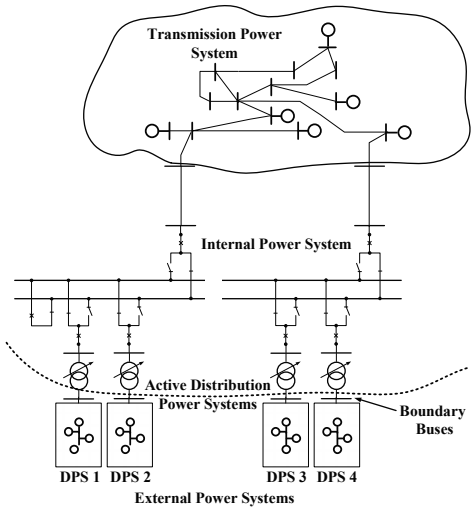

Figure 4.4. Separation of TPS and ADG into internal and external areas.

The internal area is represented by the MV busbar of the HV substation were the ADG is interconnected with the TPS. The external power system is in this case the entire ADG. A

remote area is not defined as the overall response of the entire ADG is of interest, but it is considered in the transient stability analysis of the TPS. The boundary buses are the MV buses of the transformer of the ADG with the HV substation and the PCCs of DG units connected in each active ADG.

To model the dynamic equivalency of ADG, the following steps are considered as in [40] and detailed in next Sections:

1. Identification of coherent DG units in the ADG after a fault event in the internal area
2. Network reduction of ADG
3. Dynamic aggregation of coherent groups of generators

The proposed algorithm was implemented in DIgSILENT Power Factory 14.1.6© simulation platform, using DIgSILENT Programing Language scripts−*DPL* [38]. This algorithm has a generalized character, so it can be applied to a TPS with more than one active ADG (with high penetration of synchronously based DG units). Figure 4.5 summarize this algorithm.

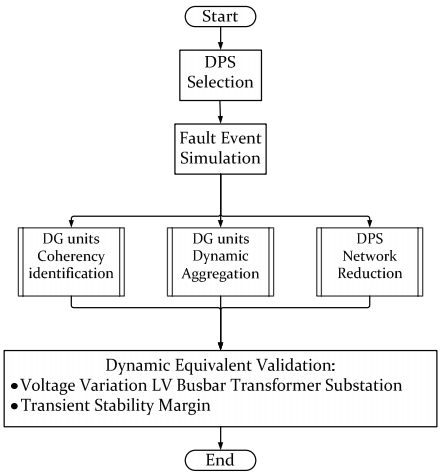

Figure 4.5. Algorithm to obtain the dynamic equivalent of ADG.

4.2.1. Benchmark ADG system and HV Substation Topology

The topology of the benchmark ADG and HV substation is illustrated in Figure 4.6. It consists of 4 voltage levels: 0.69, 6.6, 22 and 132 kV and 11 small scale hydro units based on synchronous technology equipped with exciters and governors. The data for the distribution lines, transformers and generators are given in the Appendix 3, Tables A3.1−A3.6.

For simplification, an IEEE ESAC8B model was adopted to represent the AVR and excitation system, and a HYGOV model from simulation platform library [38] was used to

represent the hydro governor. The corresponding controllers' data is provided in Tables A3.7 and A3.8.

The total length of the ADG lines is 51.55 km. The point of interconnection with TPS is in the busbar TRAFO_TPS which is modelled as a double bus–bar with tie connection. The topology of the busbar TRAFO_TPS is depicted in Figure 4.6.

A 132/22kV transformer interconnects the ADG with TPS. The model of the TPS is simplified by considering the nearest medium hydro unit (P_G=35 [MW]), a local industrial load (P_L = 0.721 MW) and a strong slack bus with S_k''=6000 MVA.

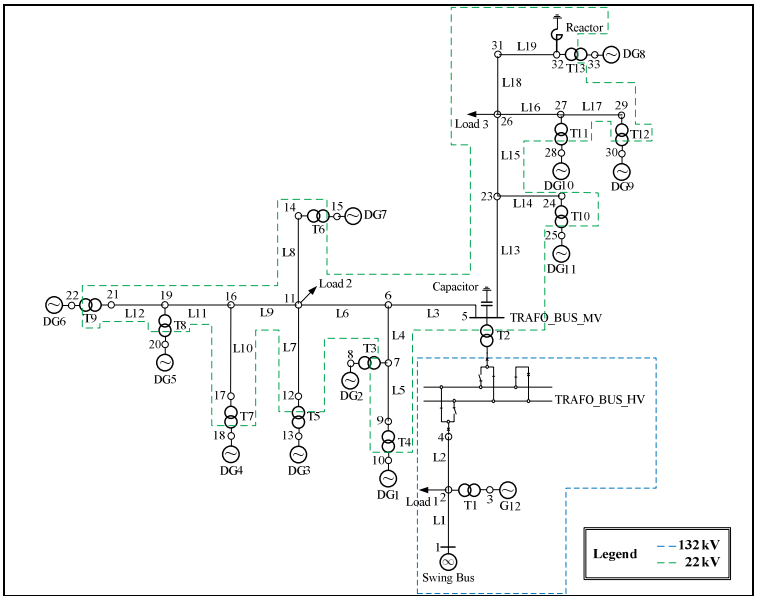

Figure 4.6. Test ADG topology.

4.2.2. Identification of coherent DG units in the ADG

For the identification of coherent DG units a mechanical coherency method based on the Euclidean distances between DG units is applied, as described in reference [46]. The main idea behind this method is to identify the DG units which are coherent or swing together after a fault has occurred in the internal area. For this a bolted three phase short circuit is applied at TRAFO_BUS_MV with duration of 150 ms. This study case will be refereed as the **Base Case**. In the post-fault period the rotor angle of all DG units were recorded and the Euclidean Distance – d_{ij} (as in equation 4.13) between DG units i and j was computed in order to identify the cluster of coherent generators [46].

$$d_{i,j} = \sqrt{\sum_{t=t_1}^{T} \left(\delta_i(t) - \delta_j(t)\right)^2} \tag{4.13}$$

According to [34], two synchronous generator units are considered to be coherent if the distance between their rotor angle variations is smaller than 0.17 radians or 10 degrees.

Further, this method is applied for the benchmark ADG depicted in Figure 4.6 for a fault event occurring at bus TRAFO_BUS_MV.

Figure 4.7 presents the rotor angle variations for all DG units connected in the benchmark power system and Figure 4.8 depicts the clustering process of the DG units. In Table 4.1 the matrix of Euclidean Distance between each of the generators is computed using (4.13).

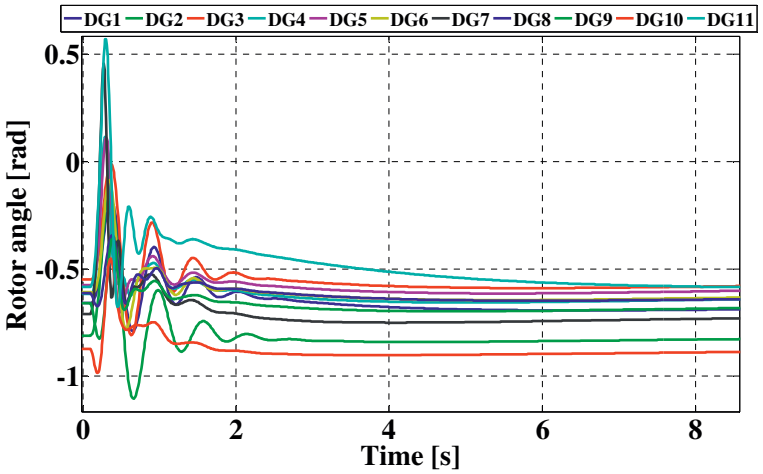

Figure 4.7. Rotor angle variation after fault occured at bus TRAFO_BUS_LV for CCT.

Table 4.1. Matrix of Euclidean Distances for the test ADG.

$[ED] =$

	DG_1	**DG_2**	**DG_3**	**DG_4**	**DG_5**	**DG_6**	**DG_7**	**DG_8**	**DG_9**	**DG_10**	**DG_11**	**DG_12**
DG_1	0	0.966	0.582	0.966	0.973	0.971	1	0.690	0.878	0.780	0.861	0.993
DG_2	0.966	0	0.774	0.086	0.112	0.106	0.260	0.680	0.408	0.576	0.444	0.231
DG_3	0.582	0.774	0	0.774	0.783	0.781	0.816	0.382	0.660	0.521	0.637	0.808
DG_4	0.966	0.086	0.774	0	0.110	0.110	0.262	0.679	0.406	0.575	0.442	0.235
DG_5	0.973	0.112	0.783	0.110	0	0.077	0.232	0.689	0.423	0.587	0.458	0.199
DG_6	0.971	0.106	0.781	0.110	0.077	0	0.237	0.687	0.420	0.584	0.455	0.207
DG_7	1	0.260	0.816	0.262	0.232	0.237	0	0.727	0.483	0.631	0.514	0.117
DG_8	0.690	0.680	0.382	0.679	0.689	0.687	0.727	0	0.545	0.360	0.516	0.718
DG_9	0.878	0.408	0.660	0.406	0.423	0.420	0.483	0.545	0	0.407	0.175	0.469
DG_10	0.780	0.576	0.521	0.575	0.587	0.584	0.631	0.360	0.407	0	0.367	0.620
DG_11	0.861	0.444	0.637	0.442	0.458	0.455	0.514	0.516	0.175	0.367	0	0.500
DG_12	0.993	0.231	0.808	0.235	0.199	0.207	0.117	0.718	0.469	0.620	0.500	0

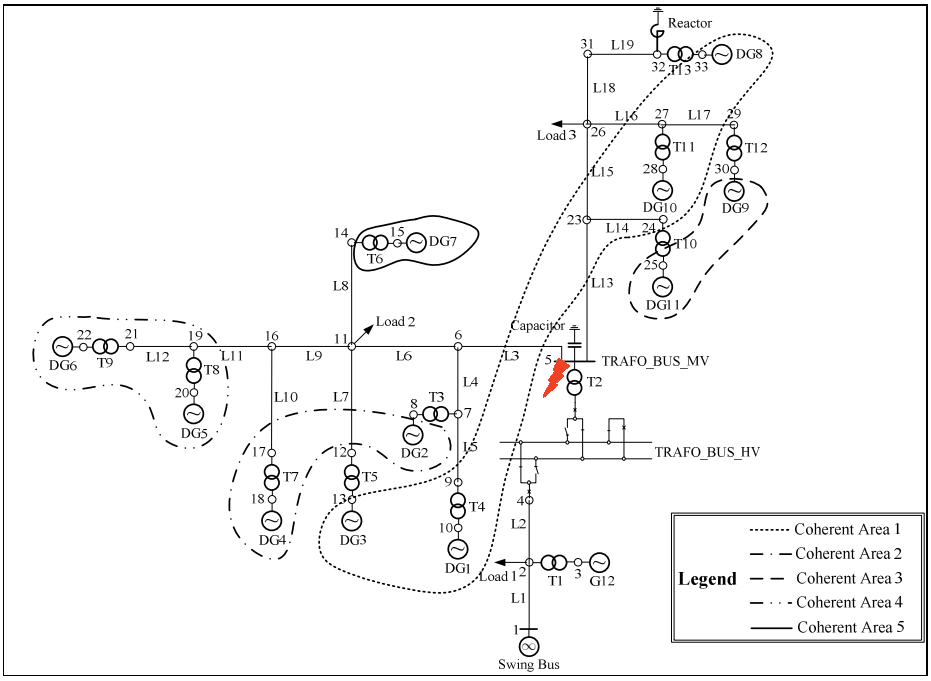

Figure 4.8. Decomposition of the system by the criterion of Euclidean Distance define as in (4.13) (Fault: Symmetric Three Phase, Bus: TRAFO_BUS_MV, CCT=150 ms)

As presented in [57] the coherency identification is impacted by the disturbance index and by the system's element significance. One can therefore observe that the coherency identification will depend on these two factors. In Sub–Section 4.2.2.A.1, this observation will be investigated in detail for the test ADG.

4.2.3. The Disturbance Impact Index

As shown in [57] the occurrence of a disturbance in a power system and the dynamic behavior afterword is determined by the disturbance characteristics and by the electrical distance between the points where the disturbance occurred and the affected element (generator, load, line). Therefore this disturbance index can be expressed as in (4.14), with:

- A coefficient measuring the electrical distance of node i, $Y_{i.a}$
- A coefficient measuring the effect of disturbance at node $i, \Delta P_i$

$$\gamma_i = \frac{Y_{ia} \Delta P_i t_a^2}{2H_i} \tag{4.14}$$

With:

- t_a the duration of the disturbance

Disturbance Index

- ΔP_i the active power imbalance during the disturbance
- H_i the inertia time constant of the generator connected at the i^{th} bus
- $Y_{i,a}$ the admittance value between the i^{th} bus and the location of disturbance a

By computing the disturbances for the test grid, the following values are obtained:

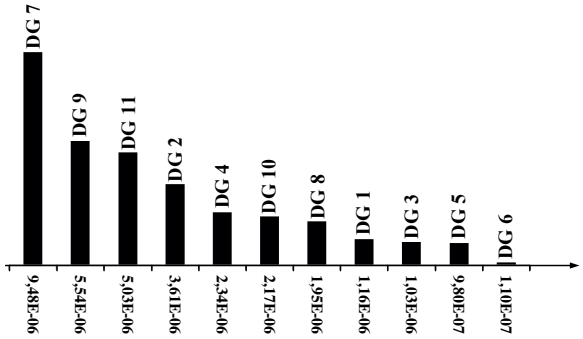

Figure 4.9. Disturbance Impact Indices defined by (4.14)
(Fault: Symmetric Three Phase, Bus: TRAFO_BUS_MV, CCT=150 ms)

Table 4.2. The Values of Disturbance Impact Index

Generator	7	9	11	2	4	10
γ_i	0.000009	0.000005	0.000005	0.000003	0.000002	0.000002
Generator	8	1	3	5	6	–
γ_i	0.000002	0.0000012	0.000001	0.000001	0.00000011	

The ΔP_1 of the DG 1 is computed based on the variation presented in Figure 4.10. *a*) and *b*).

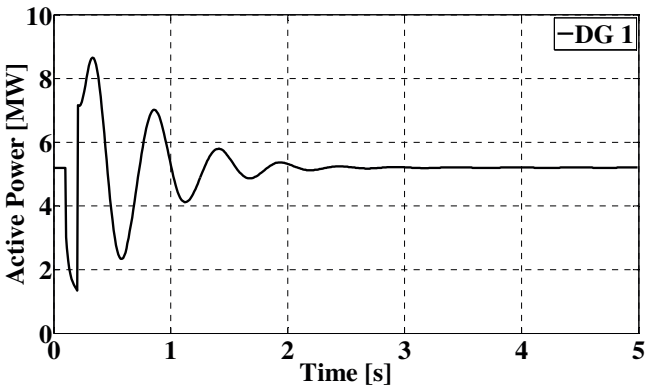

Figure 4.10. *a*) Active power variation of DG1
(Fault: Symmetric Three Phase, Bus: TRAFO_BUS_MV, CCT=150 ms)

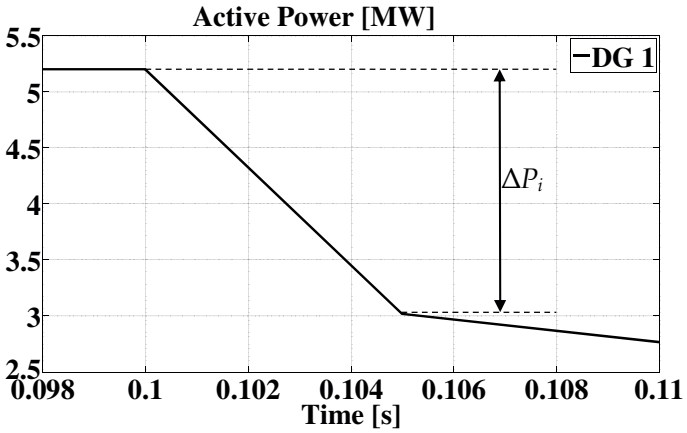

Figure 4.10. *b*) ΔP_i computation
(Fault: Symmetric Three Phase, Bus: TRAFO_BUS_MV, CCT=150 ms)

As presented in the reference [57], this index can be used to reduce the modeling complexity of different groups of generators in obtaining a dynamic equivalent of an external power system.

Using this index, some study cases are investigated in order to study the impact of the disturbance location and of magnitude–time duration on the identification of the groups of coherent generators.

By using the same test system as in previous studies, the disturbance index will be used to study the impact on the coherent generators identification process.

Three new study cases were carried out in order to investigate the above objectives are:

4.2.3. A) The impact of disturbance duration on the identification of coherent generators

In order to quantify the impact of the disturbance duration on the process of the identification of coherent generators a new study case was produced. This consists of changing the fault duration from 150 to 15 ms (but keeping the fault location). The corresponding rotor angle variations are presented in Figure 4.11.

The disturbance indices are presented in Figure 4.12.

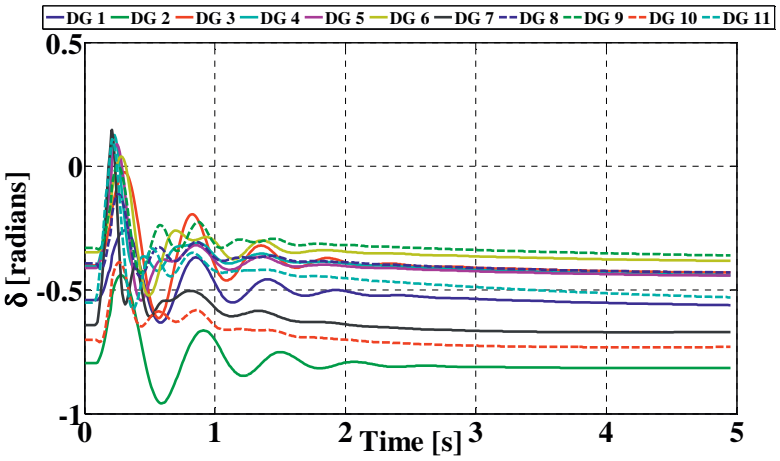

Figure 4.11. Rotor angle variations
(Fault: Symmetric Three Phase, Bus: TRAFO_BUS_MV, CCT=15 ms)

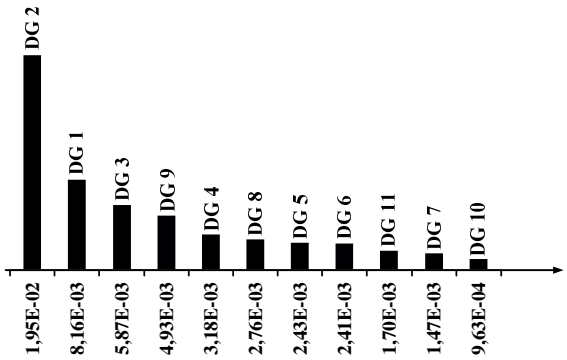

Figure 4.12. Disturbance Impact Indices defined by (4.14)
(Fault: Symmetric Three Phase, Bus: TRAFO_BUS_MV, CCT=15 ms)

Table 4.3. The Values of Disturbance Impact Index

Generator	2	1	3	9	4	8
γ_i	0.019543	0.008159	0.005867	0.004929	0.003182	0.00276
Generator	5	6	11	7	10	–
γ_i	0.002429	0.002413	0.00276	0.001473	0.000963	

Applying the fault as described above the following clustering of the DG is obtained, as presented in Figure 4.13.

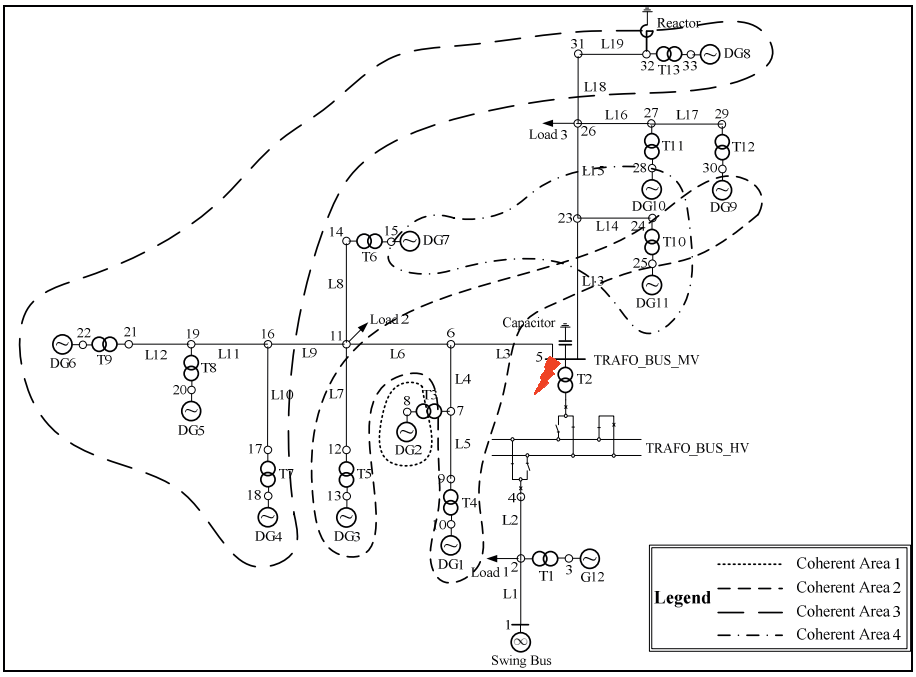

Figure 4.13. Decomposition of the system by the criterion of Euclidean Distance defined as in (4.13) (Fault: Symmetric Three Phase, Bus: TRAFO_BUS_MV, CCT=150 ms)

Using the disturbance indices obtained in 4.3, the resulted coherent areas are depicted in Figure 4.13, giving 4 coherent areas.

4.2.3. B) The impact of disturbance location on the identification of coherent generators

In order to study the impact of the fault location on the identification the same fault as in the base study case presented in Sub–Section 4.2.3.A it is applied at bus 23. With this new location the calculated disturbance indices are as presented in Figure 4.14.

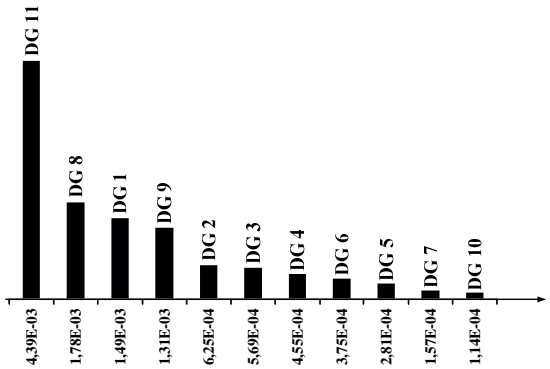

Figure 4.14. Disturbance Indices defined by (4.14)
(Fault: Symmetric Three Phase, Bus: 23, CCT=15 ms)

Table 4.4. The Values of Disturbance Impact Index

Generator	11	8	1	9	2	3
γ_i	0.00439	0.00178	0.001487	0.001313	0.000625	0.000569
Generator	4	6	5	7	10	–
γ_i	0.000455	0.000375	0.000281	0.000157	0.000114	

In the same manner as above, the decomposition of the power system in coherent areas is done as in Figure 4.15.

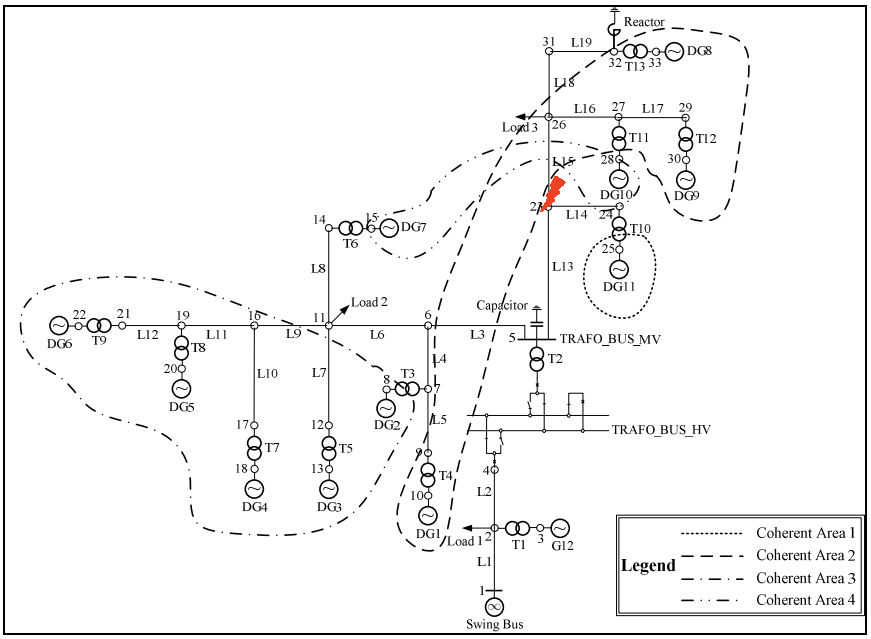

Figure 4.15. Decomposition of the system by the criterion of Euclidean Distance define as in (5.22) (Fault: Symmetric Three Phase, Bus: 23, CCT=15 ms)

4.2.3.C) The impact of disturbance type on the identification of coherent generators

In this study case a single phase to ground (with zero fault resistance and reactance) was applied at TRAFO_BUS_MV in order to observe this impact. The calculated disturbance indices are as presented in Figure 4.16 and the system decomposition in Figure 4.17.

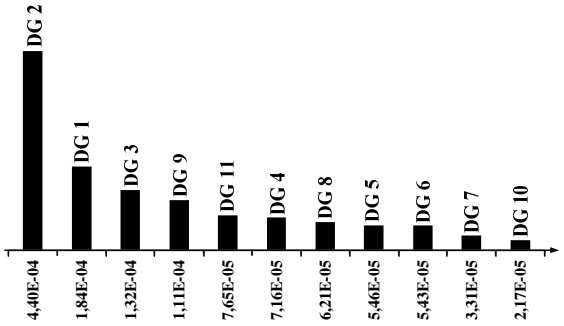

Figure 4.16. Decomposition of the system by the criterion of Euclidean Distance define as in (4.14) (Fault: Single Phase to Ground, Bus: TRAFO_BUS_MV, CCT=15 ms)

Table 4.5. The Values of Disturbance Impact Index

Generator	2	1	3	9	11	4
γ_i	0.00043	0.00018	0.00013	0.00011	0.00007	0.00007
Generator	8	5	6	7	10	–
γ_i	0.00006	0.00005	0.00005	0.00003	0.00002	

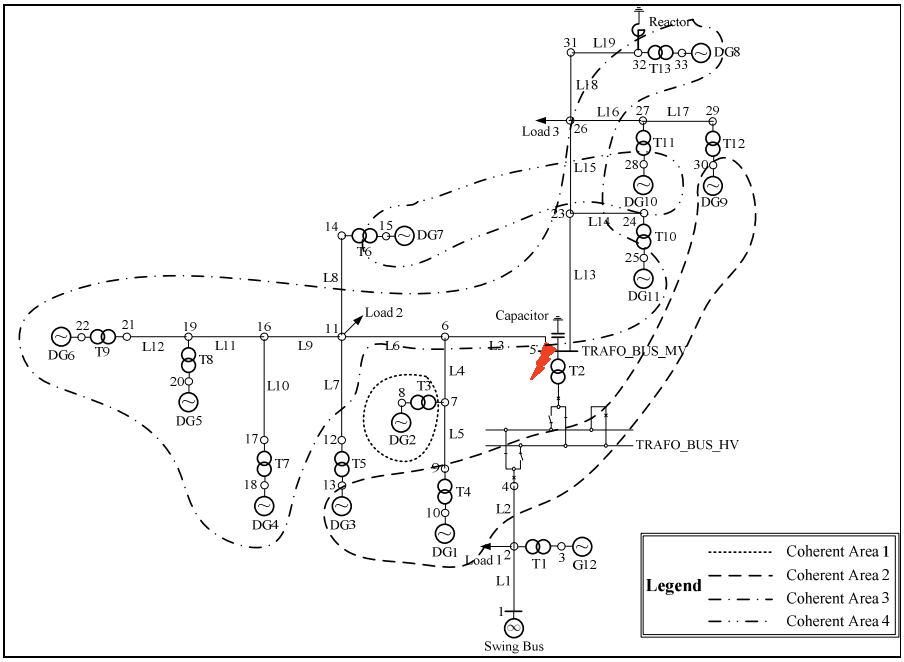

Figure 4.17 Decomposition of the system by the criterion of Euclidean Distance define as in (5.22) (Fault: Single Phase to Ground, Bus: TRAFO_BUS_MV, CCT=150 ms)

These results show that the decomposition of the test power system is not unique. It also shows that by applying different disturbances with different time duration, location or disturbance characteristics, the identification of the coherent groups of generators will be affected in a different manner.

4.2.4. Network reduction of ADG

The network equivalent was estimated using an Extended Ward equivalent because this method can roughly preserve the original ADG network response both in terms of active and reactive power flows, as discussed in Publication **B** [14]. The theory of network reduction for obtaining the Wards and Extended Wards equivalents was presented in Subsection 3.2.2 C2).

4.2.5. Dynamic aggregation of coherent groups of generators

Using the decomposition of the test power system present in Figure 4.11 and presented in the next Table 4.6 the coherent groups of generators are as presented next.

Table 4.6. Coherent Groups of Generators for the Test Distribution Grid

Coherent Group 1	1	3	8	10
Coherent Group 2	4	2		
Coherent Group 3	9	11		
Coherent Group 4	5	6		
Coherent Group 5	7			

After the coherent groups of generators are identified, the equivalent sets of generators-transformers are formed and the new equivalent parameters for these sets and their correspondent controllers are computed. The new parameters for the equivalent synchronous generators and controllers' parameters are produced according to the method presented in Sub−Section 3.2.2. B.2).

The parameters of the aggregated generators and of the exciter control systems are presented in the Table 4.7:

Table 4.7. Parameteres of the Equivalent Generators and Excitation Systems

Parameters		Equivalent Generator 1	Equivalent Generator 2	Equivalent Generator 3	Equivalent Generator 4	Equivalent Generator 5
Generator	X_d	0.4525	0.8396	0.9868	0.9908	1.5
	X_q	0.3382	0.6089	0.7576	0.7552	1
	X'_d	0.0471	0.1212	0.1014	0.1009	0.15
	X'_q	0.0726	0.1484	0.1471	0.1479	0.3
	X''_d	0.0316	0.0674	0.0510	0.0507	0.1
	X''_q	0.0393	0.0741	0.0654	0.0973	0.1
	$T'_{d,0}$	2.8374	2.9806	3.2107	3.8204	2
	$T'_{q,0}$	–	–	–	–	–
	$T''_{d,0}$	0.0193	0.0189	0.0203	0.0267	0.015
	$T''_{q,0}$	0.0911	0.1691	0.1150	0.1500	0.1
	H	6.2	3.2	2	2.5	0.5
AVR	K_E	1	1	1	1.5	1
	T_E	0.5006	20.42	1.2866	1.2629	1.2

As can be observed from Table 4.7, the standard parameters of the equivalent generators validate the conditions described in [41] regarding these parameters, namely:

$$X_d \geq X_q > X'_q \geq X'_d > X''_q \geq X''_d \tag{4.15}$$

$$T'_{d,0} > T''_{d,0} \tag{4.16}$$

$$T'_{q,0} > T''_{q,0} \tag{4.17}$$

Figure 4.18 presents the resulting dynamic equivalent of the benchmark ADG based on an Extended Ward network reduction of the original power system.

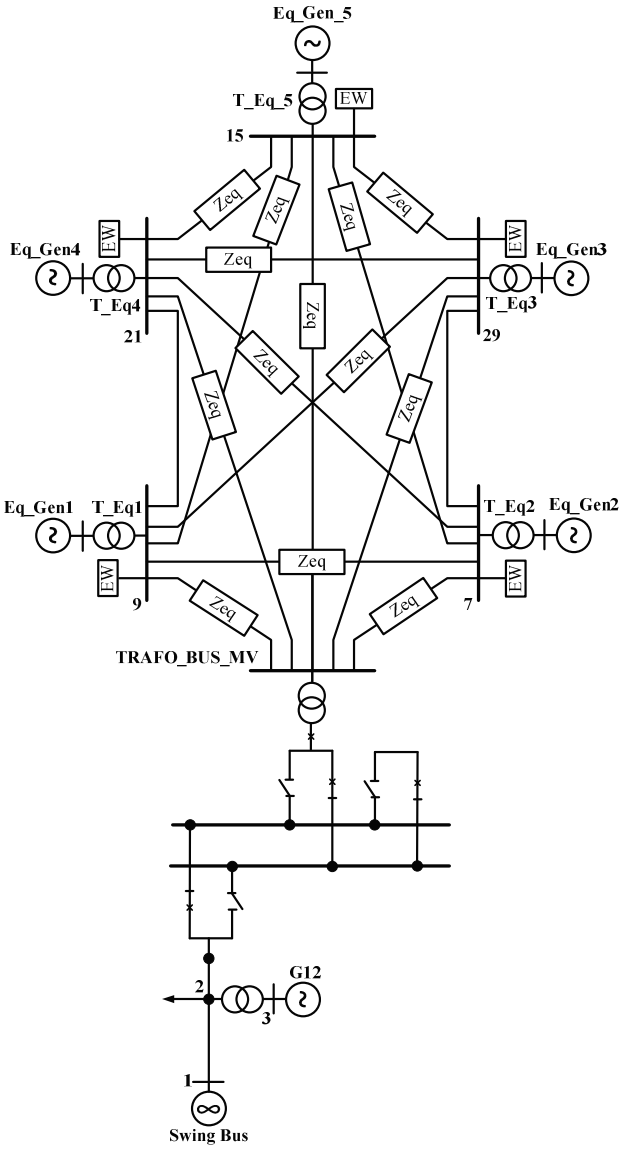

Figure 4.18. Extended Ward equivalent of original benchmark ADG for transient stability assessment into bulk TPS.

4.2.6. Method Validation

Two criteria are considered for validating the dynamic equivalent of the benchmark ADG. The first one refers to the preservation of the voltage magnitudes and angles variation at the bay busbar were ADG is connected. Figures 4.19 and 4.20 present these two responses for both original and the dynamic equivalent of the benchmark system.

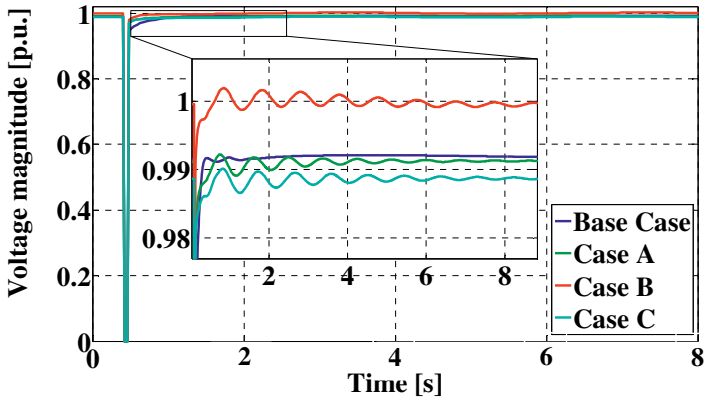

Figure 4.19. Voltage magnitude variations (original and reduced cases)

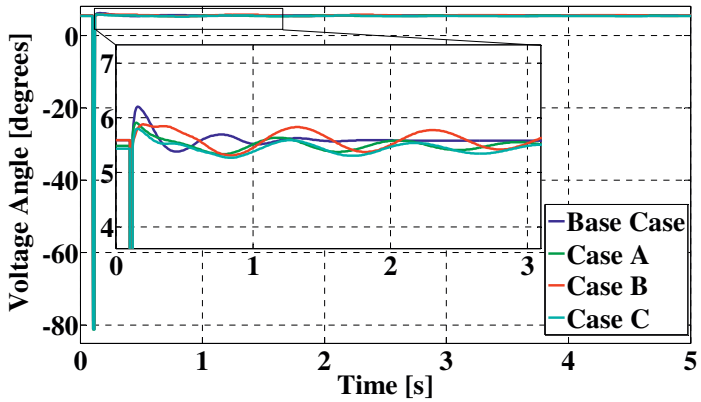

Figure 4.20. Voltage phase variations (original and reduced cases)

Figure 4.21presents the rotor angle variations of the equivalent generator 2 for the study cases described in Sub–Section 4.2.2.

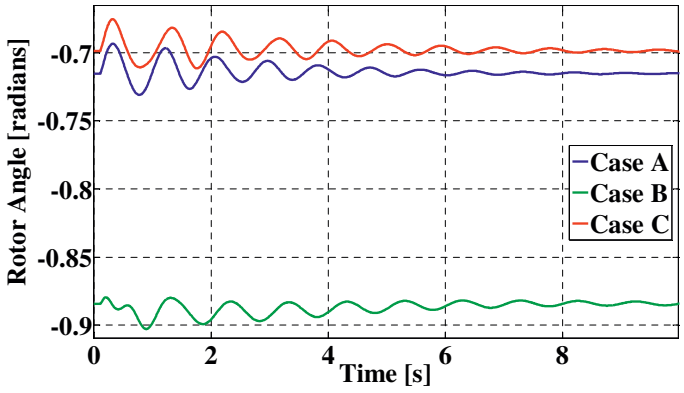

Figure 4.21. Rotor angle variations for the equivalent generator 2. (for 4.2.2 cases)

The average error was computed for each of the two series of voltage magnitude and angle variations. For the voltage magnitude variation, an average error of 0.0021 was obtained while for the voltage angle the error was 0.0951.

Table 4.6. Average errors for voltage magnitude and phase angle (compared to the original case)

Study Case	Reduced Case	Case 5.2.2.1. *a)*	Case 5.2.2.1. *b)*	Case 5.2.2.1. *c)*
$\bar{\varepsilon}_{\|V\|}[\%]$	0.21	0.066	0.81	0.31
$\bar{\varepsilon}_{\arg\{V\}}[\%]$	9.51	10.30	0.079	15.97

The second validation criterion is the transient stability margin, which gives information about the reserve of deceleration area according to the Equal Area Criterion, detailed described in [40]. According to this reference, the transient stability margin can be defined as:

$$K_t = \frac{t_{CCT} - t_{actual,CCT}}{t_{CCT}} \tag{4.18}$$

The simulations for both the original and the reduced ADG (base case and additional cases *a),b),c), d)*), showed the critical clearing time (CCT) as presented in Table 4.7. Considering an actual clearing time of 64ms (2 cycle breaker clearing time: 36 ms, primary and auxiliary relays times: 28 ms) [41], the transient stability margins, K_t, presented in Table 4.7 are obtained.

Table 4.7. Transient stability margins

Study Case	Original Case	Reduced Case	Case 5.2.2.1. *a)*	Case 5.2.2.1. *b)*	Case 5.2.2.1. *c)*
t_{CCT} [s]	0.5006	0.497	0.1922	0.4088	0.1927
K_t [p.u.]	0.872	0.871	0.667	0.843	0.668

4.3. Summary

Chapter 4 has presented a study regarding the adequacy of ADG modeling for rotor angle transient stability for TPS studies. It was shown that the computed reduced order models are disturbance dependent. The goal was to produce dynamic equivalents when a short circuit occurred in the connection point between the TPS and the ADG. This is to ensure that the dynamics associated with the DGs and their controllers will be preserved in the reduced model. It was observed that the reduced models of the ADG are disturbance dependent. This was assessed by looking into the disturbance impact index. The main conclusions to be drawn is that the coherency identification among the DGs units is dependent of the fault duration, location and type.

Chapter 5

Dynamic Equivalents of Active Distribution Grids for Rotor Angle Small Signal Stability

The chapter is based on **Publication D**, **E** and **F** *and presents the investigations regarding the model reduction of Active Distribution Grids (ADG) for small signal stability analysis. The Chapter describes the small signal equivalents method. First, the classical method of slow coherency will be investigated for the introduced test ADG. Then, a new method to identify the coherent generators in ADG is presented. Based on this method a dynamic equivalent for the ADG is proposed using a parameter identification approach.*

5.1. Problem statement

The first part of this Chapter introduces a classical method to identify the groups of coherent generators and to aggregate them in equivalent generators. This method is known as the slow coherency and it was introduced in [58]. The method will be investigated further for the test ADG by increasing the complexity of the generators modelling from the electromechanical model to the transient model with excitation system. This is done in order to observe the effect of using more complex generator models and including effect of the excitation system on the slow coherency grouping algorithm.

As is presented in [57], the small signal equivalents (or modal equivalents, as presented by other authors) present the advantage that these equivalents are not dependent on the location, type and magnitude of the disturbance. In order to observe the adequacy of the reduced models a small analysis is performed. The purpose of this analysis is to observe if the reduced model preserve the main oscillatory modes of the original grid. Further in this Chapter a new method is proposed to determine the electromechanical coherency between synchronously based distributed generators. An investigation was conducted in order to observe if the coherency phenomena shows up in the inter−area modes as in TPS. It was observed that these modes are well damped for these particular grids and usually the coherency show up within different modes with higher damped frequencies (corresponding to the local plant modes). As the linear analysis fails to identify the coherent DGs within different oscillation modes, a method based on the time domain decomposition of the state variables for each oscillation mode is proposed. This method allows the computation of the instantaneous Euclidean Distance in polar coordinates. This is done in order to cluster the DG units in a test ADG. In the end of the Chapter the method is extended with a parameter identification algorithm in order to aggregate the DG units from the test ADG.

5.1.1. The Concept of Rotor Angle Small Signal Stability

5.1.1. A) Linearization

As presented in [40] and [41] the power system can be described by the set of algebraic and differential equations, well known as the Differential–Algebraic–Equations (or DAE). The, set of differential equations describe the dynamics associated with the operation of electrical machines and their control devices. As the set of algebraic equations, describes the stator and network equations [41].

This set of equations can be represented as in (5.1) [41]:

$$\begin{cases} \dot{x} = f(x, y, u) \\ 0 = g(x, y, u) \end{cases} \tag{5.1}$$

x – state variables
y – algebraic variables
u – input variables

The linearized form of the system of equations (5.1) around an equilibrium operating point (x_0, u_0) is [41]:

$$\begin{cases} \Delta\dot{x} = \mathbf{A}\Delta x + \mathbf{B}\Delta y \\ 0 = \mathbf{C}\Delta x + \mathbf{D}\Delta y \end{cases} \tag{5.2}$$

where:
A – state matrix
B – input matrix
C – output matrix
D – feed–forward matrix

5.1.1. B) Eigenvalues, Characteristic Equation and Stability

The solutions λ of the **A** matrix is given by the non–trivial solution of the *characteristic equation*:

$$\det(\mathbf{A} - \lambda\mathbf{I}) = 0 \tag{5.3}$$

Equation (5.3) can have ***n*** solutions: $\lambda_1,...,\lambda_n$ which represents the eigenvalues of **A**. The resulting eigenvalues can be real or complex. The complex ones show up in pairs.

Complex eigenvalues show up in conjugate pairs and represents an oscillatory mode. Equation (5.4) presents a complex conjugate pair of eigenvalues:

$$\lambda_{1,2} = \alpha \pm j\Omega \tag{5.4}$$

With the frequency of oscillation in Hz:

$$f = \frac{\Omega}{2\pi} \tag{5.5}$$

And damping ratio in 1/s:

$$\zeta = -\frac{\alpha}{\sqrt{\alpha^2 + \Omega^2}} \tag{5.6}$$

5.1.1. C) Eigenvectors and free motion time response

As presented in [41] for each λ_i eigenvalues a vector $\mathbf{\Phi}_i$ exist which satisfies the following equation:

$$\mathbf{A\Phi} = \lambda\mathbf{\Phi} \tag{5.7}$$

This eigenvectors are called the *right eigenvectors* or the *mode shape* and they give the relative activity of the state variable x_i in the corresponding mode λ_i.

Similarly, left eigenvectors can be defined, $\mathbf{\Psi}_i$:

$$\mathbf{\Psi A} = \mathbf{\Psi}\lambda \tag{5.8}$$

The *left eigenvectors* measures the relative contribution of the state variable x_i in the corresponding mode λ_i.

Using the eigenvalues and right and left eigenvectors, the free motion time response of the system can be written for the *n* modes of oscillation [41]:

$$\Delta x_i(t) = \mathbf{\Phi}_{i,1}\mathbf{\Psi}_{i,1}\Delta x_i(0)e^{\lambda_1 t} + \ldots + \mathbf{\Phi}_{n,1}\mathbf{\Psi}_{n,1}\Delta x_n(0)e^{\lambda_n t} \tag{5.9}$$

In order to make the time response presented in (5.9) real, the eigenvalues and eigenvectors must have appropriate complex values.

5.2. Classical Methods − Slow Coherency Theory

As presented in Section 5.1, small signal equivalents are used to produce a reduced order model and present the advantage that their computation is not dependent by the location, duration and magnitude of the disturbance, as for the equivalent used in transient stability. All of these methods of small signal equivalence techniques are based on the modal analysis results: eigenvalues and eigenvectors.

In this Section the theory of slow coherency will be presented to observe how suitable this method is to produce small signal equivalent for ADGs. Further it will be investigated how the slow coherency grouping algorithm is affected by increasing the model complexity of the generator and by including the excitation system.

The theory of slow coherency was developed by Dr. Joe Chow and is described in detail in [59] and [60].

As presented in [59], a group of generators is considered slow coherent when they are swinging against other groups of generators with respect to the slower inter−area modes. The singular perturbation method is used in [58] to produce the separation of the time scale of the slow variables (corresponding to the slow inter−area modes) from the faster (corresponding to the local modes of oscillation within the areas).

5.2.1. Slow Coherency Theory. Generalities

The slow coherency concept involves two time scales, one of the slower inter−area modes, and the second of the higher frequency local modes. The slow coherency is defined in [58], as in the following.

Definition: According to [58], if $\lambda_1,...,\lambda_r$ are the slowest r modes of the system response, then the i^{th} machine and the j^{th} machine are slowly coherent if the difference of their angles $x_i(t)$ and $x_j(t)$, defined as:

$$x_i(t) - x_j(t) = z_{ij}(t) \tag{5.10}$$

do not include any of the r slowest modes.

In this case, the slow inter−area dynamics and the fast intra−area dynamics are suitable for two time scale analysis using the singular perturbation method, as presented in the same reference [58]. This method can be applied to the systems in the *state separable form*:

$$\begin{cases} \dfrac{d\xi}{dt} = f(\xi, \eta, t) \\ \varepsilon \dfrac{d\eta}{dt} = g(\xi, \eta, t) \end{cases} \tag{5.11}$$

Where: ξ − represent the ″slow″ states and η − represent the ″fast″ ones.

With $\varepsilon = 0$ the separation between the two time scales will be large, then the system (5.11) becomes [58]:

$$\begin{cases} \dfrac{d\xi}{dt} = \mathrm{f}(\xi, \eta, \mathrm{t}) \\ 0 = \mathrm{g}(\xi, \eta, \mathrm{t}) \end{cases} \tag{5.12}$$

As presented by the same author system models don't always appear in this form, therefore a transformation of the state variables needs to be done in order to obtain a system in the form of (5.12).

In the following some definitions are presented, which later will be used to describe the grouping algorithm proposed by the authors in [58] and [59].

5.2.1.1. Ideal decomposable and non−exact decomposable *r* systems

According to [58], an **ideal decomposable *r* system** is defined as: *"a system in which the slow coherency is exact and the number of coherent areas is equal to the number of slow modes"*. This definition is expressed by (5.10).

If there is a small contribution of the slower modes in (5.10), then this system can be defined as a non−exact decomposable *r* system.

5.2.1.2. Reference and non−reference set of machines. Grouping matrix

In [58], an example is presented in order to define the reference and non−reference set of machines and the grouping matrix. By using an arbitrary selection of the reference machines angles (components of a *r*-vector x^1) and of the non−reference ones (components of a *r*-vector x^2), a grouping matrix can be defined as L_g (of dimensions (n-r)x(r), with n being the total number of machines angles). This matrix is used to assign machines to areas and it will have the same number of columns in x^2 as the number of machines in x^1 [58]. Using this, it can be said that the machine x_j^1 is slow coherent with x_i^2 if the (i,j) entry in L_g is 1.

Example *In* [58] *is presented an example which illustrates how the L_g matrix is produced for a three area−five machine system*

$$L_g = \begin{array}{c} \\ x_1 \\ x_4 \end{array} \begin{array}{c} \begin{array}{ccc} x_2 & x_3 & x_5 \end{array} \\ \begin{bmatrix} 0 & 0 & 1 \\ 1 & 0 & 0 \end{bmatrix} \end{array} \tag{5.13}$$

This can be translated into that: the machine corresponding to x_1 is from the same slow coherent area as x_5. Using the L_g matrix, (5.10) can be rewritten as:

$$x^2(t) - L_g x^1(t) = z^2(t) \tag{5.14}$$

Where $z^2(t)$ are the corresponding functions $z_{ij}(t)$ and are defined as:

$$z^2(t) = \begin{bmatrix} x_1 - x_5 \\ x_4 - x_2 \end{bmatrix} \tag{5.15}$$

With the particular transformation of coordinates, (5.14) can be rewritten as (with L not necessarily a grouping matrix) [58]*:*

$$\begin{bmatrix} x^1 \\ z^2 \end{bmatrix} = \begin{bmatrix} I & 0 \\ -L & I \end{bmatrix} \begin{bmatrix} x^1 \\ x^2 \end{bmatrix} \tag{5.16}$$

More of the general transformation of coordinates can be found in [58].

5.2.2. Slow Coherency Grouping Algorithm

In [58] and [59] the grouping algorithm for identification of the slow coherent areas, is presented for a non−exactly *r* decomposable systems. As presented above for these type of systems, (5.10) is approximately satisfied, meaning that there are some small contributions to the $z_{ij}(t)$. Resulting from this it can be concluded that i^{th} and j^{th} are near−coherent [58]. As presented in [59], the scope of the slow coherency grouping algorithm is to find the L_d matrix which will be approximate in the form of L_g. Where L_d is the dichotomic matrix solution of Ricatti equation $R(L)$=0.

<u>STEP 1.</u> The computation of the *V* basis for the sub−matrix A_ω (A_ω defined further in Section 5.3)

Geometric representation
As presented in [58], considering *V* a (*n*x*r*) general matrix representing the basis of the eigensubspace *V* corresponding to the slow modes of A_ω (A_ω defined in the next Section 5.3 being a sub−matrix of the system matrix *A*):

$$V = \begin{bmatrix} V_1 \\ V_2 \end{bmatrix} \tag{5.17}$$

where V_1 (dimensions *r*x*r*) represents a submatrix of *V*.
Then,

$$L_d = L_g = V_2 V_1^{-1} \tag{5.18}$$

represents the only solution of the Ricatti equation *R(L)*. Submatrix V_1 is non−singular if no machines from the same area are in x^1. If V_1 is singular, L_d does not exist and these represent the advantage of this grouping algorithm: two reference machines cannot be allocated to the same coherent area.

In order to find the near−coherent areas, one has to find the *r* ″most linearly independent vectors″. With the matrix *V* rearranged as submatrix V_1 containing the row vectors corresponding to the reference machine (5.17), it can be re−written:

$$VV_1^{-1} = \begin{bmatrix} I \\ L_d \end{bmatrix} \tag{5.19}$$

As presented in [58], in each row of L_d the entries can show up as:

- close to 1 which corresponds to the projection of the vector on the corresponding reference vector
- close to 0 which corresponds to the projection of the vector on the other reference vectors

STEP 2. Gaussian elimination of *V*

To find the most *r* linear independent row vectors (used further as reference rows) a Gaussian elimination, with complete pivoting of *V* is applied [59].

STEP 3. Computation of L_d

Computing V_1 from above, the L_d is found using :

$$V_1^T L_d^T = V_2^T \tag{5.20}$$

STEP 4. LU decomposition of V_1 and approximation of L_d by an L_g

In the final step a LU decomposition of V_1 is produced and the grouping matrix L_g (having just 0 and 1 values) is approximated based on the resulting L_d.

Next, the algorithm of slow coherency grouping will be applied for the reduced system matrix $\mathbf{A}_\omega$ of the test ADG. In the following it is described how to compute the reduced system matrix $\mathbf{A}_\omega$ for different models of synchronous generators.

5.3. Electromechanical Models of Multi−Machine Active Distribution Grids

In this Sub−Chapter these different models to represent a multi machine ADG will be described the ″classical″, transient and transient with excitation system models.

5.3.1. Electromechanical (or ″Classical″) Model of Multi−Machine Active Distribution Grids

As presented in [61] and [62] the multi−machine model is the simplest one to represent the power system dynamics. This model was generally used in the slow coherency grouping algorithm and is represented by the two electromechanical equations:

$$\begin{cases} M_i\dot{\omega}_i = P_{m,i} - P_{e,i} - D_i\omega_i & (5.21.a) \\ \dot{\delta}_i = \omega_0\omega_i & (5.21.b) \end{cases}$$

Where the electrical output of each of generator is defined as:

$$P_{e,i} = \sum_{\substack{j=1 \\ j\neq i}}^{N} E_i'E_j'\left[B_{ij}^{red}\sin\left(\delta_i - \delta_j\right)\right] + E_i'G_{ii}^{red\ 2} \tag{5.22}$$

With $i = \overline{1,N}$ and:

E_i' −the voltage behind the transient reactance (assumed constant)

G_{ii}^{red} and B_{ij}^{red} are the real and imaginary parts of the reduced Y_{red} matrix to the internal nodes of the generators.

Linearizing (5.21) and (5.22) around the equilibrium point $\left(\delta_i^{(0)},\omega_i^{(0)}\right)$ with [63]:

$$\begin{cases} \Delta\dot{\delta}_i = \delta_i - \delta_i^{(0)} & (5.23.a) \\ \Delta\dot{\omega}_i = \omega_i - \omega_i^{(0)} & (5.23.b) \end{cases}$$

The system of equations (5.21) becomes (considering $\Delta P_{m,i}$=0), considering n_g generators:

$$\begin{cases} \Delta\dot{\delta}_i = \Omega\Delta\omega_i & (5.24.a) \\ \Delta\dot{\omega}_i = \dfrac{1}{M_i}\left[\Delta P_{e,i} - D_i\Delta\omega_i\right] & (5.24.b) \end{cases}$$

Where $\Delta P_{e,i}$ are commonly known as the ″synchronizing coefficients″ given by:

$$\Delta P_{e,i} = \sum_{j\in n_g}\frac{\partial P_{e,i}}{\partial\delta_j}\Delta\delta_j \quad , \quad i = \overline{1,n_g} \tag{5.25}$$

(5.25) can be expanded into:

$$K_{S,ij} = \Delta P_{e,ij} = \begin{cases} \dfrac{\partial P_{e,i}}{\partial \delta_j} = E_i' E_j' B_{ij}^{red} \cos\left(\delta_i - \delta_j\right), & i, j = \overline{1, n_g}, i \neq j \\ \dfrac{\partial P_{e,i}}{\partial \delta_i} = -\sum\limits_{\substack{j \in n_g \\ j \neq i}} \dfrac{\partial P_{e,i}}{\partial \delta_j} & , \ i = \overline{1, n_g} \end{cases} \tag{5.26}$$

As presented in [63], a state space representation can be defined by introducing the following notations:

$$\begin{aligned} &\boldsymbol{\Delta\dot{\delta}} = \left[\Delta\delta_1 ... \Delta\delta_{n_g}\right]^T, \left(n_g \times 1\right) \\ &\boldsymbol{\Delta\dot{\omega}} = \left[\Delta\omega_1 ... \Delta\omega_{n_g}\right]^T, \left(n_g \times 1\right) \\ &\mathbf{M}^{-1} = diag\left(\frac{1}{2H_i}\right), \left(n_g \times n_g\right) \qquad \begin{matrix} i = \overline{1, n_g} \\ j = \overline{1, n_g} \end{matrix} \\ &\mathbf{D} = diag\left(D_i\right), \left(n_g \times n_g\right) \\ &\boldsymbol{\Delta P_e} = \left[\Delta P_{e,ij}\right], \left(n_g \times n_g\right) \end{aligned} \tag{5.27}$$

Using (5.24) a state space model can be derived as in [64]:

$$\underbrace{\begin{bmatrix} \boldsymbol{\Delta\dot{\delta}} \\ \boldsymbol{\Delta\dot{\omega}} \end{bmatrix}}_{\dot{\mathbf{x}}} = \underbrace{\begin{bmatrix} 0 & \Omega\mathbf{I}_{\left(n_g \times n_g\right)} \\ \mathbf{M}^{-1}\boldsymbol{\Delta P_e} & \mathbf{M}^{-1}\mathbf{D} \end{bmatrix}}_{\bar{\mathbf{A}}} \underbrace{\begin{bmatrix} \boldsymbol{\Delta\delta} \\ \boldsymbol{\Delta\omega} \end{bmatrix}}_{\mathbf{x}} \tag{5.28}$$

The reference names this model as the electromechanical model with damping and $\bar{\mathbf{A}}$ the state matrix with damping.
If $\boldsymbol{D} \simeq 0$ the electromechanical model without damping becomes [62] [65]:

$$\underbrace{\begin{bmatrix} \boldsymbol{\Delta\dot{\delta}} \\ \boldsymbol{\Delta\dot{\omega}} \end{bmatrix}}_{\dot{\mathbf{x}}} = \underbrace{\begin{bmatrix} 0 & \Omega\mathbf{I}_{\left(n_g \times n_g\right)} \\ \mathbf{M}^{-1}\boldsymbol{\Delta P_e} & 0 \end{bmatrix}}_{\bar{\mathbf{A}}} \underbrace{\begin{bmatrix} \boldsymbol{\Delta\delta} \\ \boldsymbol{\Delta\omega} \end{bmatrix}}_{\mathbf{x}} \tag{5.29}$$

In the first part of this work the purpose is to study the slow coherency grouping for the reduced matrix $\mathbf{A}_\omega$, defined by:

$$\mathbf{A}_\omega = \mathbf{M}^{-1}\boldsymbol{\Delta P_e} \tag{5.30}$$

5.3.2. Transient Model of Multi−Machine Power Systems

In the previous Section the ″classical″ or electromechanical model of the synchronous generators was used to compute the reduced system matrix $\mathbf{A}_\omega$. As this model does not represent the rotor dynamics, it can be assumed that grouping of DGs by the slow coherency algorithm can produce slightly different areas compared to more detailed models. Therefore, this Section presents the transient model for small signal analysis of a multi−machine ADGs with high penetration of DG units. The model is presented in [64].

The reference [64] describes two formulations of the small signal multi−machine model:

1. using the current balance form of the network equations, also known as the EPRI approach
2. using the power balance form of the network equations, also known as the Generalized Heffron−Phillips model

In the following, the second formulation will be considered for the presentation of the transient small signal multi−machine of ADGs.

In this model the synchronous machine is represented as a two axis model with a field winding on the direct axis and a damper winding on the quadrature axis.

The electrical and mechanical dynamic equations for the two axis model are described in the following, (correspondent to each i^{th} machine, $i=\overline{1,m}$ with m being the number of machines).

The mechanical dynamic equations are the same as 5.21:

$$\begin{cases} M_i\dot{\omega}_i = P_{m,i} - P_{e,i} - D_i\omega_i & (5.31.a) \\ \dot{\delta}_i = \omega_0\omega_i & (5.31.b) \end{cases}$$

The electrical dynamic equations are:

$$\begin{cases} T'_{d0,i}\dot{E}'_{q,i} = -E'_{q,i} - \left(X_{d,i} - X'_{d,i}\right)I_{d,i} + E_{fd,i} & (5.32.a) \\ T'_{q0,i}\dot{E}'_{d,i} = -E'_{d,i} + \left(X_{q,i} - X'_{q,i}\right)I_{q,i} & (5.32.b) \end{cases}$$

Or in a general form (5.31) and (5.32) becomes:

$$\begin{cases} \mathbf{M}\dot{\boldsymbol{\omega}} = \mathbf{P}_m - \mathbf{P}_e - \mathbf{D}\boldsymbol{\omega} & (5.33.a) \\ \dot{\boldsymbol{\delta}} = \Omega\boldsymbol{\omega} & (5.33.b) \end{cases}$$

$$\begin{cases} \mathbf{T}'_{d0}\dot{\mathbf{E}}'_q = -\mathbf{E}'_q - \left(\mathbf{X}_d - \mathbf{X}'_d\right)\mathbf{I}_d + \mathbf{E}_{fd} & (5.34.a) \\ \mathbf{T}'_{q0}\dot{\mathbf{E}}'_d = -\mathbf{E}'_d + \left(\mathbf{X}_q - \mathbf{X}'_q\right)\mathbf{I}_q & (5.34.b) \end{cases}$$

Where:

$$
\begin{aligned}
&\boldsymbol{\Delta\dot{\delta}} = \left[\Delta\dot{\delta}_1 ... \Delta\dot{\delta}_{n_g}\right]^T, \left(n_g \times 1\right) \\
&\boldsymbol{\Delta\dot{\omega}} = \left[\Delta\dot{\omega}_1 ... \Delta\dot{\omega}_{n_g}\right]^T, \left(n_g \times 1\right) \\
&\boldsymbol{\Delta\dot{E}'_q} = \left[\Delta\dot{E}'_{q,1} ... \Delta\dot{E}'_{q,n}\right]^T, \left(n_g \times 1\right) \\
&\boldsymbol{\Delta\dot{E}'_d} = \left[\Delta\dot{E}'_{d,1} ... \Delta\dot{E}'_{d,n}\right]^T, \left(n_g \times 1\right) \qquad i = \overline{1, n_g} \\
&\mathbf{M}^{-1} = diag\left(\frac{1}{2H_i}\right), \left(n_g \times n_g\right) \qquad j = \overline{1, n_g} \\
&\mathbf{D} = diag\left(D_i\right), \left(n_g \times n_g\right) \\
&\boldsymbol{\Delta P_e} = \left[\Delta P_{e,ij}\right], \left(n_g \times n_g\right)
\end{aligned}
\tag{5.35}
$$

The electrical power output $P_{e,i}$ is defined by:

$$
P_{e,i} = E'_{d,i} I_{d,i} + E'_{q,i} I_{q,i} - \left(X'_{d,i} - X'_{q,i}\right) I_{d,i} I_{q,i} \tag{5.36}
$$

(S1) Simplification 1:

For small time constants $T'_{d0,i}$, $E'_{d,i}$ becomes very fast and (5.34.b) becomes and algebraic equation:

$$
E'_{d,i} = \left(X_{q,i} - X'_{q,i}\right) I_{q,i} \tag{5.37}
$$

With ***Simplification 1***, the dynamic equations becomes (general form):

$$
\begin{cases}
\mathbf{M\dot{\omega}} = \mathbf{P_m} - \mathbf{P_e} - \mathbf{D\omega} & \text{(5.38.a)} \\
\dot{\boldsymbol{\delta}} = \boldsymbol{\omega}_0 \boldsymbol{\omega} & \text{(5.38.b)}
\end{cases}
$$

And

$$
\mathbf{T'_{d0}\dot{E}'_q} = -\mathbf{E}'_q - \left(\mathbf{X_d} - \mathbf{X}'_d\right)\mathbf{I_d} + \mathbf{E}_{fd} \tag{5.39}
$$

The stator algebraic equations becomes:

$$
\begin{cases}
U_i \sin\left(\delta_i - \theta_i\right) + R_{a,i} I_{d,i} - X_{q,i} I_{q,i} = 0 \\
E'_{q,i} - U_i \cos\left(\delta_i - \theta_i\right) - R_{a,i} I_{q,i} - X'_{q,i} I_{d,i} = 0
\end{cases} \tag{5.40}
$$

The stator algebraic equations are written with the following notations:

$$
\begin{cases}
U_{d,i} = U_i \sin\left(\delta_i - \theta_i\right) \\
U_{q,i} = U_i \cos\left(\delta_i - \theta_i\right)
\end{cases} \tag{5.41}
$$

Network equations are represented using the power balance form (the balance of real and reactive power at the generator buses) [64]:

$$\begin{cases} I_{d,i}U_i\sin(\delta_i-\theta_i)+I_{q,i}U_i\cos(\delta_i-\theta_i)+P_{L,i}(U_i) \\ \qquad -\sum_{k=1}^{n}U_iU_kY_{ik}\cos(\theta_i-\theta_k-\alpha_{ik})=0 \\ I_{d,i}U_i\cos(\delta_i-\theta_i)-I_{q,i}U_i\sin(\delta_i-\theta_i)+Q_{L,i}(U_i) \\ \qquad -\sum_{k=1}^{n}U_iU_kY_{ik}\sin(\theta_i-\theta_k-\alpha_{ik})=0 \end{cases}, i=\overline{1,m} \tag{5.42}$$

And:

$$\begin{cases} P_{L,i}(U_i)-\sum_{k=1}^{n}U_iU_kY_{ik}\cos(\theta_i-\theta_k-\alpha_{ik})=0 \\ Q_{L,i}(U_i)-\sum_{k=1}^{n}U_iU_kY_{ik}\sin(\theta_i-\theta_k-\alpha_{ik})=0 \end{cases}, i=\overline{m+1,n} \tag{5.43}$$

$\Rightarrow$ The model corresponding from (5.30) to (5.39) without the equation of the excitation system will be mention further as the transient model of the multi−machine ADGs.

As the set of variables presented in (5.36), is not adequate for the future investigation of effects of field circuit dynamics excitation and excitation system, (5.39) can be rewritten in terms of field flux and inductances (according to the references [41] and [49]).

This is needed as the simulation environment uses the approach described in [41] and the following set of variables to model the synchronous generators.

The complete set of variables to model the synchronous generator according to [41] is:

$$\left[\omega,\delta,\psi_{fd},\psi_{1d},\psi_{1q},\psi_{2q}\right] \tag{5.44}$$

The signification of each variable is presented in the List of Symbols.

In order to obtain the adequate model of representation of the synchronous generator (for considering the effects of synchronous machine field dynamics), (5.34.a) can be simplified by introducing the following notations:

The emf $E'_{q,i}$ behind the transient reactance $X'_{d,i}$ for each of the i^{th} machine is defined as [45]:

$$E'_{q,i}=\omega_0\frac{L_{ads,i}}{L_{fd,i}}\psi_{fd,i} \tag{5.45}$$

Where:

$L_{fd,i}$ −inductance of the excitation winding *fd*

Considering $U_{q,i}$ defined by:

$$U_{q,i}\cong\omega_0\psi_{d,i} \tag{5.46}$$

And as:

$$\psi_{d,i} = -L_{d,i} I_{d,i} + L_{md,i} I_{f,i} \tag{5.47}$$

Results:

$$U_{q,i} \cong -\omega_0 L_{d,i} I_{d,i} + \omega_0 L_{md,i} I_{f,i} = -X_{d,i} I_{d,i} + E_{Iq,i} \tag{5.48}$$

For open−circuit operation $I_{d,i} = I_{q,i} = 0$

$$E_{Iq,i} = U_{q,i} \cong \omega_0 L_{md,i} I_{f,i} \tag{5.49}$$

In the transient operation, $U_{q,i}$ equals:

$$U_{q,i} = -X'_{d,i} I_{d,i} + E'_{q,i} \tag{5.50}$$

From (5.48) and (5.50) results:

$$E_{Iq,i} = \left(X_{d,i} - X'_{d,i}\right) I_{d,i} + E'_{q,i} \tag{5.51}$$

Considering (5.51), (5.31.a) can be rewritten as:

$$\dot{E}'_{q,i} = \frac{-E'_{q,i} - \left(X_{d,i} - X'_{d,i}\right) I_{d,i} + E_{fd,i}}{T'_{d0,i}} \tag{5.52}$$

Or

$$\dot{E}'_{q,i} = \frac{E_{fd,i} - E_{Iq,i}}{T'_{d0,i}} \tag{5.53}$$

Considering (5.46), (5.50) and that $T'_{d0,i}$ is defined as:

$$T'_{d0,i} = \frac{L_{fd}}{R_{fd}} \tag{5.54}$$

Then (5.53) which describe the dynamics of the excitation flux, can be simplified to:

$$\dot{\psi}_{fd,i} = \omega_0 \left(E_{fd,i} - R_{fd,i} I_{fd,i}\right) \tag{5.55}$$

$R_{fd,i}$ −resistance of the excitation winding *fd*

Or in a general manner for all *n* machines:

$$\dot{\boldsymbol{\Psi}}_{fd} = \boldsymbol{\omega}_0 \left(\mathbf{E}_{fd} - \mathbf{R}_{fd} \mathbf{I}_{fd}\right) \tag{5.56}$$

5.3.2.1. Effect of the field flux linkage on the synchronizing torque

In this Sub–Section the steps to compute the synchronizing torques $\mathbf{\Delta P}_e = \left[\Delta P_{e,ij}\right], \left(n_g \times n_g\right)$ are presented, included the effect of field flux variations. The theory behind this phenomenon is detailed in [41] and resumed as in the following.

(S2) Simplification 2:
The amortisseur effects are neglected
(S3) Simplification 3:
The machines are operated with constant field voltage
(S4) Simplification 4:
At ω_r=1 [p.u.] P_e= T_e.
(S5) Simplification 5:
A constant mechanical power/torque is considered (ΔP_m= ΔT_m=0*).*

The set of state variables in this case is:

$$\begin{matrix}\left[\omega_i, \delta_i, \psi_{fd,i}\right] \\ \left(\dot{\omega}_i, \dot{\delta}_i, \dot{\psi}_{fd,i}, \dot{\nu}_i\right) \\ \left(\dot{\omega}_i, \dot{\delta}_i\right)\end{matrix} \tag{5.57}$$

By linearizing the set of equations (5.38) to (5.56) (by considering $\omega_0 = 1\text{p.u.}$ then $P_e = T_e$) with this, the following linearized equations can be written (in a matrix form), as presented in [41] for each machine:

$$\begin{bmatrix} \Delta\dot{\omega}_i \\ \Delta\dot{\delta}_i \\ \Delta\dot{\psi}_{fd,i} \end{bmatrix} = \begin{bmatrix} a_{11,i} & a_{12,i} & a_{13,i} \\ a_{21,i} & 0 & 0 \\ 0 & a_{32,i} & a_{33,i} \end{bmatrix} \begin{bmatrix} \Delta\omega_i \\ \Delta\delta_i \\ \Delta\psi_{fd,i} \end{bmatrix} + \begin{bmatrix} b_{11,i} & 0 \\ 0 & 0 \\ 0 & b_{32,i} \end{bmatrix} \begin{bmatrix} \Delta T_{m,i} \\ \Delta E_{fd,i} \end{bmatrix} \tag{5.58}$$

The linearization constants $\left[a_{11,i}, a_{12,i}, a_{13,i}, a_{21,i}, a_{32,i}, a_{33,i}\right]$ and $\left[b_{11,i}, b_{32,i}\right]$ are defined as in [41].

By linearizing the stator algebraic equation (5.42) it can be observed that:

$$\Delta I_{d,i} = f\left(\Delta\delta_i, \Delta\psi_{fd,i}\right) = \alpha_{\delta_i}\Delta\delta_i + \alpha_{\psi_{fd,i}}\Delta\psi_{fd,i} \tag{5.59}$$

Where: α_{δ_i} –linearization constant due $\Delta\delta_i$

$\alpha_{\psi_{fd,i}}$ –linearization constant due $\Delta\psi_{fd,i}$

These linearization constants can be obtained as presented in [41].

Inserting the definition of $\Delta I_{d,i}$ in the network equations (5.44), it can be observed that square matrices can be calculated between each *i* and *j* machines, as the form of:

$$\mathbf{A}_{11}=\left[a_{11}\right]_{(ij)}=\begin{bmatrix} a_{11,11} & \cdots & a_{11,1m} \\ \vdots & \ddots & \vdots \\ a_{11,n1} & \cdots & a_{11,nm} \end{bmatrix} i=\overline{1,n},\ j=\overline{1,m} \tag{5.60}$$

In a generalized manner, (5.60) can be rewritten as:

$$\begin{bmatrix} \Delta\dot{\omega} \\ \Delta\dot{\delta} \\ \Delta\dot{\Psi}_{fd} \end{bmatrix}=\begin{bmatrix} \mathbf{A}_{11} & \mathbf{A}_{12} & \mathbf{A}_{13} \\ \mathbf{A}_{21} & 0 & 0 \\ 0 & \mathbf{A}_{32} & \mathbf{A}_{33} \end{bmatrix}\begin{bmatrix} \Delta\omega \\ \Delta\delta \\ \Delta\Psi_{fd} \end{bmatrix}+\begin{bmatrix} \mathbf{B}_{11} & 0 \\ 0 & 0 \\ 0 & \mathbf{B}_{32} \end{bmatrix}\begin{bmatrix} \Delta\mathbf{T}_m \\ \Delta\mathbf{E}_{fd} \end{bmatrix} \tag{5.61}$$

From the above equations the next linearization constants can be written as they are defined in [41] by using a generalized manner:

$$\mathbf{K}_1=-\mathbf{M}\mathbf{A}_{12} \tag{5.62}$$

$$\mathbf{K}_2=-\mathbf{M}\mathbf{A}_{13} \tag{5.63}$$

$$\mathbf{K}_3=-\frac{\mathbf{B}_{32}}{\mathbf{A}_{33}} \tag{5.64}$$

$$\mathbf{K}_4=-\frac{\mathbf{A}_{32}}{\mathbf{B}_{32}} \tag{5.65}$$

$$\mathbf{T}_3=-\frac{\mathbf{I}}{\mathbf{A}_{33}} \tag{5.66}$$

With these constants of linearization, the block diagram representation with constant E_{fd} of the synchronous machines can be presented as shown in Figure 5.1.

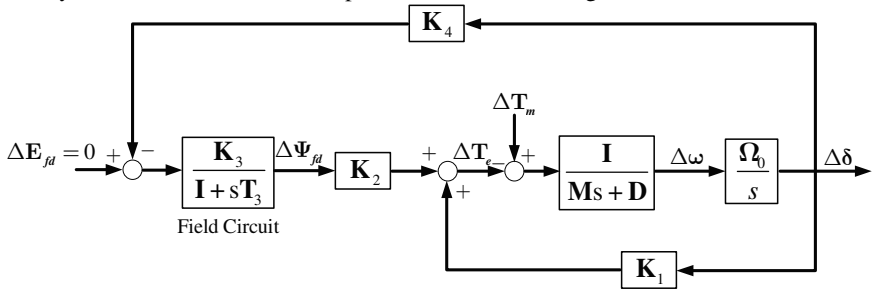

Figure 5.1. Generalized block diagram representation with constant E_{fd} [41].

As presented in Figure 5.1 and according to [41], the field flux variations are caused by variations of the rotor angle feedback, through the linearization constant K_4.

According to [41], the changes in ΔT_e due to $\Delta\psi_{fd}$ cause by $\Delta\delta$ can be expressed as, for the i^{th} machine:

$$\left.\frac{\Delta T_{e,i}}{\Delta\delta_i}\right|_{due\ to\ \Delta\psi_{fd}} = \frac{K_{2,i}K_{3,i}K_{4,i}}{1+sT_{3,i}} \tag{5.67}$$

For $s=j\omega=0$, a steady state limit can be defined [41] from:

$$\Delta P_{e,i} = \Delta T_{e,i}\Big|_{due\ to\ \Delta\psi_{fd}} = -K_{2,i}K_{3,i}K_{4,i}\Delta\delta_i \tag{5.68}$$

This limit is:

$$K_{2,i}K_{3,i}K_{4,i} = K_{1,i} \tag{5.69}$$

In [41] the contribution of $\Delta\psi_{fd}$ to the synchronizing and damping torque components depending on the oscillating frequency is described.

For the interest in this work is the total steady–state synchronizing torque coefficient, taking into consideration the effect of field flux linkage, this can be defined for each i^{th} machine as [41]:

$$K_{S,ij}\Big|_{due\ to\ \Delta\psi_{fd}} = \Delta P_{e,ij}\Big|_{due\ to\ \Delta\psi_{fd}} = K_{1,ij} - K_{2,ij}K_{3,ij}K_{4,ij} \tag{5.70}$$

Therefore, a similar matrix as the one defined in (5.29) can be obtained in a generalized manner:

$$\mathbf{A}_{\omega} = \mathbf{K}_1 - \mathbf{K}_2\mathbf{K}_3\mathbf{K}_4 \tag{5.71}$$

According to the same author, the overall impact, over the synchronizing torques, by considering the effect of field flux linkage, is to: ″reduce slightly the synchronizing torques component and to increase the damping torques component″ [41].

5.3.2.2. Effect of the excitation system on the synchronizing torque

In order to observe the impact of the excitation system on the slow coherency identification, the machine model is completed with the one of the excitation systems. In this case, a thyristor excitation system (or the IEEE ST1A model [54]) is considered. This model will replace the IEEE ESAC8B model used to describe the AVR in Chapter 4.

As presented in [41], the system is represented by a high exciter gain K_A (without transient gain reduction or derivative feedback) and a voltage transducer with the time constant T_R. Figure 5.2 presents the macro–blocks of this excitation system.

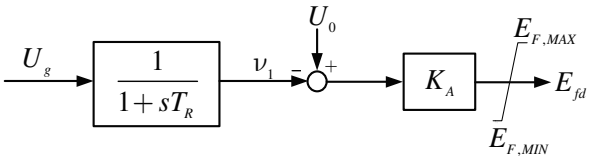

Figure 5.2. A simplified excitation system model.

In this Sub-Section the set of equations (5.30–5.57) is extended so that the equations describing the dynamics of the excitation system are included. The main scope is to observe how the synchronizing torque definition is impacted by the linearizing constants which results from this model extension.

The new state variables are:

$$\left[\omega_i, \delta_i, \psi_{fd,i}, \nu_i\right] \tag{5.72}$$

The excitation system dynamic equation is given by:

$$T_{A,i}\dot{\nu}_i = -E_{fd,i} + K_{A,i}\left(U_{0,i} - U_{g,i}\right) \tag{5.73}$$

Or in a general formulation:

$$\mathbf{T_A}\dot{\mathbf{N}} = -\mathbf{E_{fd}} + \mathbf{K_A}\left(\mathbf{U}_0 - \mathbf{U_g}\right) \tag{5.74}$$

Where:

$$\begin{aligned}
&\boldsymbol{\Delta\dot{\delta}} = \left[\Delta\dot{\delta}_1 ... \Delta\dot{\delta}_{n_g}\right]^T, \left(n_g \times 1\right) \\
&\boldsymbol{\Delta\dot{\omega}} = \left[\Delta\dot{\omega}_1 ... \Delta\dot{\omega}_{n_g}\right]^T, \left(n_g \times 1\right) \\
&\boldsymbol{\Delta\dot{\Psi}_{fd}} = \left[\Delta\dot{\psi}_{fd,1} ... \Delta\dot{\psi}_{fd,n}\right]^T, \left(n_g \times 1\right) \\
&\boldsymbol{\Delta\dot{N}} = \left[\Delta\dot{\nu}_1 ... \Delta\dot{\nu}_n\right]^T, \left(n_g \times 1\right) \qquad i = \overline{1, n_g} \\
&\mathbf{M}^{-1} = diag\left(\frac{1}{2H_i}\right), \left(n_g \times n_g\right) \qquad j = \overline{1, n_g} \\
&\mathbf{D} = diag\left(D_i\right), \left(n_g \times n_g\right) \\
&\boldsymbol{\Delta P_e} = \left[\Delta P_{e,ij}\right], \left(n_g \times n_g\right)
\end{aligned} \tag{5.75}$$

⇒ The model corresponding from (5.39) to (5.41) without the equation of the excitation system will further be mentioned as the transient model with the excitation system of the multi–machine ADGs.

As presented in [41] by considering the excitation system equation, the system presented in (5.39, 5.58 and 5.41) can be linearized and have the following form:

$$\begin{bmatrix} \Delta\dot{\omega}_i \\ \Delta\dot{\delta}_i \\ \Delta\dot{\psi}_{fd,i} \\ \Delta\dot{\nu}_i \end{bmatrix} = \begin{bmatrix} a_{11,i} & a_{12,i} & a_{13,i} & 0 \\ a_{21,i} & 0 & 0 & 0 \\ 0 & a_{32,i} & a_{33,i} & a_{34,i} \\ 0 & a_{42,i} & a_{43,i} & a_{44,i} \end{bmatrix} \begin{bmatrix} \Delta\omega_i \\ \Delta\delta_i \\ \Delta\psi_{fd,i} \\ \Delta\nu_i \end{bmatrix} + \begin{bmatrix} b_{11,i} \\ 0 \\ 0 \\ 0 \end{bmatrix} \left[\Delta T_{m,i}\right] \tag{5.76}$$

The rest of the linearization constants $\left[a_{34,i}, a_{42,i}, a_{43,i}, a_{44,i}\right]$ can be calculated as in [41].

Again, by linearizing the stator algebraic equation (5.42) it can be observed that:

$$\Delta I_{d,i} = f\left(\Delta\delta_i, \Delta\psi_{fd,i}, \Delta\nu_i\right) = \alpha_{\delta,i}\Delta\delta_i + \alpha_{\psi_{fd,i}}\Delta\psi_{fd,i} + \alpha_{\nu_i}\Delta\nu_i \tag{5.77}$$

Where: α_{δ_i} –linearization constant due $\Delta\delta_i$

$\alpha_{\psi_{fd,i}}$ –linearization constant due $\Delta\psi_{fd,i}$

α_{ν_i} –linearization constant due $\Delta\nu_i$

As in Sub–Section 5.3.2, the equations (5.76) can be written in a generalized manner:

$$\begin{bmatrix} \Delta\dot{\boldsymbol{\omega}} \\ \Delta\dot{\boldsymbol{\delta}} \\ \Delta\dot{\boldsymbol{\Psi}}_{fd} \\ \Delta\dot{\mathbf{N}} \end{bmatrix} = \begin{bmatrix} \mathbf{A}_{11} & \mathbf{A}_{12} & \mathbf{A}_{13} & 0 \\ \mathbf{A}_{21} & 0 & 0 & 0 \\ 0 & \mathbf{A}_{32} & \mathbf{A}_{33} & \mathbf{A}_{34} \\ 0 & \mathbf{A}_{42} & \mathbf{A}_{43} & \mathbf{A}_{44} \end{bmatrix} \begin{bmatrix} \Delta\boldsymbol{\omega} \\ \Delta\boldsymbol{\delta} \\ \Delta\boldsymbol{\Psi}_{fd} \\ \Delta\mathbf{N} \end{bmatrix} + \begin{bmatrix} \mathbf{B}_{11} \\ 0 \\ 0 \\ 0 \end{bmatrix} \left[\Delta\mathbf{T}_m\right] \tag{5.78}$$

In addition to the linearization constants presented above (in Sub–Section 5.3.2), two others must be defined, in order to obtain the block diagram scheme.

$$\mathbf{K}_5 = \mathbf{A}_{42}\mathbf{T}_R \tag{5.79}$$

And

$$\mathbf{K}_6 = \mathbf{A}_{43}\mathbf{T}_R \tag{5.80}$$

Where: $\mathbf{T}_R = diag\left(T_{R,i}\right)$–diagonal matrix representing the time constant of the voltage transducer for each *i* excitation system.

With the definition of the new linearization constants, the extended and generalized block diagram can be presented as in Figure 5.3, according to [41]:

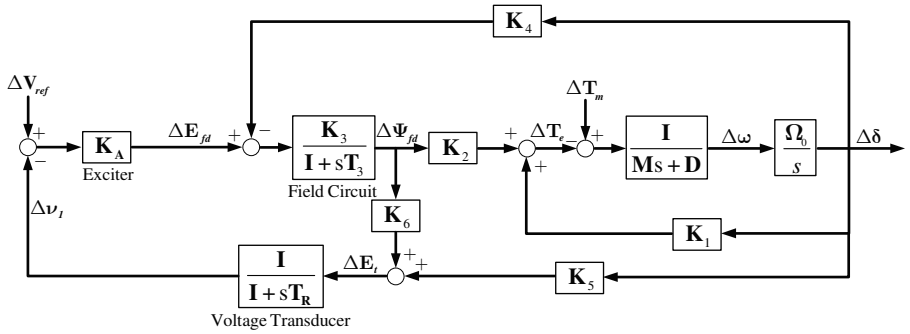

Figure 5.3. Generalized block diagram representation with excitation system [41].

With this, the steady state synchronizing torque coefficient definition (impacted by the effect of the excitation system) is of interest. Considering the equations of the field flux and air –gap torque variations due to the change in $\Delta\psi_{fd}$, as defined in [41]:

Then, the synchronizing torques due to $\Delta\psi_{fd}$ are:

$$K_{S,ij}\Big|_{due\ to\ \Delta\psi_{fd}} = \frac{-K_{2,ij}K_{3,ij}\left(K_{4,ij}+K_{5,ij}K_{A,i}\right)}{1+K_{3,ij}K_{6,ij}K_{A,i}} \tag{5.81}$$

And, the total synchronizing torque can be defined:

$$K_{S,ij}^{total} = K_1 + K_{S,ij}\Big|_{due\ to\ \Delta\psi_{fd}} \tag{5.82}$$

$$\mathbf{A}_{\omega} = \mathbf{K}_S^{total} = \mathbf{K}_1 + \mathbf{K}_S\Big|_{due\ to\ \Delta\psi_{fd}} \tag{5.83}$$

As presented above, **the overall impact**, of including the effect of the excitation system over the synchronizing torques, depends on the sign of the constant K_5, [41].

- *K_5 positive*: "introduces a negative synchronizing torque and a positive damping torque component"
- *K_5 negative*: "introduces a positive synchronizing torque and a negative damping torque component"

Comments:

- In this Section, three definitions of the synchronizing torque of the synchronous generator were obtained for multi–machine power systems. These three definitions correspond to the three models considered in this research: electromechanical, transient with constant excitation flux and transient with excitation system.
- In Section 5.4, these definitions will be used to investigate the impact on the grouping of generators in a grid, by using the aforementioned slow coherency concept.

5.4. Identification of Slow Coherent Distributed Generators in a test ADG

In the first part of this Sub−Section the ″tolerance−based grouping″ produced by Dr. Joe Chow in [59] is resumed. In the next parts, an analysis is performed in order to observe the impact of model selection for multi−machines in the ADG on the identification of slow coherent groups. The three models as obtained in Sub−section 5.3 will be considered.

In the continuation of this Section the impact of excitation system modeling is investigated on the identification of slow coherent distributed generators (by using the subtransient multi−machine model).

5.4.1. Tolerance−Based Grouping Algorithm

In order to obtain accurate coherent groups of generators the ″tolerance−based grouping″ algorithm developed by Dr. Joe Chow in [59] is used.

The ″tolerance−based grouping″ algorithm, as presented in [59]develops a measure of the slow coherency between the generators. The algorithm is based on the right−eigenvectors columns, which are normalized to unity.

A distance measure is introduced between the i^{th} and j^{th} rows of the V (right−eigenvectors), corresponding to machines i and j. This distance is defined by (5.84):

$$d_{ij} = v_i v_j^T \left(\left| v_i \right| \left| v_j \right| \right) \tag{5.84}$$

For perfectly coherent generators d_{ij}=1 meaning that $v_i = v_j$. As presented in [59], typically a tolerance coefficient is defined ($\gamma = 0.9 - 0.95$), for two machines to be considered coherent, if $d_{ij} > \gamma$.

Using this, a coherency matrix can be defined, to be used in the slow coherency identification algorithm:

$$\left(C_m\right)_{ij} = d_{ij} - \gamma \tag{5.85}$$

The contour plots of C_m for the test ADG will be presented for the different models of the generators.

5.4.1. A) Electromechanical (or ″Classical″) Model of Multi−Machine Active Distribution Grids

Considering the same test ADG introduced in Chapter 4 shown in Figure 5.4, the system is modeled and linearized using Power System Toolbox−PST, [66].

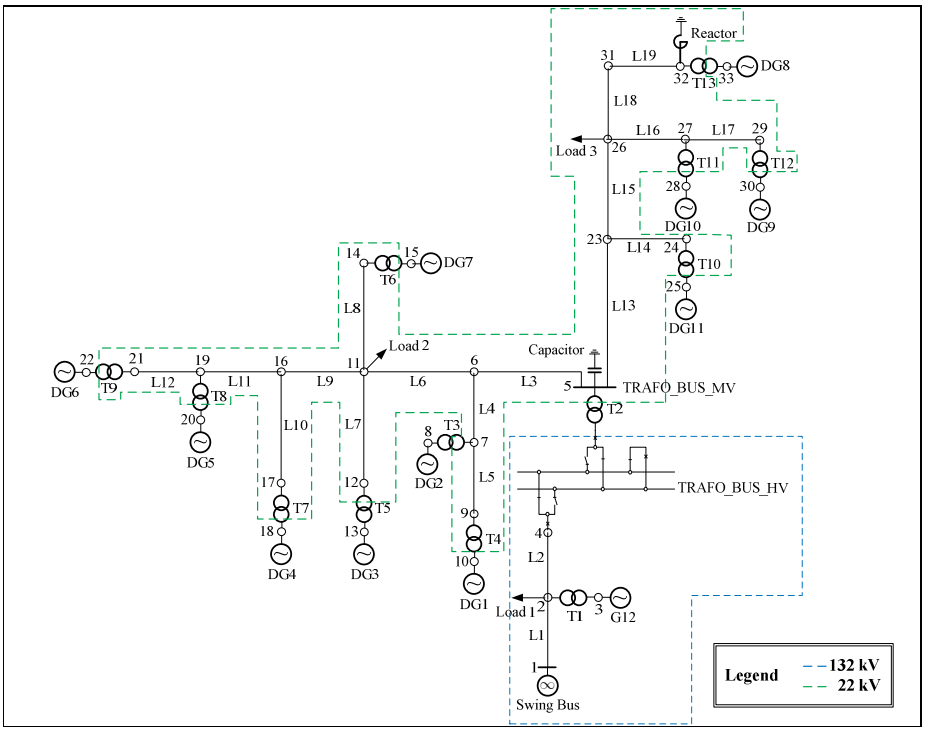

Figure 5.4. Test ADG topology.

With the definition of $\mathbf{A}_\omega$ as next, as (5.29):

$$\mathbf{A}_\omega = \mathbf{M}^{-1}\Delta\mathbf{P}_e \tag{5.86}$$

The sub−matrix $\mathbf{A}_\omega$ and the corresponding right−eigenvectors for the ″classical″ electromechanical model is presented in following pages. The eigenvalues of the $\mathbf{A}_\omega$ are all real as the $\mathbf{A}_\omega$ is symmetrical:

$$\lambda[\mathbf{A}_\omega] = \begin{bmatrix} -7.058 \\ -6.984 \\ -6.110 \\ -2.695 \\ -1.732 \\ -1.712 \\ -1.468 \\ -1.089 \\ -0.816 \\ -0.710 \\ -0.652 \\ -0.484 \\ -7.002 * \left(10^{-9}\right) \end{bmatrix}$$

The contour plot of C_m for the test ADG (by considering the electromechanical model) is presented in Figure 5.5. This contour was produced for the 7 slowest modes.

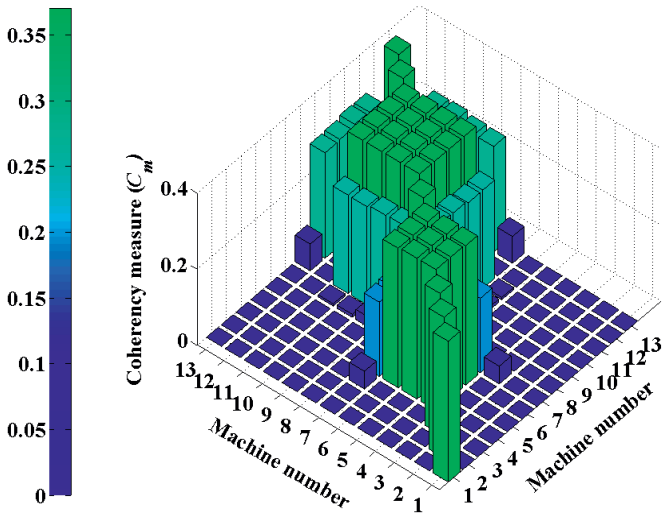

Figure 5.5. C_m values for the test ADG
(with the representation of generators using electromechanical model)

By considering the desired number of slow coherent areas to be 7, the following grouping matrix L_g is obtained for the machines, as presented in Table 5.1.

Table 5.1. Grouping matrix L_g for the 7−area partition
(with the representation of generators using electromechanical model)

$$[L_g] =$$

12	0	0	0	0	0
1	0	0	0	0	0
3	0	0	0	0	0
2	0	0	0	0	0
4	5	6	0	0	0
7	8	9	10	11	0
13	0	0	0	0	0

Based on the grouping matrix is presented in Table 5.1. Figure 5.6 presents the 7 slow−coherent areas in the ADG topology.

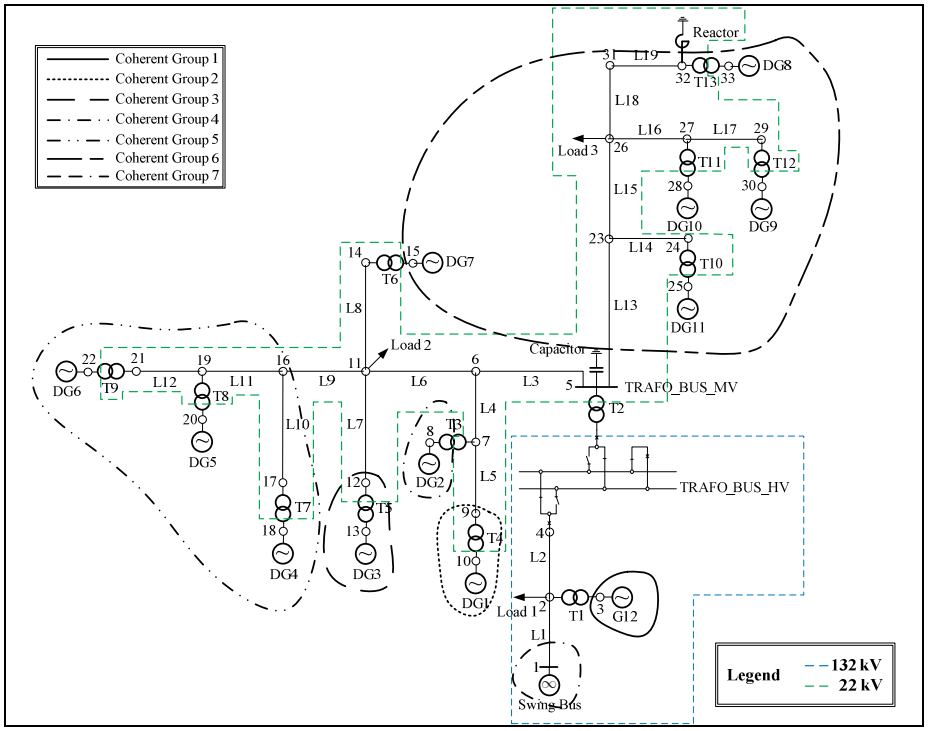

Figure 5.6. 7−areas partition of the ADG
(with the representation of generators using electromechanical model)

5.4.1. B) Transient Model of Multi−Machine Active Distribution Grids

In this Sub−Section, the results referring to the matrix of the transient synchronizing torque coefficients (defined by (5.73)) are presented. Considering the same number of groups (7 coherent areas), the grouping matrix L_g is obtained similar as for the electromechanical case. See Table 5.1.

The contour plot of C_m for the test ADG (by considering the electromechanical model) is presented in Figure 5.7. This contour was produced for the 7 slowest modes and by considering $\gamma = 0.8$.

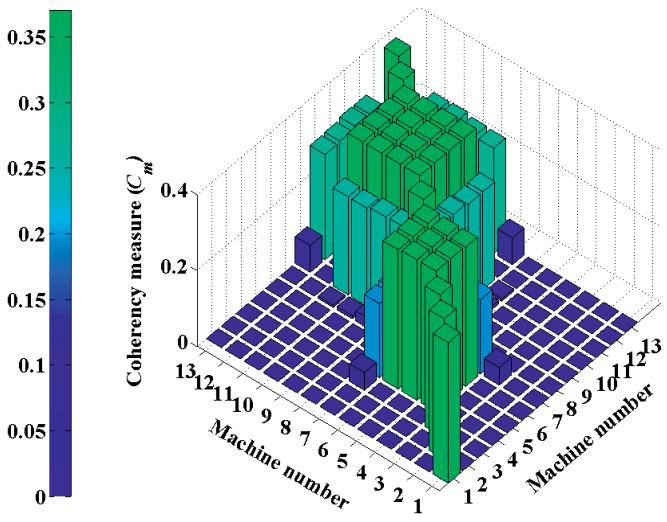

Figure 5.7. C_m values for the test ADG
(with the representation of generators using transient model)

5.4.1. C) Transient Model with Excitation System of Multi−Machine Active Distribution Grids

Further, the matrix of the transient synchronizing coefficients considering the excitation system (defined in (5.86)) is used to observe how the grouping of machines is impacted.

Considering the same number of groups (7 coherent areas), the grouping matrix L_g is obtained as in Table 5.2.

Table 5.2. Grouping matrix L_g for the 7−area partition
(with the representation of generators using transient model with excitation system)

$[L_g] =$

12	0	0	0
1	0	0	0
3	0	0	0
2	0	0	0
4	5	6	0
8	9	0	0
13	7	10	11

This contour was produced for the 7 slowest modes and by considering $\gamma = 0.6$.

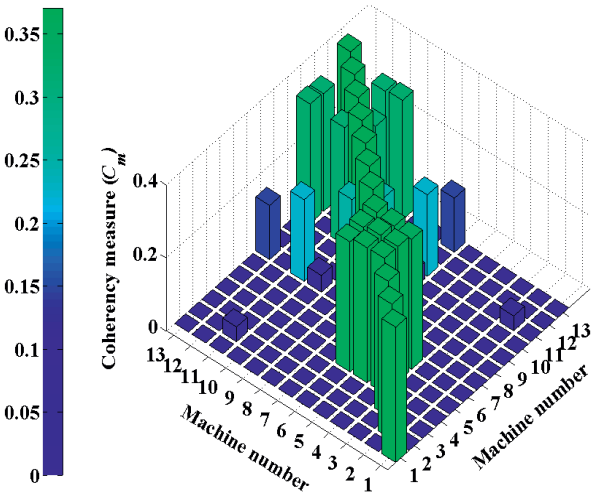

Figure 5.8. C_m values for the test ADG
(with the representation of generators using transient with excitation system model)

This grouping is shown in Figure 5.9. It can be observed from the contour plot that between DG 10 and 11 there exist a tight linkage. If the tolerance coefficient is decreased to 0.6 then it is shown that between the group of DGs 10 and 11 and 7 there exist relative good linkage combined with the one of swing machine. For practical reasons, the swing machine will be isolated from the cluster of generators 7, as this machine is modeled as a strong grid.

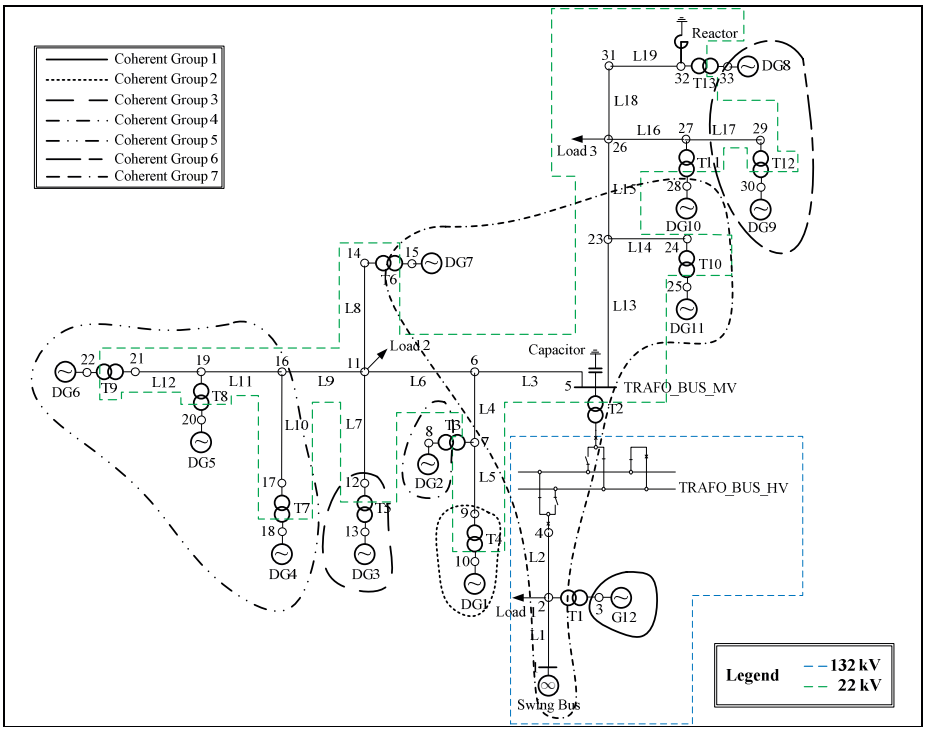

Figure 5.9. 7−areas partition of the ADG
(with the representation of generators using transient model with excitation system)

Table 5.3. Sub–matrix ($\mathbf{A}_{\omega}$) for classical electromechanical multi–machine model.

$[\mathbf{A}_{\omega}] =$

	DG_1	**DG_2**	**DG_3**	**DG_4**	**DG_5**	**DG_6**	**DG_7**	**DG_8**	**DG_9**	**DG_10**	**DG_11**	**DG_12**	**DG_13**
DG_1	-0.755	0.143	0.031	0.02	0.019	0.022	0.010	0.012	0.017	0.007	0.012	0.027	0.43
DG_2	0.069	-0.653	0.032	0.02	0.020	0.023	0.011	0.013	0.018	0.007	0.012	0.026	0.396
DG_3	0.033	0.061	-0.772	0.074	0.073	0.083	0.039	0.010	0.014	0.005	0.01	0.022	0.344
DG_4	0.047	0.084	0.168	-1.287	0.165	0.186	0.056	0.013	0.019	0.007	0.013	0.031	0.493
DG_5	0.047	0.084	0.166	0.164	-1.357	0.263	0.055	0.013	0.020	0.008	0.013	0.031	0.489
DG_6	0.053	0.094	0.188	0.187	0.268	-1.504	0.063	0.015	0.022	0.008	0.015	0.034	0.553
DG_7	0.277	0.524	0.935	0.602	0.599	0.678	-6.962	0.091	0.125	0.052	0.085	0.183	2.807
DG_8	0.069	0.116	0.051	0.031	0.031	0.034	0.016	-2.232	0.465	0.203	0.096	0.065	1.050
DG_9	0.073	0.122	0.053	0.033	0.032	0.036	0.016	0.387	-2.313	0.264	0.102	0.069	1.120
DG_10	0.205	0.365	0.156	0.098	0.096	0.108	0.050	0.975	1.410	-6.895	0.270	0.189	2.967
DG_11	0.249	0.457	0.194	0.123	0.121	0.136	0.064	0.368	0.481	0.208	-6.129	0.227	3.495
DG_12	0.004	0.009	0.003	0.002	0.002	0.002	0.0012	0.0022	0.003	0.001	0.002	-0.646	0.611
DG_13	0.00025	0.00043	0.00018	0.00012	0.00011	0.000128	6E-05	0.000102	0.000148	5.86E-05	0.0001	0.002	-0.003

Table 5.4. Right eigenvectors corresponding to the $\mathbf{A}_{\omega}$ of classical electromechanical model.

$$[V]=$$

0.277	0.398	-0.157	0.300	0.922	-0.048	-0.001
0.277	0.439	-0.195	0.385	-0.371	-0.047	-0.001
0.277	0.454	-0.184	-0.679	-0.090	-0.382	-0.008
0.277	0.332	-0.100	-0.313	-0.019	0.569	-0.776
0.277	0.332	-0.100	-0.310	-0.019	0.555	0.580
0.277	0.316	-0.093	-0.286	-0.016	0.446	0.244
0.277	0.221	-0.053	-0.147	-0.008	0.101	0.007
0.277	0.137	0.004	-0.0007	0.018	0.046	0.005
0.277	0.134	0.004	-0.00063	0.017	0.044	0.004
0.277	0.122	0.002	-0.00083	0.012	0.032	0.003
0.277	0.120	0.0004	-0.001	0.009	0.027	0.002
0.277	0.065	0.933	0.002	-0.003	-0.005	-0.0001
0.277	-0.001	-0.002	-1.21E-06	-5.31E-05	-8.79E-05	-3.86E-06

Table 5.5. Sub–matrix $\mathbf{A}_{\omega}$ for transient multi–machine model.

$[\mathbf{A}_{\omega}] =$

	DG_1	**DG_2**	**DG_3**	**DG_4**	**DG_5**	**DG_6**	**DG_7**	**DG_8**	**DG_9**	**DG_10**	**DG_11**	**DG_12**	**DG_13**
DG_1	-0.755	0.143	0.031	0.020	0.019	0.022	0.010	0.012	0.017	0.007	0.012	0.027	0.43
DG_2	0.069	-0.649	0.032	0.020	0.020	0.023	0.011	0.013	0.018	0.007	0.012	0.026	0.396
DG_3	0.033	0.0613	-0.772	0.074	0.073	0.083	0.039	0.010	0.014	0.005	0.010	0.022	0.344
DG_4	0.047	0.084	0.168	-1.280	0.165	0.186	0.056	0.013	0.019	0.007	0.013	0.031	0.493
DG_5	0.047	0.084	0.166	0.164	-1.348	0.263	0.055	0.013	0.020	0.008	0.013	0.031	0.489
DG_6	0.053	0.094	0.188	0.187	0.268	-1.492	0.063	0.015	0.022	0.008	0.015	0.034	0.553
DG_7	0.277	0.524	0.935	0.602	0.599	0.678	-6.871	0.091	0.125	0.052	0.085	0.183	2.807
DG_8	0.069	0.116	0.0511	0.031	0.031	0.034	0.016	-2.214	0.465	0.203	0.096	0.065	1.050
DG_9	0.073	0.122	0.053	0.033	0.032	0.036	0.016	0.387	-2.292	0.264	0.102	0.069	1.120
DG_10	0.205	0.365	0.156	0.098	0.096	0.108	0.050	0.975	1.410	-6.831	0.270	0.189	2.967
DG_11	0.249	0.457	0.194	0.123	0.121	0.136	0.064	0.368	0.481	0.208	-6.089	0.227	3.495
DG_12	0.004	0.009	0.0038	0.002	0.002	0.002	0.001	0.0022	0.003	0.0012	0.002	-0.642	0.611
DG_13	0.0002	0.0004	0.00018	0.00012	0.0001	0.0001	6E-05	0.0001	0.00015	5.86E-05	0.0001	0.002	-0.004

Table 5.6. Sub–system matrix $\mathbf{A}_{\omega}$ for transient with excitation system multi–machine model.

$[\mathbf{A}_{\omega}] =$

	DG_1	**DG_2**	**DG_3**	**DG_4**	**DG_5**	**DG_6**	**DG_7**	**DG_8**	**DG_9**	**DG_10**	**DG_11**	**DG_12**	**DG_13**
DG_1	-0.755	0.143	0.031	0.020	0.019	0.022	0.010	0.012	0.017	0.007	0.012	0.027	0.43
DG_2	0.109	-0.609	0.071	0.060	0.059	0.062	0.050	0.053	0.058	0.047	0.051	0.065	0.435
DG_3	0.033	0.061	-0.772	0.074	0.073	0.083	0.039	0.010	0.014	0.005	0.010	0.022	0.344
DG_4	-0.001	0.035	0.119	-1.328	0.116	0.137	0.007	-0.034	-0.028	-0.04	-0.034	-0.017	0.444
DG_5	-0.013	0.023	0.104	0.103	-1.409	0.202	-0.005	-0.047	-0.041	-0.053	-0.047	-0.029	0.428
DG_6	-0.047	-0.006	0.088	0.087	0.167	-1.592	-0.037	-0.084	-0.077	-0.091	-0.084	-0.065	0.453
DG_7	0.318	0.565	0.976	0.643	0.640	0.719	-6.830	0.132	0.166	0.093	0.125	0.224	2.848
DG_8	-0.066	-0.019	-0.085	-0.104	-0.105	-0.101	-0.120	-2.351	0.329	0.067	-0.039	-0.070	0.913
DG_9	-0.168	-0.120	-0.188	-0.209	-0.210	-0.206	-0.225	0.145	-2.535	0.021	-0.139	-0.173	0.877
DG_10	0.196	0.355	0.147	0.089	0.087	0.099	0.041	0.966	1.401	-6.840	0.261	0.180	2.957
DG_11	0.286	0.494	0.231	0.160	0.158	0.173	0.101	0.406	0.519	0.245	-6.051	0.264	3.532
DG_12	0.041	0.045	0.040	0.038	0.038	0.039	0.037	0.038	0.039	0.037	0.038	-0.606	0.648
DG_13	0.0009	0.0011	0.00089	0.0008	0.0008	0.0008	0.0007	0.0008	0.0008	0.0007	0.0008	0.0027	-0.003

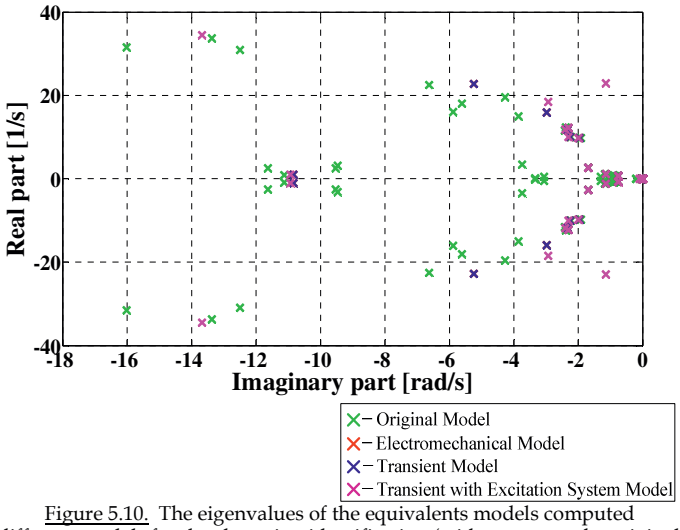

Figure 5.10. The eigenvalues of the equivalents models computed with 3 different models for the clustering identification (with respect to the original model)

Figure 5.10 shows the eigenvalues when the 3 models of the generators are used for DGs clustering: original, electromechanical model for generators, transient model and transient model with excitation system. The equivalent models of the grid are preserving the original electromechanical eigenvalues in a good manner. For a better observation of this in Table 5.7, the electromechanical modes are represented both by the damped frequency Hz and damping ratio [p.u.]. The errors of damped frequencies and damping ratio are presented in Tables 5.8 a) and b) and 5.9 a) and b). From these Tables it can be observed that by modeling the excitation system, the Modes 1, 5, 6, 7 and 8 present a better approximation compared to the electromechanical and transient models. In Appendix 4 the full list of eigenvalues are presented.

Table 5.7. Identified original eigenvalues in the equivalent models

	Original Model		**Electromechanical and Transient Model**		**Transient with Excitation System Model**	
	Frequency [Hz]	**Damping Ratio** [p.u.]	**Frequency** [Hz]	**Damping Ratio** [p.u.]	**Frequency** [Hz]	**Damping Ratio** [p.u.]
Mode 1	1.954	0.189	1.947	0.184	1.952	0.183
Mode 2	1.837	0.204	1.857	0.195	1.873	0.198
Mode 3	1.602	0.215	1.597	0.218	1.600	0.223
Mode 4	1.565	0.191	1.564	0.195	1.568	0.197
Mode 5	0.415	0.542	0.416	0.541	0.416	0.541
Mode 6	0.188	0.703	0.188	0.695	0.189	0.691
Mode 7	0.145	0.996	0.160	0.995	0.156	0.995
Mode 8	0.1443	0.701	0.116	0.717	0.117	0.715

Table 5.8. a) Damped frequencies errors of the original model with respect to the electromechanical and transient models

	Original Model	**Electromechanical and Transient Model**	**Error**
	Frequency [Hz]	**Frequency** [Hz]	[%]
Mode 1	1.954	1.947	0.7
Mode 2	1.837	1.857	2
Mode 3	1.602	1.597	0.5
Mode 4	1.565	1.564	0.1

Table 5.8. b) Damped frequencies errors of the original model with respect to the transient with excitation system model

	Original Model	**Transient with Excitation System Model**	**Error**
	Frequency [Hz]	**Frequency** [Hz]	[%]
Mode 1	1.954	1.952	0.2
Mode 2	1.837	1.873	3.6
Mode 3	1.602	1.6	0.2
Mode 4	1.565	1.568	0.3

Table 5.9. a) Damping ratios errors of the original model with respect to the electromechanical and transient models

	Original Model	**Electromechanical and Transient Model**	**Error**
	Damping Ratio [p.u.]	**Damping Ratio** [p.u.]	[%]
Mode 1	0.189	0.184	0.5
Mode 2	0.204	0.195	0.9
Mode 3	0.215	0.218	0.3
Mode 4	0.191	0.195	0.4

Table 5.9. b) Damped ratios errors of the original model with respect to the transient with excitation system model

	Original Model	**Transient with Excitation System Model**	**Error**
	Frequency [Hz]	**Frequency** [Hz]	[%]
Mode 1	0.189	0.183	0.6
Mode 2	0.204	0.198	0.6
Mode 3	0.215	0.223	0.8
Mode 4	0.191	0.197	0.6

5.4.1. D) Impact of Excitation System on the Identification of Slow Coherent Areas

In this Sub−Section, the impact of the excitation system on the identification of slow coherent areas in the test ADG is investigated. The scope is to observe how the change in the amplifier gain K_A impacts the slow coherent areas identification. Therefore, a variation of $K_A = [400; 1000; 2000]$ is produced for the excitation system of DG 4.It can be observed from Figure 5.11 that by increasing K_A, generator DG 4 is excluded from the coherent area,

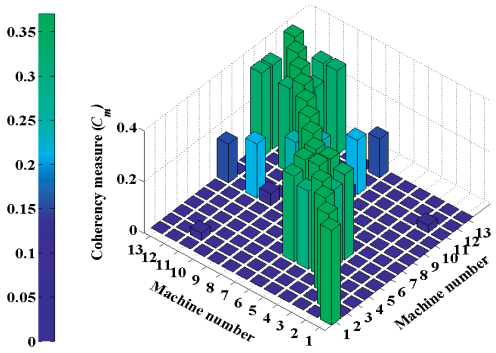

a)K_A=400 p.u.

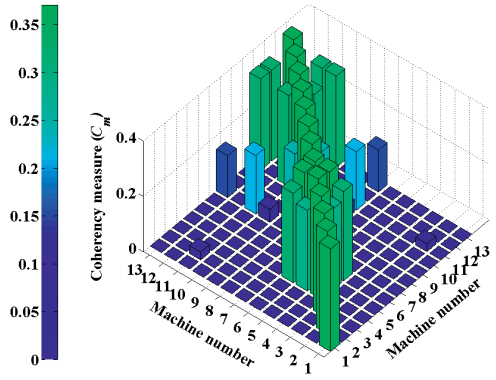

b)K_A=1000 p.u.

consisting of DG 4, DG 5 and DG 6.

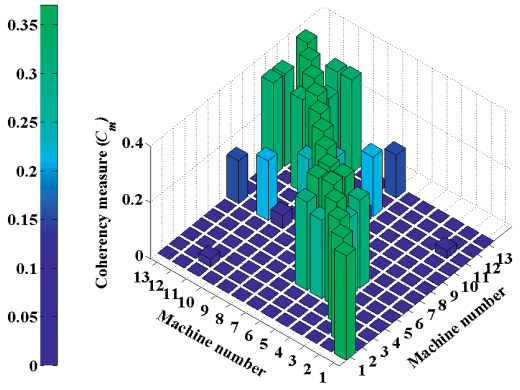

c)K_A=2000 p.u.

Figure 5.11. Impact of Excitation System on the Identification of Slow Coherent Areas

As can be observed from Table 5.8, usually in distribution systems with small scale hydro units the low frequency inter-area modes are well damped with respect to the transmission system. Therefore it can be seen that for ADGs with high penetration of small scale hydro, units the coherency phenomena occurs for DGs at modes with higher damped frequencies, which can be confirmed by running a small signal time domain analysis. Usually these oscillation modes are associated with local plant modes. When DGs are subject to small disturbances (small variations in load or generated power) it can be observed that the coherency between DGs happens within oscillations modes with higher damped frequencies and the groups of generators show up coherent within different oscillation modes. Normally the magnitude of excitation is so small that by observing the time response of some state variables these groups of coherent generators are very difficult to identify.

As in this case the coherency happens within different oscillation modes, the linear analysis fails to identify properly these groups as they results from the small signal time domain simulation. Therefore a tool is needed to decompose the time responses and to observe the magnitude and phase for each oscillation mode in order to determine how coherency happens in this case. In the next Section such a tool is proposed which allows the identification of coherent generators and the modes which now can be considered having a grid wide perspective.

5.5. Clustering Distributed Generation by Instantaneous Euclidean Distance in Polar Coordinates

5.5.1. Introduction

As presented in Sub–Section 5.4.1. D) the particularity of ADGs with high penetration of small scale hydro units make the linear analysis not sufficient to determine the coherent groups of generators. Therefore a new method is proposed in this work which can determine the coherent generators using the time responses of the state variables for each oscillation mode. The first part of this Sub–Section addresses the definitions of the electromechanically coherency concept between the synchronous generators, presented in Sub–Chapter 4.2.1. Two generators are called electromechanically coherent after a disturbance occurs if their correspondent rotor angles or speed variations exhibits the same trend of oscillation, [67]. This can be quantified by calculating the difference between two rotor angles and comparing it with an admissible tolerance, [33]. The approach is simple and easy to apply, if the aforementioned signals are known a priori. However if generators are equipped with different types of exciters systems, this approach is not valid, [68]. In this case, even if the magnitudes of oscillations are comparable, it can happen that the phases of these oscillations are not the same, as demonstrated in [48] and [68]. Therefore, one can conclude that the electromechanical coherency concept is a concept dependent on both magnitude and phase variations of the rotor angle oscillations [68]. As presented in Sub– Section 4.2.1, the methods developed to investigate the coherency concept address this by mean of the magnitude, of the phase or by a mix concept of the two, [40] [68]. In this Section a new method is proposed to identify the concept of the electromechanical coherency between DG units. The proposed method allows the computation of the instantaneous Euclidean Distance in polar coordinates for clustering Distributed Generation units in a test power system. This is done by taking into consideration, both the magnitude and the phase of oscillations (in a unified tool). As will be demonstrated, the proposed method gives better results with respect to the metric Euclidean Distance. The method is based on electromechanical modes decomposition (or *"free motion time responses"*) of the state variables for small hydro units, as presented in [11]. This approach was chosen, due to the simplified manner in which the computation of the instantaneous magnitude and phase can be performed.

There are several transforms available to compute the phase of a real signal; the most popular are the following three, [69]:

1. Fourier Transform
2. Hilbert Transform
3. Wavelet Transform

However, in this case as the system state representation is known, the *"free motion time responses"* represents a very simple tool to decompose the time responses of the state variables for each of the oscillation modes. The magnitude and phase computation will then be straightforward as for general complex numbers.

5.5.2. Method Description

5.5.2.1. Electromechanical coherency concept overview

This Section summarizes the concepts of the electromechanical coherency as discussed in 4.2.1.

Two recorded signals from the i^{th} and j^{th} generators can be represented in polar coordinates as in (5.87) and (5.88):

$$x_i(t) = \boldsymbol{X}_i(t) e^{\phi_{x,i}(t)} \tag{5.87}$$

$$y_i(t) = \boldsymbol{Y}_i(t) e^{\phi_{y,i}(t)} \tag{5.88}$$

where:

– $\boldsymbol{X}_i(t)$ and $\boldsymbol{Y}_i(t)$ are the instantaneous magnitudes of the rotor angle signals $x_i(t)$ and $y_i(t)$

– $\phi_{x,i}(t)$ and $\phi_{y,i}(t)$ are the instantaneous phases of the rotor angle signals $x_i(t)$ and $y_i(t)$

Generally, the coherency concept is tackled in literature by three main groups of methods:

Coherency of magnitude [40]

$$\left|\boldsymbol{X}_i(t) - \boldsymbol{Y}_i(t)\right| < \varepsilon_m, \quad t \in [t_0, t_n] \tag{5.89}$$

This approach is mainly used to identify the electromechanical coherency together with the computation of the metric Euclidean Distance between i^{th} and j^{th} units, over a time interval, as proposed in [46], by (5.90):

$$d_{i,j} = \sqrt{\sum_{t=t_1}^{T} \left(x_i(t) - x_j(t)\right)^2} \tag{5.90}$$

Coherency of phase this is presented in [33] [47]

$$\left|\phi_{x,i}(t) - \phi_{y,i}(t)\right| < \varepsilon_m, \quad t \in [t_0, t_n] \tag{5.91}$$

Coherency of magnitude and phase [47] [48] for which both (5.89) and (5.91) need to be validated over a time interval $t \in [t_0, t_n]$, were t_0 and t_n – represents the starting and ending time of the signal recording.

5.5.2.2. Clustering DG units via Instantaneous Euclidean Distance in Polar Coordinates

Why clustering of DG units using the Instantaneous Euclidean Distance in Polar Coodinates?

1. Why instantaneous?

As power systems are dynamic systems, these systems are changing continuously their state of operation during a time period, due to small or large disturbances. Different disturbances will excite certain oscillation modes visible in some state variables, due to a higher relative activity of the state variables in those modes. This is quantified by the mode shapes or the observability eigenvectors. As will be presented next, the time domain response of certain states are defined as the sum of the state's responses for each oscillation mode. So, for identifying how generators can be cluster in coherent groups after a disturbance, time responses of this disturbance during a time interval are used. In this time interval certain dominant oscillation modes can be recognized, for which the instantaneous magnitudes and phase angles are of interest. There are several methods to compute the magnitude and phase of a real signal. The most known are Fourier and Hilbert Transforms, detailed in [67] and [70].
According to [70], the Hilbert transform of a function $x(t)$ is defined as:

$$H\left(f(t)\right) = -\frac{1}{\pi t} f(t) \tag{5.92}$$

This further can be expressed in integral form as:

$$H\left(f(t)\right) = -\frac{1}{\pi}\int_{-\infty}^{\infty} \frac{f(\tau)}{\tau - t} d\tau \tag{5.93}$$

As presented in [70], in order to compute the imaginary part of a real signal described by a periodic function, the Hilbert transform will produce a phase shift of $\pi/2$ which will result in an analytic signal in complex form, as:

$$z(t) = x(t) - iy(t) \tag{5.94}$$

Where

$$y(t) = H\left(x(t)\right) \tag{5.95}$$

With this the instantaneous amplitude $a(t)$ and phase $\varphi(t)$ of $x(t)$ can be computed [70]:

$$a(t) = \sqrt{x(t)^2 + y(t)^2} \tag{5.96}$$

$$\varphi(t) = \arctan\frac{y(t)}{x(t)} \tag{5.97}$$

In this PhD work a method based on the time domain decomposition is proposed to compute the magnitude and phase of a real signal. In this case the real signal is the time response of a state variable for a certain dominant oscillation mode. The method is validated against the Hilbert transform.

2. Why Euclidean Distance in Polar Coordinates

As presented above the concept of electromechanical coherency was treated separately into two different concepts: the coherency of magnitude and of phase. Euclidean Distance in polar coordinates allows the computation of the coherency as a unified concept.

This Section presents a new method to investigate the electromechanical coherency of magnitude and phase concept.

The method is based on the computation of the instantaneous Euclidean Distance – *ED(t)* in polar coordinates at each instant of time *t*. The method is based on modes decomposition time responses of the state variables for obtaining the instantaneous magnitude and phase and computation of *ED(t)*, as discussed in [41].

In this approach only the electromechanical modes with the frequency of oscillations between [0.25 − 2] Hz is considered for the time domain decomposition. [11]

The idea is to use the time responses of modes decomposition of speed of the DGs, in order to identify the number of clusters of DG units, when the test ADG is affected with a small disturbance. The secondary frequency control is not modeled in this research.

Considering that the speed registered for each of the DG units can be expressed in terms of the electromechanical oscillatory modes, right and left eigenvectors as described in [41], then for the i^{th} and j^{th} generators:

$$\Delta\omega_i(t) = \Phi_{i,1}c_{i,1}e^{\lambda_1 t} + \Phi_{i,2}c_{i,2}e^{\lambda_2 t} + \cdots + \Phi_{i,k}c_{i,k}e^{\lambda_k t} \tag{5.98}$$

$$\Delta\omega_j(t) = \Phi_{j,1}c_{j,1}e^{\lambda_1 t} + \Phi_{j,2}c_{j,2}e^{\lambda_2 t} + \cdots + \Phi_{j,k}c_{j,k}e^{\lambda_k t} \tag{5.99}$$

Where: $\Delta\omega_i(t)$ and $\Delta\omega_j(t)$ are small variation of speed of the DGs, Φ_i and Φ_j are the right eigenvectors, c_k – represent the magnitude of the excitation of k^{th} mode and λ_k – represent the k^{th} oscillatory mode.

Or, rewriting (5.98) and (5.99) in the complex form:

$$\Delta\omega_i(t) = \mathbf{\Psi}_{i,1}e^{\psi_{i,1}t} + \mathbf{\Psi}_{i,2}e^{\psi_{i,2}t} + \cdots + \mathbf{\Psi}_{i,k}e^{\psi_{i,k}t} \tag{5.100}$$

$$\Delta\omega_j(t) = \mathbf{\Psi}_{j,1}e^{\psi_{j,1}t} + \mathbf{\Psi}_{j,2}e^{\psi_{j,2}t} + \cdots + \mathbf{\Psi}_{j,k}e^{\psi_{j,k}t} \tag{5.101}$$

where: $\mathbf{\Psi}_{i,k}, \mathbf{\Psi}_{j,k}$ and $\psi_{i,k}, \psi_{j,k}$ represent complex numbers having the form: $\alpha + j\beta$.

In order to identify the electromechanical modes of oscillations, the *"free motion time responses"* of the speed registered for each of the DGs should be calculated as discussed in [41]. If the topology of the ADG is known, then this time response can be easily modeled in a simulation platform, by running a modal analysis and registering the right and left eigenvectors and electromechanical modes of oscillations. This method it is suitable for off-line studies and the computation of instantaneous magnitudes and phases is done by running an iterative modal analysis for the known ADG, at each time step *t*. After the dominant electromechanical modes of oscillation are identified, their correspondent instantaneous magnitudes and phases can be computed, considering that the real and imaginary parts for each free motion time response coefficient can be written as in (5.102) and (5.103):

$$\mathrm{Re}\left\{\Delta\omega_i^k\right\}=\mathrm{Re}\left\{\boldsymbol{\Psi}_{i,k}e^{\psi_{i,k}t}\right\} \tag{5.102}$$

$$\mathrm{Im}\left\{\Delta\omega_i^k\right\}=\mathrm{Im}\left\{\boldsymbol{\Psi}_{i,k}e^{\psi_{i,k}t}\right\} \tag{5.103}$$

With (5.102) and (5.103), the instantaneous magnitudes $\boldsymbol{\Lambda}_{i,k}(t)$ and phase $\phi_{i,k}(t)$ of each k^{th} electromechanical mode of oscillation and for each i^{th} DG unit, can be computed as:

$$\boldsymbol{\Lambda}_{i,k}(t)=\sqrt{\left(\mathrm{Re}\left\{\boldsymbol{\Psi}_{i,k}e^{\psi_{i,k}t}\right\}\right)^2+\left(\mathrm{Im}\left\{\boldsymbol{\Psi}_{i,k}e^{\psi_{i,k}t}\right\}\right)^2} \tag{5.104}$$

$$\phi_{i,k}(t)=\tan^{-1}\left(\frac{\mathrm{Im}\left\{\boldsymbol{\Psi}_{i,k}e^{\psi_{i,k}t}\right\}}{\mathrm{Re}\left\{\boldsymbol{\Psi}_{i,k}e^{\psi_{i,k}t}\right\}}\right) \tag{5.105}$$

Using the instantaneous magnitudes and phases as defined in (5.104) and (5.105), the average instantaneous Euclidean Distance – ED_{ij}, between generators i^{th} and j^{th} can be written as:

$$ED_{ij}=\sqrt{\left[\frac{\sum_{t=1}^{T}\left[\boldsymbol{\Lambda}_i^2(t)+\boldsymbol{\Lambda}_j^2(t)-2\boldsymbol{\Lambda}_i(t)\boldsymbol{\Lambda}_i(t)\cos\left(\phi_i(t)-\phi_j(t)\right)\right]}{N}\right]} \tag{5.106}$$

Where N is the number of samples registered at each time instant t

Then, by computing the ED_{ij} between each i^{th} and j^{th} generators with $i, j\in\Gamma$ (where Γ is the set of generators from the external area), the i^{th} and j^{th} generators can be recognized as electromechanically coherent, by identifying the minimum averaged instantaneous Euclidean Distance – ED_{ij} :

$$\min\left(ED_{ij}\right) \tag{5.107}$$

Or in other words, (5.106) can be calculated for each instant of time t and the i^{th} and j^{th} generators can be considered electromechanical coherent if the $ED_{ij,k}$ for each k^{th} mode of oscillation validates the condition from (5.107).

5.5.2.3. Study Case

In this Section the DG units connected to the test ADG used in this work are clustered by using the method described in Section 5.5.2.2. The test model for the ADG was already introduced in Chapter 4. The system were simulated and implemented using DIgSILENT Power Factory 14.1.6® platform.

In this research the TPS is modeled as the internal power system (represented by the strong TPS behind the bus 7500_132 kV).The ADG simulation model is presented in Figure 5.12.

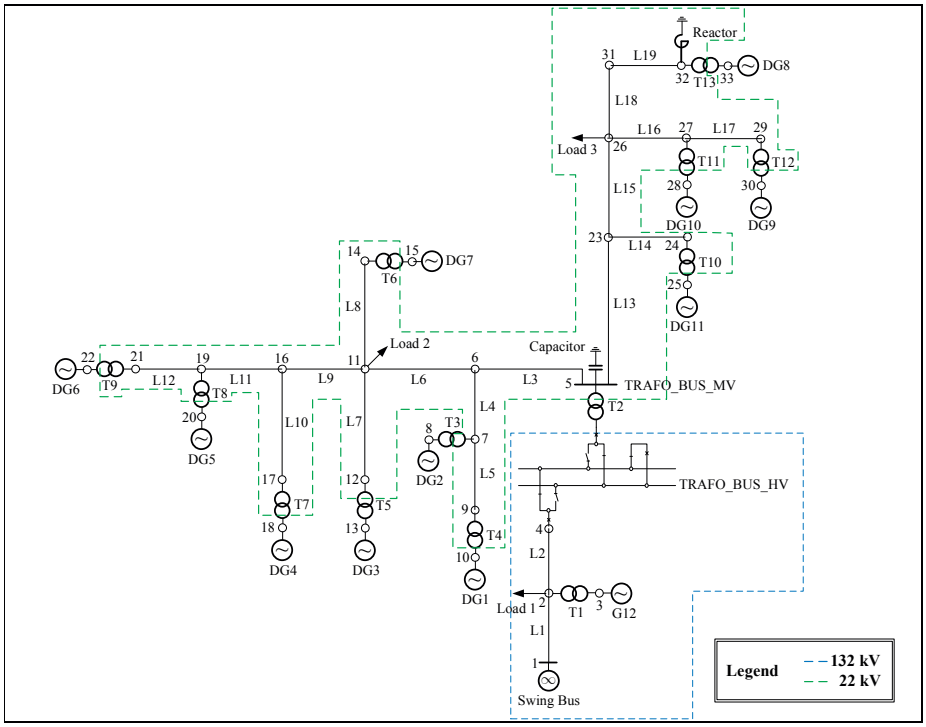

Figure 5.12. Test ADG topology.

To validate the proposed method to determine electromechanical coherency between DG units, a small disturbance was introduced to the test ADG. This disturbance is represented by an increase of 5% of the speed reference of the medium size hydro power plant connected at the bus 3. The speeds of al DG units were recorded and are presented in Figure 5.13.

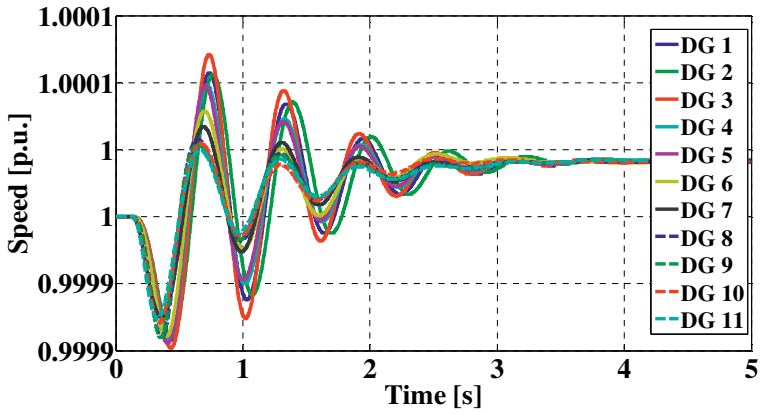

Figure 5.13. Speed variations of DG units after a small disturbance

If we investigate the DG units which belong to Cluster 1 in Figure 5.14, one can observe that the magnitudes of the oscillations are comparable but their phases are shifted.

After computing the metric Euclidean Distance defined by (5.103) between each real valued signal representing the speed of the DG units, the following clusters were obtained:

Table 5.10. Clusters of DG Units By Using the Metric Euclidean Distance

Clusters	DG Units
Cluster 1	DG 1, DG 2, DG 3
Cluster 2	DG 4, DG 5, DG 6, DG 7
Cluster 3	DG 8, DG 9, DG 11
Cluster 4	DG 10

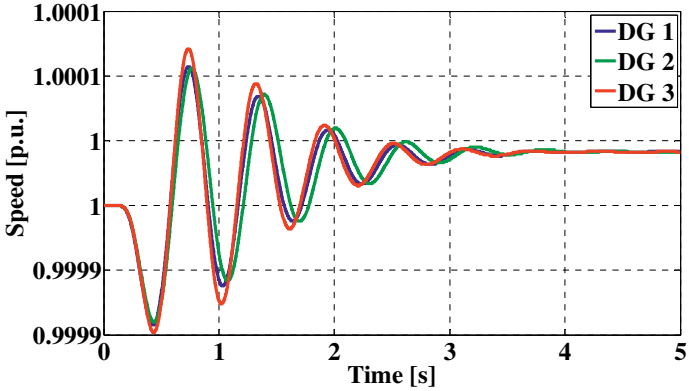

Figure 5.14. Speed variations of DG units after a small disturbance

- **Identification of the dominant electromechanical modes**

To identify the dominant electromechanical modes, a filtering technique was used to select the modes with the frequencies of oscillations between 0.25 and 2 Hz. Running the modal analysis for the test ADG, the dominant electromechanical modes, presented in Table 5.11 were identified.

Table 5.11. Dominant Electromechanical Modes of Oscillations

Electromechanical Modes	**Real Part**	**Imaginary Part**	**Damped Frequency**	**Damping Ratio**
–	**[1/s]**	**[rad/s]**	**[Hz]**	**[%]**
Mode 1	−2.375	±12.283	1.971	18.984
Mode 2	−2.413	±11.546	1.874	20.457
Mode 3	−2.223	±10.069	1.602	21.558
Mode 4	−1.916	±9.834	1.565	19.123
Mode 5	−3.730	±3.423	0.545	73.670
Mode 6	−9.477	±3.172	0.505	94.829
Mode 7	−1.688	±2.613	0.416	54.262
Mode 8	−9.518	±2.569	0.409	96.543
Mode 9	−11.627	±2.546	0.405	97.685

4. *Coherency identification in ADGs: Time domain simulation versus Observability eigenvectors*

As presented above, the coherency among generation units can be identified by running a time domain simulation, or a modal analysis. When the modal analysis is chosen to identify coherency among the generation units, observability eigenvectors (also called mode shapes) are of interest.

This is not any longer true for ADGs as those modes corresponding to the inter−area modes for TPSs are well damped. For these types of grids the coherency can be recognized within several local plant modes. This can be proven by looking in the list of the eigenvalues presented in Tables 5.11 and 5.14.

Considering speed as a state variable and by plotting the observability eigenvectors for some of the local plant modes, the coherency among DG units can be identified. This can be observed by plotting the observability eigenvectors for modes 2 and 3 (see Table 5.11) and modes 14 and 17 (see Table 5.14) as in Figure 5.17.

Normally for TPSs the clusters of coherent generators can be identified by running a time domain simulation of a small disturbance or by observing the phase of the observability eigenvectors. For the case of the test ADG it was shown that there aren't oscillation modes similar with the inter−area modes for TPSs for which the same coherency can be recognized as by running a time domain simulation. As presented above for ADGs the coherency

observed in a time domain simulation (see Figure 5.15) can be similarly identified by looking in particular local plant modes, as presented in Figure 5.15.

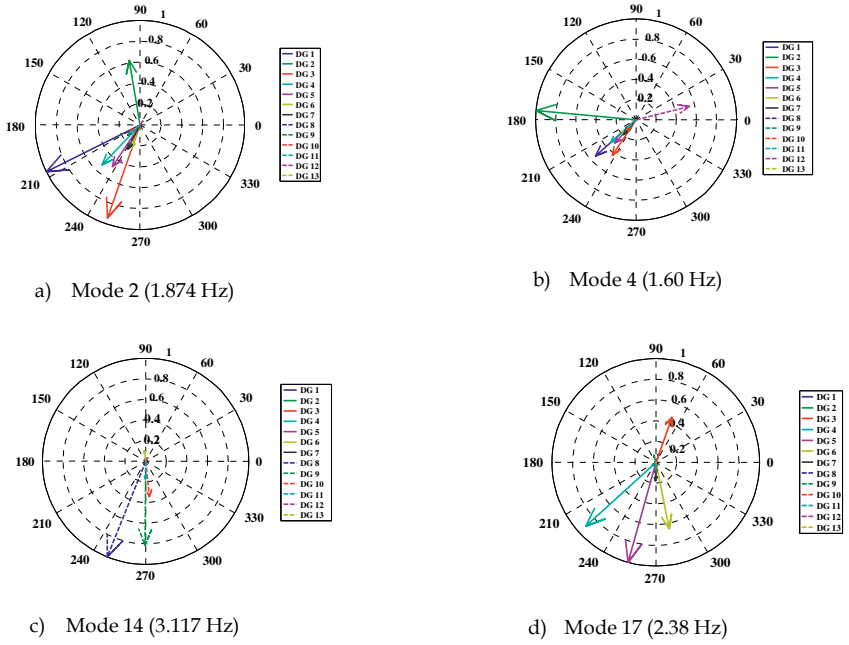

a) Mode 2 (1.874 Hz)

b) Mode 4 (1.60 Hz)

c) Mode 14 (3.117 Hz)

d) Mode 17 (2.38 Hz)

Figure 5.15. Observability eigenvectors for different local plant modes.

From the time domain simulation presented in Figure 5.13 two oscillation modes can be identified as dominant: mode 3 – 1.602 Hz and mode 4 – 1.565 Hz. Let us investigate the observability of eigenvectors of these modes are investigated in Figure 5.16.

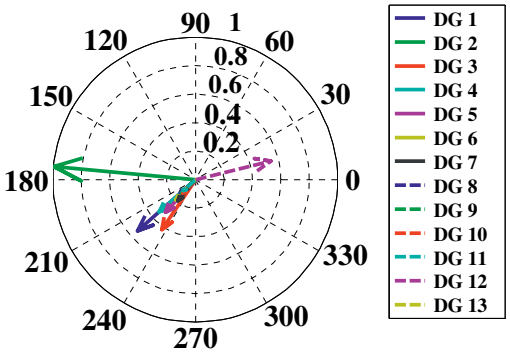

a) Mode 3 (1.602 Hz)

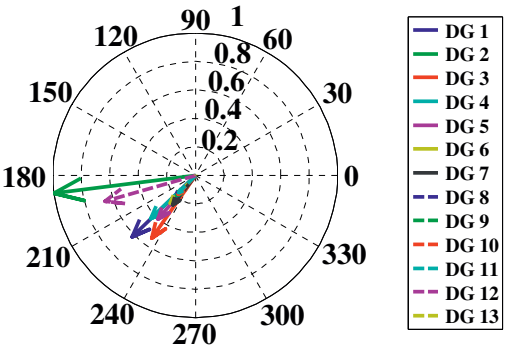

b) Mode 4 (1.565 Hz)

Figure 5.16. Observability eigenvectors for Modes 3 and 4.

From Figures 5.16 a) and b) it can be observed that even the magnitudes of the observability eigenvectors are similar with the magnitudes of oscillations recognizable in the speed signals from Figure 5.13, the phase angles of the observability eigenvectors and the time instants where the speed oscillations points are different, as can be observed from Figure 5.17.

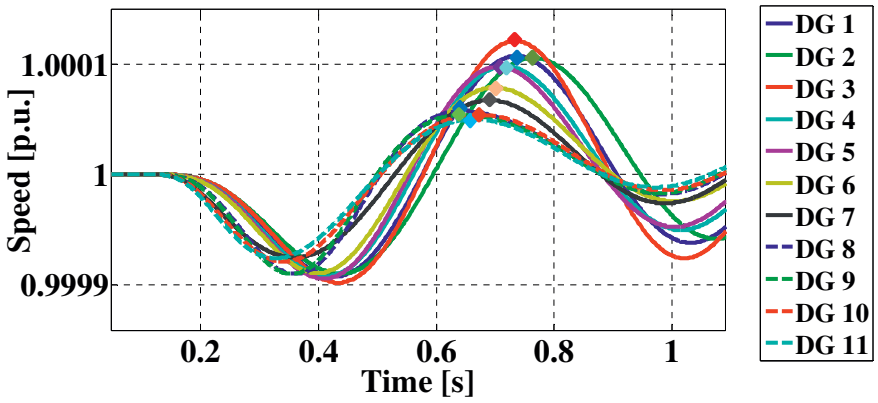

Figure 5.17. Speed signals of DGs.

This happens as in the time domain response defined by (5.92) the observability (right) eigenvectors are multiply with the corresponding controllability (left) eigenvectors, so a phase shift appears. This product between the right (observability) and left (controllability) eigenvectors corresponds to the participation factor, defined according to [41] as:

$$p_{ki} = \phi_{ki}\psi_{ik} \tag{5.108}$$

According to [41] the participation factors measures the net participation of the k^{th} state variable in an i^{th} mode. In Figure 5.20 the participation factors (complex values) are depicted for the Modes 3 and 5 presented in Table 5.11. From these Figures it can be observed that a same clustering of the DG units is produced as by the proposed method presented in Table 5.12. As generators 2 and 12 are dominant in modes 3 and 4 they were neglected in Figures 5.18 a) and b).

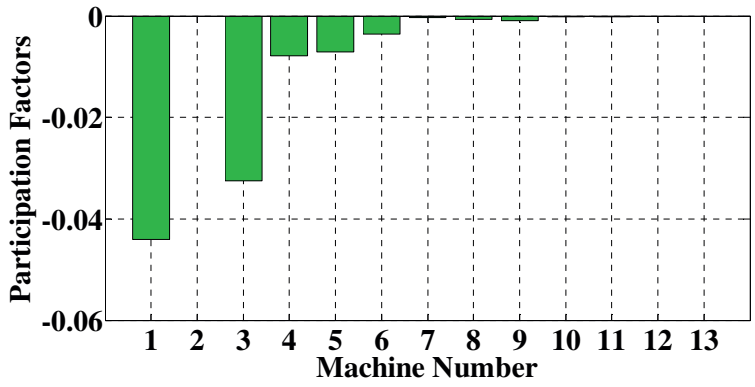

a) Mode 3 (1.602 Hz)

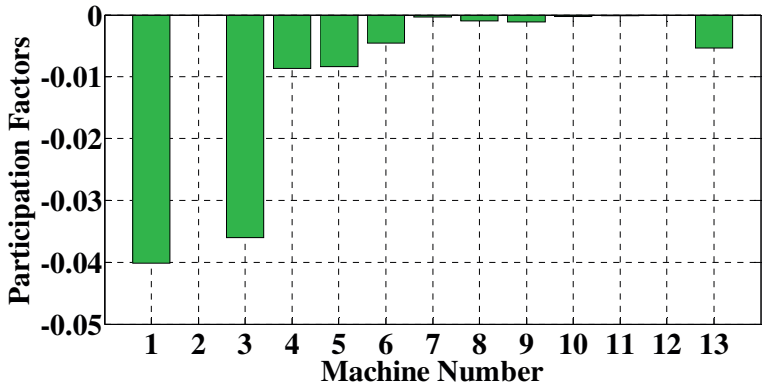

b) Mode 4 (1.565 Hz)

Figure 5.18. Participation factors for modes 3 and 4.

Therefore in the proposed method a mathematical manipulation of the time response decomposition presented in (5.92) is used to obtain the magnitudes and phases of the electromechanical modes of oscillations. Further these magnitudes and phases are used to cluster the DGs using the Euclidean distance in polar coordinates. A complete description of the mathematical manipulation of (5.92) and of the manner in which the magnitude and phase is computed for the pair complex of conjugate eigenvalues is presented in Appendix 6.

- **Modes decomposition**

As shown in [41], the time response of a state variable which describes the operation of the synchronous machine can be modelled by a linear combination of *k* dynamic modes (as done for example in (5.95) and (5.96) for the speed signals of two DG units).

The instantaneous magnitudes and phases can be calculated applying the decomposition of the speed signals for each DG unit and for the dominant electromechanical modes.

By using equations (5.101), the real electromechanical coherency between DG units can be achieved. Figure 5.19, shows the time responses and the correspondent magnitudes of the Mode 1 for the speed signal of the DG units 1, 2 and 3. Figure 5.20 shows the phases of the Mode 1 for the speed signal of the DG units 1, 2 and 3.

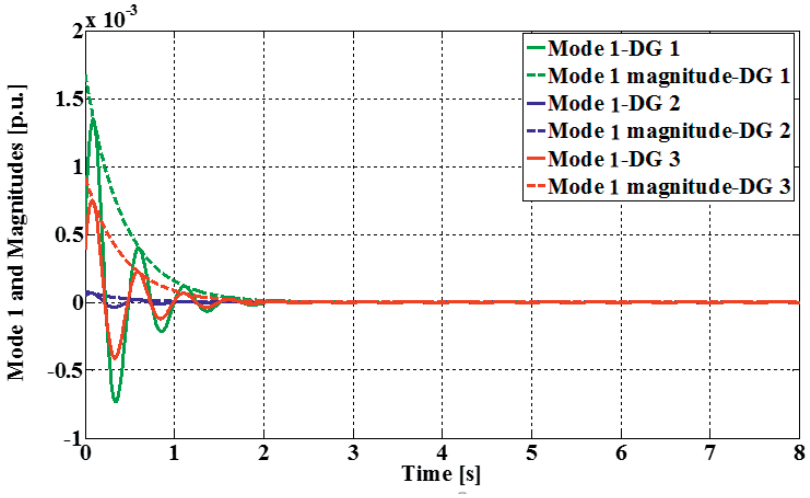

Figure 5.19. Mode 1 – magnitude of the speed signal of DG 1, 2 and 3

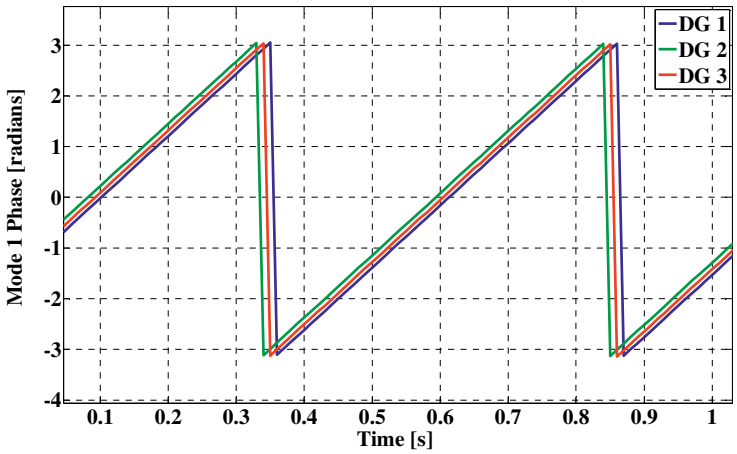

Figure 5.20. Mode 1 – phase of the speed signal of DG 1, 2 and 3

Figure 5.21 shows that the phase shift between the phase angles of DG 1, 2 and 3 for Mode 1 (presented in Figure 5.20 with respect to DG 1) are constant in time. Figure 5.22 shows the instantaneous difference between the phases computed with the method based on the time domain decomposition and compared with Hilbert transform.

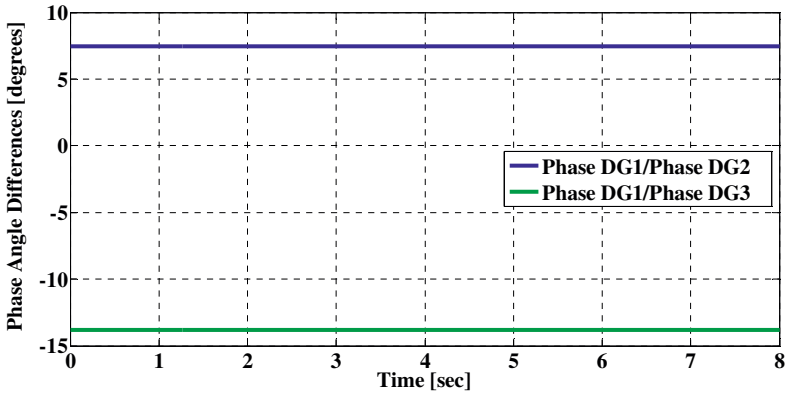

Figure 5.21. Phase angle differences of DG 2 and DG 3 with respect to DG 1.

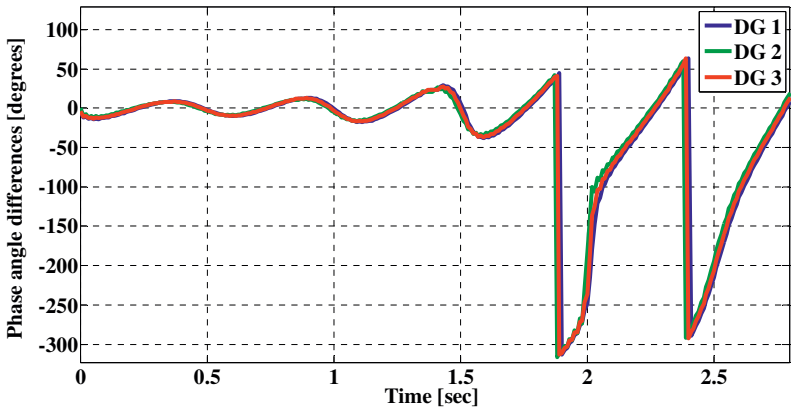

Figure 5.22. Phase angle difference using

the proposed method versus the Hilbert transform

As it is shown in the above Figures 5.20 and 5.21 presenting the modes of oscillation associated with the complex conjugate pairs of eigenvalues 1–2 and 5–6, DG 1 and 3 are oscillating coherent against DG 2.

Using the proposed method to compute the instantaneous Euclidean Distance in polar coordinates– between all DG units for Modes 5 and 6, the following DG clusters can be identified:

Table 5.12. Clusters of DG Units By Using the Instantaneous Euclidean Distance in Polar Coordinates

Clusters	**DG Units**
Cluster 1	DG 1, DG 3
Cluster 2	DG 4, DG 5, DG 6
Cluster 3	DG 7, DG 10, DG 11
Cluster 4	DG 8, DG 9
Cluster 5	DG 2

In Table 5.13 presents the ED matrix in absolute values between all DG units for Mode 5 and 6:

Table 5.13. Averaged instantaneous ED matrix

$[ED] =$

	DG_1	**DG_2**	**DG_3**	**DG_4**	**DG_5**	**DG_6**	**DG_7**	**DG_8**	**DG_9**	**DG_10**	**DG_11**	**DG_12**
DG_1	1.0000	0.9909	0.0584	0.1080	0.1060	0.1040	0.1110	0.1090	0.1090	0.1110	0.1110	0.4480
DG_2	0.9909	1.0000	0.9730	0.9990	0.9990	0.9990	1.0000	1.0000	1.0000	1.0000	1.0000	0.5530
DG_3	0.0584	0.9730	1.0000	0.0567	0.0556	0.0531	0.0597	0.0584	0.0582	0.0599	0.0598	0.4237
DG_4	0.1080	0.9990	0.0567	1.0000	0.0011	0.0039	0.0030	0.0018	0.0015	0.0032	0.0032	0.4468
DG_5	0.1060	0.9990	0.0556	0.0011	1.0000	0.0029	0.0041	0.0029	0.0026	0.0043	0.0043	0.4463
DG_6	0.1040	0.9990	0.0531	0.0039	0.0029	1.0000	0.0070	0.0057	0.0054	0.0072	0.0071	0.4466
DG_7	0.1110	1.0000	0.0597	0.0030	0.0041	0.0070	1.0000	0.0012	0.0015	0.0002	0.0002	0.4475
DG_8	0.1090	1.0000	0.0584	0.0018	0.0029	0.0057	0.0012	1.0000	0.0003	0.0014	0.0014	0.4473
DG_9	0.1090	1.0000	0.0582	0.0015	0.0026	0.0054	0.0015	0.0003	1.0000	0.0017	0.0017	0.4473
DG_10	0.1110	1.0000	0.0599	0.0032	0.0043	0.0072	0.0002	0.0014	0.0017	1.0000	0.0000	0.4475
DG_11	0.1110	1.0000	0.0598	0.0032	0.0043	0.0071	0.0002	0.0014	0.0017	0.0000	1.0000	0.4475
DG_12	0.4480	0.5530	0.4237	0.4468	0.4463	0.4466	0.4475	0.4473	0.4473	0.4475	0.4475	1.0000

5.6. Dynamic Equivalents of Active Distribution Grids Based on Model Parameters Identification

5.6.1. Generalities

In the Section a new method is proposed to compute dynamic equivalents of ADGs to be used for small signal stability studies of the main grid. The scope of the method is to produce simplified models which will preserve the dominant electromechanical modes of oscillations of ADGs. The computation of dynamic equivalents is based on the method published in [16] and described in Section 5.5 were clusters of coherent DG units are identified by calculating the instantaneous Euclidean distance in polar coordinates. The method of Section 5.5 will be extended to identify the clusters of DG units and the dominant modes in which DGs exhibits coherent behavior.

Furthermore, the time responses of the state variables associated with equivalent generators will be built within the identified dominant electromechanical modes. Using a model parameter identification tool available in commercial power system software, the parameters of equivalent generators and automatic voltage regulators will be obtained, based on the computed new state variables. To validate the method a new small signal stability calculation is produced.

5.6.2. Electromechanical modes identification

In order to identify the dominant electromechanical modes, a filtering technique was used for selecting those modes with an oscillation frequency between 0.2 and 2 Hz, [41].

A modal analysis was performed using DIgSILENT PowerFactory© for the test ADG. The dominant electromechanical modes are presented in Table 5.11 in Sub−section 5.5.2.3. C).

As will be shown during the following Sub−Sections, the proposed method performs well in identifying the dominant modes of oscillations. But when performing a clustering of units as it will be described later, the method will not consider the local plant oscillations modes.

Further the clusters presented in Sub−Section 5.5.2.3 will be considered and the set of modes used to reconstruct the equivalent signals will be extended to the set of local plant modes, presented in Table 5.14:

Table 5.14. Dominant Electromechanical Modes of Oscillations

Electromechanical Modes	**Real Part**	**Imaginary Part**	**Damped Frequency**	**Damping Ratio**
–	**[1/s]**	**[rad/s]**	**[Hz]**	**[%]**
Mode 10	−12.631	±33.876	5.391	34.936
Mode 11	−16.006	±31.575	5.025	45.214
Mode 12	−12.493	±30.870	4.913	37.514
Mode 13	−6.622	±22.514	3.583	28.217
Mode 14	−4.270	±19.588	3.117	21.298
Mode 15	−5.606	±18.064	2.875	29.639
Mode 16	−5.886	±16.068	2.557	34.396
Mode 17	−3.854	±14.954	2.380	24.956

5.6.3. Method Description

In the following the steps of computing dynamic equivalents based on model parameter identification are presented.

5.6.3.1. Clustering of DG units and dominant electromechanical modes identification

In this step the number of clusters of DG units which exhibit a coherent behavior both in magnitude and phase of oscillations, are identified using the method introduced in [41] and detailed in Sub−Section 5.5.2.2. As presented in [6], the time responses of a state variable x (in this case the speed) for each of i and j DG unit can be modelled as a linear combination of k dynamic modes, as shown in (5.109) and (5.110):

$$\Delta x_i(t) = \Phi_{i,1} c_{i,1} e^{\lambda_1 t} + \Phi_{i,2} c_{i,2} e^{\lambda_2 t} + \cdots + \Phi_{i,k} c_{i,k} e^{\lambda_k t} \tag{5.109}$$

$$\Delta x_j(t) = \Phi_{j,1} c_{j,1} e^{\lambda_1 t} + \Phi_{j,2} c_{j,2} e^{\lambda_2 t} + \cdots + \Phi_{j,k} c_{j,k} e^{\lambda_k t} \tag{5.110}$$

Where:

- $\Delta x_i(t)$ and $\Delta x_j(t)$ are the DGs small speed variations, Φ_i and Φ_j are the right eigenvectors
- c_k represents the magnitude of the excitation of the k^{th} mode
- λ_k represents the k^{th} oscillatory mode.

Or, rewriting (5.109) and (5.110) in the complex form [4]:

$$\Delta x_i(t) = \mathbf{\Psi}_{i,1} e^{\psi_{i,1} t} + \mathbf{\Psi}_{i,2} e^{\psi_{i,2} t} + \cdots + \mathbf{\Psi}_{i,k} e^{\psi_{i,k} t} \tag{5.111}$$

$$\Delta x_j(t) = \mathbf{\Psi}_{j,1} e^{\psi_{j,1} t} + \mathbf{\Psi}_{j,2} e^{\psi_{j,2} t} + \cdots + \mathbf{\Psi}_{j,k} e^{\psi_{j,k} t} \tag{5.112}$$

Where:

- $\mathbf{\Psi}_{i,k}, \mathbf{\Psi}_{j,k}$ and $\psi_{i,k}, \psi_{j,k}$ represent complex numbers having the form: $\alpha + j\Omega$.

Using the theory described in Sub–Section 5.5.2.2 is possible to compute the instantaneous Euclidean Distance $-ED_{ij}(t)$ between generators i^{th} and j^{th}. A set of clusters will be identified for each k^{th} electromechanical mode.

The ***dominant electromechanical modes*** will be recognized as those modes in which DG units are clustered as similar. Or, in other words, dominant electromechanical modes are those modes in which DG units exhibit coherent behavior.

5.6.3.2. Computation of time responses of equivalent state variables

After the numbers of DG clusters and their compositions are determined, the time response of equivalent state variables associated with each clusters equivalent generator are computed. The time response of equivalent state variables is computed using a weighting function representing the sum of the linear combinations in the *n* dominant modes multiplied with normalized participation factors for each cluster *m* and DG unit *i*. The equivalent state variables for which the time response is computed are equivalent speed (ω_{eq}), rotor angle (δ_{eq}), excitation flux ($\psi_{fd,eq}$), flux in the damping D axis ($\psi_{1d,eq}$), and flux in the damping Q axis ($\psi_{1q,eq}$). In this case, the amortisseurs in the generator model are included, and the system of equations is as in (5.113) [41]:

$$\begin{cases} s\omega = \dfrac{1}{2H}\left(T_m - T_e - K_D\omega\right) \\ s\delta = \omega_0 \Delta\omega \\ s\psi_{fd} = \dfrac{\omega_0 R_{fd}}{L_{adu}} E_{fd} - \omega_0 R_{fd} i_{fd} \\ s\psi_{1d} = -\omega_0 R_{1d} i_{1d} \\ s\psi_{1q} = -\omega_0 R_{1q} i_{1q} \\ s\psi_{2q} = -\omega_0 R_{2q} i_{2q} \end{cases} \tag{5.113}$$

As presented in [41], the model includes one *d* and *q* axis amortisseurs as shown in Figures 5.23 *a*) and *b*).

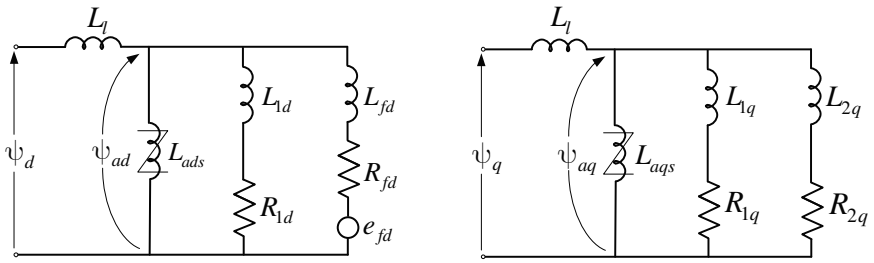

Figure 5.23. Synchronous machine equaivalent circuits with one *d* and *q* axis amortisseurs [41]

The time response of an equivalent state variable Δx_{eq} of a cluster *m*, is defined as:

$$\Delta x_{eq,m}(t) = \sum_{DG_i=1}^{M} \sum_{n=1}^{N} \left\{ \Phi_{DG_i,n} c_{DG_i,n} \left(\frac{P_{DG_i,n}}{P_{n,\max}} \right) e^{\lambda_n t} \right\} \tag{5.114}$$

Where:

DG_i – represents i^{th} DG unit belonging to cluster *m*

n – represents the dominant electromechanical mode

$P_{DG_i,n}$ – represents the participation factor of the state variable *x* of DG unit *i*, in dominant mode *n*

$$P_{n,\max} = \max\left(P_{i,n}\right) \tag{5.115}$$

Where:

$P_{n,\max}$ – represent the maximum participation factor of state variable *x* in dominant mode *n* for each DG unit *i* belonging to cluster *M*

m – number of DG units from cluster *M*

n – number of dominant electromechanical modes

5.6.3.3. Reference machine definition

The reference machine of the cluster *m* is defined as the DG unit with the maximum participation factor of state variable *x* within the dominant mode *n.* The parameters of the reference machine will be used in the next steps as an initial guess in the Model Parameter Identification function of DIgSILENT PowerFactory©.

5.6.3.4. Parameters identification of equivalent generators

Using the computed equivalent state variables for each cluster $m \in M$, the parameters of an equivalent generator associated with an AVR with the cluster *m* are identified using the

Model Parameter Identification function of DIgSILENT PowerFactory© [38]. In order to identify the parameters of equivalent generators based on the computed state variables from (5.110), a benchmark grid needs to be used. This benchmark consists of a ″stiff″ voltage source connected to the generator-transformer (GT) set, to which the parameters have to be identified. The resistance and reactance defined in the ″stiff″ voltage source are the external resistance and reactance measured (by a frequency sweep) at the terminal of the GT set of the reference machine. The benchmark grid model is presented in Figure 5.24. The reference frequency signal in per-unit of the ″stiff″ voltage source is controlled using the computed equivalent speed. In this way the equivalent generator will be ″forced″ to reproduce the same dominant oscillation modes preserved in the computed signals. The equivalent signals (ω_{eq}, δ_{eq}, $\psi_{fd,eq}$, $\psi_{1d,eq}$, $\psi_{1q,eq}$) are passed from a measurement file together with the corresponding simulated signal to a comparator which tunes the equivalent generator's parameters by minimizing an objective function. According to [38], the parameters identification algorithm is based on a least square method and the objective function is computed as in (5.116):

$$\sum_{i=1}^{n}\left[\left(M_i - S_i\right)w_i\right]^p \tag{5.116}$$

Where:

- M_i is the measured response (equivalent signals)
- S_i is the simulated response
- w_i is the weighting factor (user defined)
- p is the power (user defined)

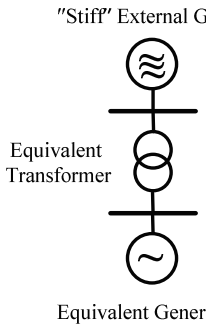

Figure 5.24. Benchmark grid for parameters identification of equivalent generator

The identification process diagram is presented in Figure 5.25.

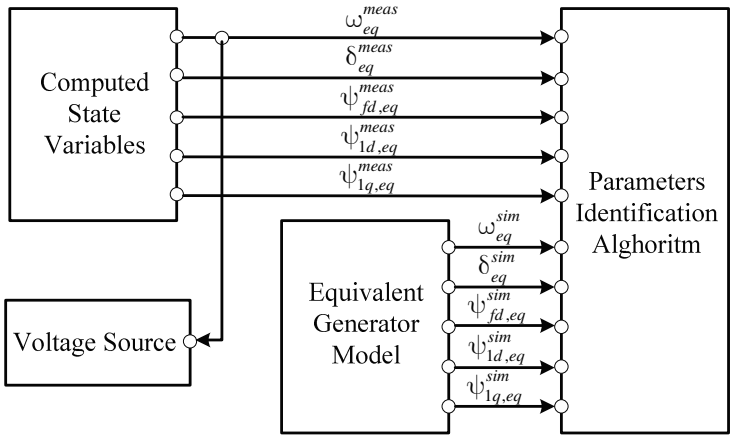

Figure 5.25. Parameter identification process diagram

The nominal apparent power S_{eq}[MVA], active power setpoints P_{eq}[MW] and inertia H_{eq}[s] of the equivalent generator (correspondent to the cluster *m*) are computed as:

$$S_{eq} = \sum_{DG_i} S_{DG_i} \tag{5.117}$$

$$P_{eq} = \sum_{DG_i} P_{DG_i} \tag{5.118}$$

$$H_{eq} = \sum_{DG_i} \frac{H_{DG_i}}{m} \tag{5.119}$$

Where:

m – number of DG units from cluster *M*

5.6.3.5. Network reduction

After identifying the parameters of the equivalent generators on the basis of the computed state variables, the ADG network is reduced to an Extended Ward Equivalent. A detailed description of the network reduction methods can be found in Sub–Section 4.2.1. B). This equivalent was chosen due its ability to roughly preserve the active and reactive power flows, as discussed in [14].

5.6.3.6. Method validation

In this step a new modal analysis computation is produced for the dynamic equivalent connected to the transmission power system. The scope is to observe if the dominant modes of oscillation were retained in the equivalent model of the ADG.

5.6.4. Results

5.6.4.1. Dominant Modes Dynamic Equivalent

In this Section, the steps described in Section 5.6.3 are applied for the test ADG, in order to obtain a dynamic equivalent which will reproduce only the dominant modes of oscillation. Using the method described in 5.6.3.1, for clustering of DG units and dominant modes identification, the following sets of clusters resulted for each of the electromechanical modes, shown in Table 5.15.

Table 5.15. Clusters of DG Units for all Electromechanical Modes

	Mode 1	**Mode 2**	**Mode 3**	**Mode 4**	**Mode 5**	**Mode 6**
DG 1	Cluster 1	Cluster 1	Cluster 1	Cluster 1	Cluster 1	Cluster 1
DG 2	Cluster 2	Cluster 1	Cluster 1	Cluster 1	Cluster 1	Cluster 2
DG 3	Cluster 2	Cluster 1	Cluster 2	Cluster 1	Cluster 1	Cluster 1
DG 4	Cluster 2	Cluster 2	Cluster 2	Cluster 2	Cluster 2	Cluster 3
DG 5	Cluster 2	Cluster 2	Cluster 2	Cluster 2	Cluster 2	Cluster 2
DG 6	Cluster 2	Cluster 1	Cluster 3	Cluster 2	Cluster 2	Cluster 2
DG 7	Cluster 1	Cluster 2	Cluster 2	Cluster 3	Cluster 3	Cluster 4
DG 8	Cluster 1	Cluster 2	Cluster 1	Cluster 3	Cluster 3	Cluster 5
DG 9	Cluster 1	Cluster 3	Cluster 4	Cluster 3	Cluster 3	Cluster 5
DG 10	Cluster 1	Cluster 2	Cluster 3	Cluster 2	Cluster 2	Cluster 3
DG 11	Cluster 1	Cluster 3	Cluster 3	Cluster 3	Cluster 3	Cluster 4

It can be observed from Table 5.15 that DG units present a coherent behavior in modes 4 (1.602 Hz) and 5 (1.565 Hz), in which the clustering is similar. Therefore, these two modes are defined as dominant modes and are used to compute the state variable of the equivalent generators, as described in 5.6.3.2. The reference machines were identified based on (5.115) for each of the three clusters, as presented in Table 5.16:

Table 5.16. ReferenceMachines in Clusters 1, 2 and

	Reference Machine
Cluster 1	DG 2
Cluster 2	DG 6
Cluster 3	DG 9

Using equation (5.115), the state variables (ω_{eq}, δ_{eq}, $\psi_{fd,eq}$, $\psi_{1d,eq}$, $\psi_{1q,eq}$) were computed for all three equivalent generators. Figures 5.26 and 5.27 present the computed state variables: speed and excitation of the equivalent generator 1 based on (5.114). A small increase of 5% was produced at the reference speed signal of the HYGOV main hydro power plant hydro–governor.

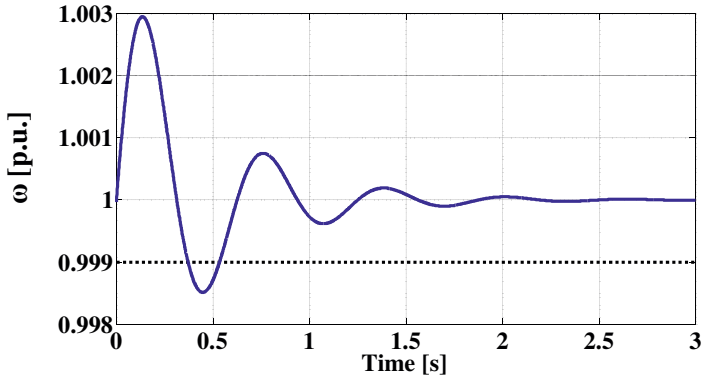

Figure 5.26. Computed speed of equivalent generator 1

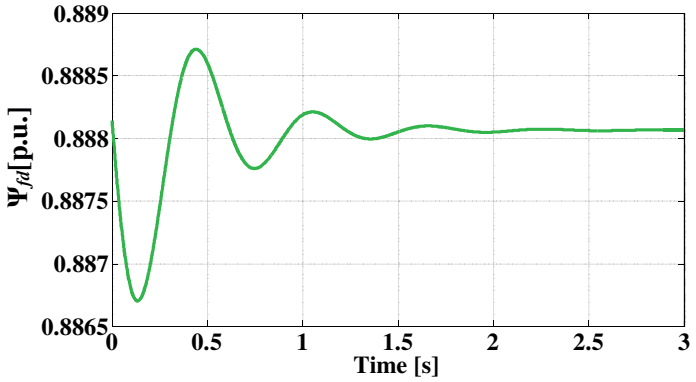

Figure 5.27. Computed excitation flux of equivalent generator 1

After network reduction is completed, the ADG is represented by a set of equivalent impedances between each of the retained buses. Voltages sources are connected at each retained bus in order to preserve the active and reactive power flows [38].

The equivalent generators are connected to the retained bus bars of reference machines presented in Table 5.16 via equivalent transformers (the nominal apparent power for each machine is as defined in (5.117)).

The structure of the dynamic equivalent is presented in Figure 5.28.

After network reduction is completed, the ADG is represented by a set of equivalent impedances between each of the retained buses. Voltages sources are connected at each retained bus in order to preserve the active and reactive power flows [38].

The equivalent generators are connected to the retained bus bars of reference machines presented in Table 5.16 via equivalent transformers (the nominal apparent power for each machine is as defined in (5.117)).

The structure of the dynamic equivalent is presented in Figure 5.28.

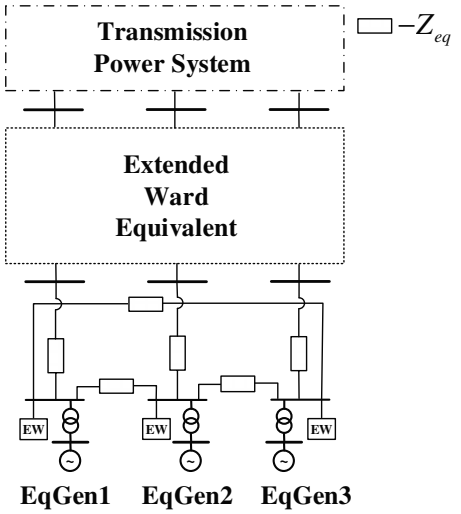

Figure 5.28. Dynamic equivalent model of the test ADG

A new small signal analysis was computed and the new electromechanical modes of oscillation are presented in Table 5.17. The dominant modes of oscillation (modes 1 and 2) were identified in the list of modes, validating the dynamic equivalent technique for the dominant modes of oscillations recognized.

Table 5.17. Electromechanical Modes Using the Dynamic Equivalent Model

Electromechanical Modes	**Real Part**	**Imaginary Part**	**Damped Frequency**	**Damping Ratio**
–	**[1/s]**	**[rad/s]**	**[Hz]**	**[%]**
Mode 1	−2.331	±10.005	1.592	22.690
Mode 2	−2.115	±9.964	1.585	20.763
Mode 3	−1.448	±8.162	1.299	17.467
Mode 4	−49.636	±8.147	1.296	98.679
Mode 5	−2.345	±5.238	0.833	40.861
Mode 6	−0.451	±5.129	0.816	8.759
Mode 7	−1.861	±4.021	0.640	42.001
Mode 8	−2.103	±3.827	0.609	48.159
Mode 9	−1.671	±2.534	0.403	55.051

Figure 5.29 presents the speed time responses for all of the three equivalent generator units.

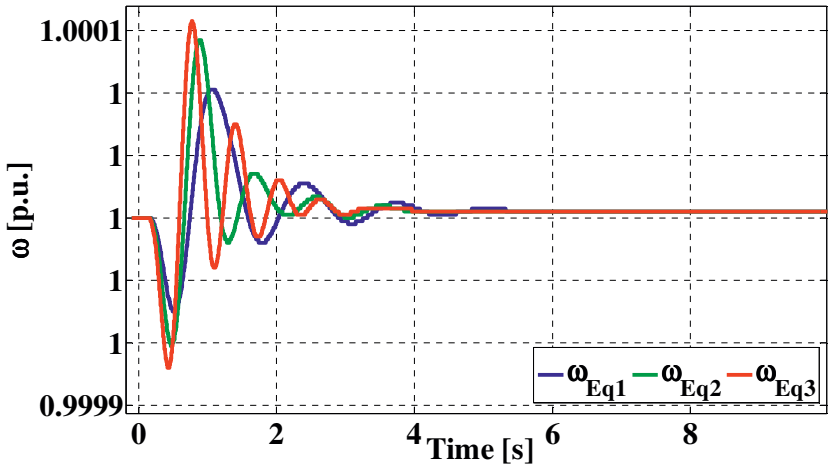

Figure 5.29. Speed responses of the equivalent generators

Figure 5.30 presents the eigenvalues for the original and reduced models. As can be observed, the equivalent preserves the modes with the following frequencies: 1.592, 1.585 and 0.403 [Hz]. These frequencies are the approximation of the modes: 1.6026, 1.5651 and 0.416 [Hz].

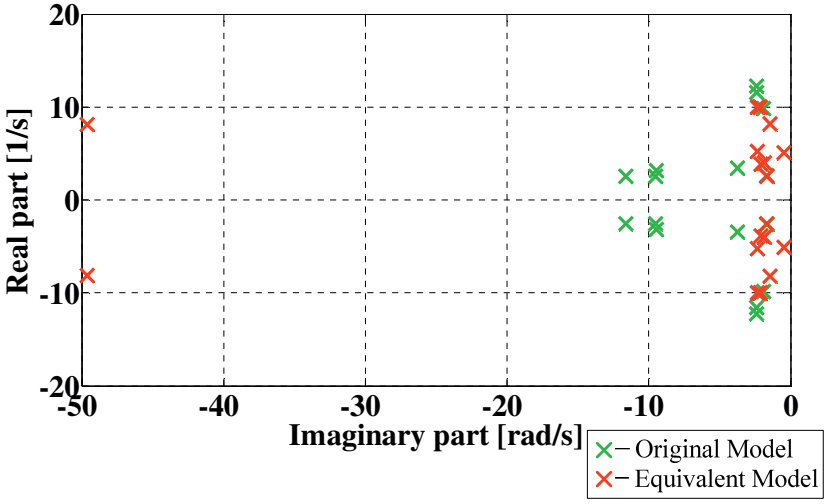

Figure 5.30. Eigenvalues for the original and reduced models.

Table 5.18 presents the frequencies and damping ratios of the recognized modes for the equivalent model from the original one of the ADG. The errors and the average error are presented in [%].

Table 5.18. Electromechanical Modes Using the Dynamic Equivalent Model

Damped Frequency [Hz]			**Damping Ratio [%]**		
Original Model	Equivalent Model	Error [%]	Original Model	Equivalent Model	Error [%]
1.6026	1.592	1.06	21.561	22.69	1.129
1.5651	1.585	1.99	19.126	20.763	1.637
0.416	0.403	1.3	54.256	55.051	0.795

5.6.4.2. Multi−Modes Dynamic Equivalent

In this Section the list of electromechanical oscillation modes presented in Table 5.11 is extended with the local plant modes presented in Table 5.14. The equivalent speed signals rebuilt with these complex conjugate modes are presented in Figure 5.31.

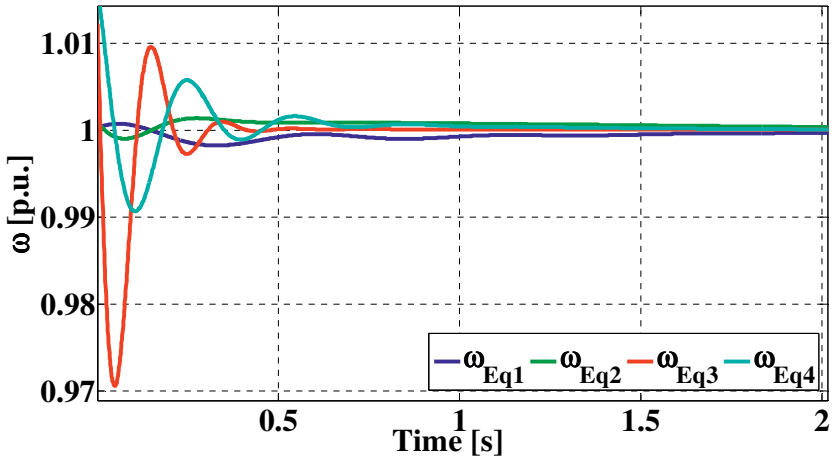

Figure 5.31. Speed responses of the equivalent generators

As presented in Section 5.6.3.3, reference generators must be defined in order to identify the parameters of the equivalent generators.

Table 5.19 presents the reference generators. The clusters of generators are referred to Table 5.19 from Sub−Section 5.5.2.3. C).

Table 5.19. Reference Machines in Clusters 1, 2, 3 and 4

	Reference Machine
Cluster 1	DG 3
Cluster 2	DG 6
Cluster 3	DG 10
Cluster 4	DG 9

In Figure 5.32 the eigenvalues of the equivalent and reduced model are plotted. From Figure 5.34 it can be observed that this equivalent provides a better approximation of the original modes: 1.6026, 1.5651 and 0.416 [Hz].

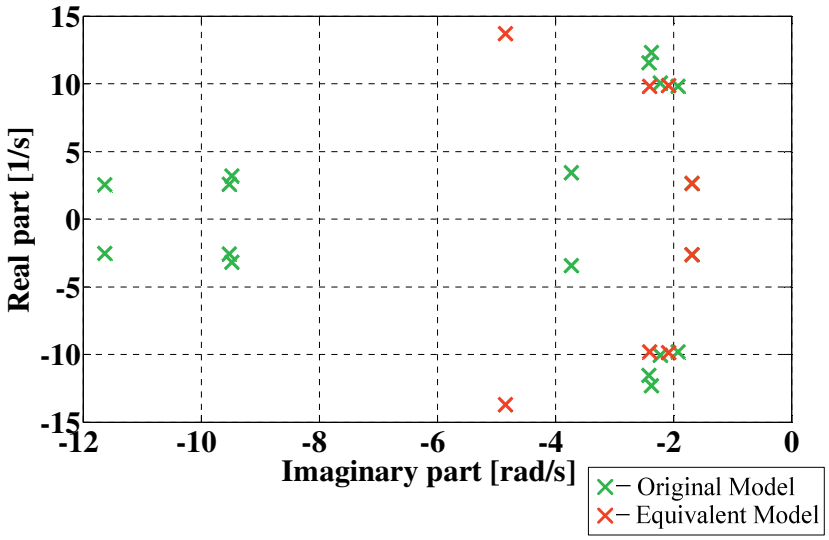

Figure 5.32. Eigenvalues of the equivalent and reduced model

Figure 5.33 presents the speed time responses for all of the three equivalent generator units.

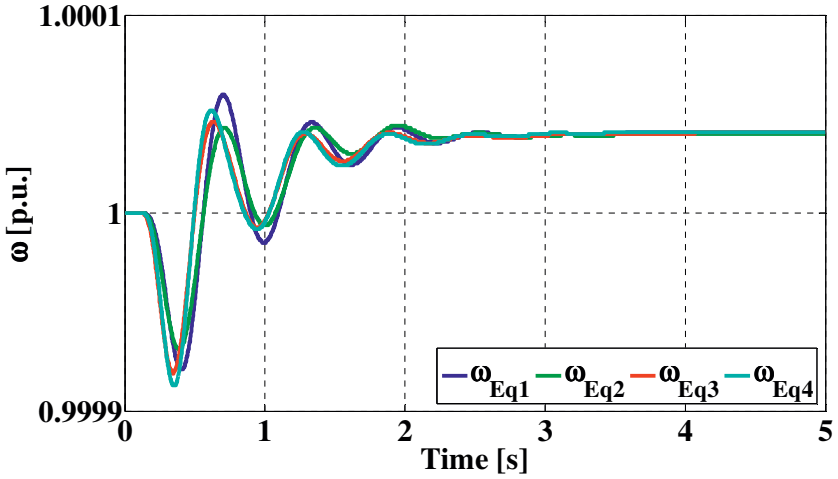

Figure 5.33. Speed responses of the equivalent generators

In Table 5.20 the frequencies and damping ratios of the dominant modes for the original and multi−modes equivalent model of the ADG are presented. The errors and the average error are presented in [%].

Table 5.20. Electromechanical Modes Using the Dynamic Equivalent Model

Damped Frequency [Hz]			**Damping Ratio [%]**		
Original Model	Equivalent Model	Error [%]	Original Model	Equivalent Model	Error [%]
1.6026	1.572	3.0125	21.561	20.633	0.987
1.5651	1.557	0.3521	19.126	23.757	4.633
0.4158	0.416	0.0709	54.256	54.030	0.161

5.7. Summary

In Sections 5.3 and 5.4 a classical method to cluster generators was presented. This method is based on the slow coherency theory developed by Dr. Joe Chow in [59]. Using the slowest inter–area modes to group the generators into areas it was observed for the test ADG that by modeling the synchronous generators using the electromechanical and transient models, the resulting groups of generators differ from the ones when the excitation system is included. Including the excitation more accurate groups of coherent generators are obtained similar with the ones observed by running a small signal time domain simulation. This has to do with the modeling of the excitation systems and with the particularity of ADG systems. This particularity is that for distribution grids with high penetration of small scale hydro units the inter–area modes are very well damped. Therefore the groups of coherent generators show up in local plant modes. The coherency recognition in these particular grids become more complex as the coherency is not identifiable in just one mode, but in a mix of several modes.

From this point the linear analysis fails to identify correctly the groups of generators and a new method as the one proposed in Section 5.5 can give better results. This method is based on decomposition of the state variables' time domain responses for each of the oscillation modes. By using this, magnitude and phase of the state variable can be observed over a time range for each of the modes. By using this information, further a simple method can be used to determine the groups of coherent generators in the ADG. This method allows also the identification of the oscillation modes which now presents a grid wide perspective. The time domain decomposition is a powerful tool which can allow the aggregation of coherent groups of generators. This method is extended in order to compute the equivalent signals of the aggregated generators as presented in Section 5.6. The dynamic parameters of these generators can be determined using model parameter identification algorithm.

Chapter 6

Discussions

In this Chapter, the results presented in the previous Chapters are discussed.

6.1. Grid Code Requirements: similarities, harmonization and drawbacks

In the first part of Chapter 2, an overview of different national grid codes related to the integration of DG units has been presented. The surveyed grid codes are from both transmission and distribution level of the power system, as some of the countries introduce requirements for DG connection in their national transmission grid codes.

This is mainly due to the fact that DG penetration grade in their national power system is not so high and the need for a distinct distribution grid code has not been necessary. In the survey a comparison and analysis of the main steady state and transient requirements was conducted. Some similarities were observed through this survey and a trend towards a harmonization of the European codes which nowadays is in the act and known as the ENTSO-E grid code.

It was observed that the technical connection guidelines in the national grid codes are varying from country to country. The principle reasons for this are the degree of DG penetration and the robustness of the national power systems. It can also be concluded from the overview that in the most recent grid codes related to DG integration, system operators are asking for more demanding capabilities during fault occurrence in the grid (fault ride through, reactive current injection or absorption).

These requirements were absent in previous versions of grid codes, where a disconnection of the DG unit was permissible. It was observed that most of the grid codes (especially those issued in countries with large amount of DG penetration) are making a clear distinction in the requirements between DG units which presents a power electronic interface and those based on synchronous generators. Also, the trend is to divide these requirements with respect to the specifics of the generation site where DG units are installed e.g.: onshore and offshore requirements (offshore requirements are related to wave energy and offshore wind power plants). Some international publications (from IEEE and ENTSO-E) were also investigated, having a regulatory harmonization approach and presenting some new features for DG connection requirements.

In the first part of Chapter 3, the main topics which were not covered in the grid codes' LV–FRT requirements were found as the inadequacy of external power system modeling and the absence of voltage phase angle variation. These drawbacks were investigated in detail and main discussions are summarized in the following.

Four models were considered for modeling of the external grid, especially concerning on the capabilities of a DG unit to withstand a three phase fault are investigated:

- a Thévenin equivalent
- a multi-machine power system
- dynamic equivalents based on **Ward** and **Extended Ward**

Computer based simulations were carried out to achieve the dynamic response of the DG unit (modeled in this case as a small scale hydro unit) when a three phase fault occur at the PCC, using all four aforementioned models for external grid representation. For the Thévenin equivalent the model described in the existing grid codes was used, and for the multi-machine power system a benchmark power system was studied.

To obtain the wide area dynamic equivalents of the benchmark power system, a dynamic aggregation of synchronous generators technique based on the coherency method was applied. As for the power system reduction, Ward and Extended Ward equivalency methods were applied. The results show that by using a Thévenin equivalent, overall inaccurate LV−FRT results are obtained for the main parameters of DG unit (rotor angle, voltage magnitude and angle variation, active and reactive power).

This is mainly due to the fact that a Thévenin equivalent does not represent the electromechanical dynamics as a complete model representation of power system would do. In terms of active and reactive power variations after the fault, it was observed that the first oscillations present smaller magnitudes with respect to the connection of DG unit in the benchmark power system and in corresponding equivalents. This can be a critical observation as these magnitudes will be used by the DG developers to choose the generator ratings and controllers. The benchmark power system was modeled to represent all dynamics associated with an ADG and TPS as well the inter-area dynamics between these power systems. It is obvious that by increasing the detail in the power system representation, the accuracy of the results will increase. But a trade-off must be performed between the range of electromechanical dynamics covered by the complexity of the model, the effort to simulate the model in a commercial software and simulation time. By using wide area dynamic equivalents of the benchmark power system it was observed that the original response was roughly preserved, mostly by using a dynamic Extended Ward equivalent. This is mainly due to a more accurate representation of reactive power flow. Some errors are introduced by the equivalency process, mainly due to the aggregation method used and the process of power system reduction technique.

In the second part of Chapter 3, it was shown from dynamic computer simulations of the system under study that the expected transient response of a hydro power DG-unit equipped with a synchronous generator strongly depends on both change in amplitude and phase angle of the terminal voltage caused by the fault in question, especially the active power response. An analysis taking only voltage change as the perturbation will in many cases most likely lead to erroneous conclusions regarding transient stability of the unit and critical clearing time.

In addition, the study shows that the type (and parameterization) of the unit's automatic voltage controller in this case have a significant impact on the unit's Critical Clearing Time. Also, it was observed that by decoupling the magnitude and phase angle of voltage, there will be large differences in rotor angle excursions meaning that the appreciation of the transient stability margin is erroneous.

6.2. Dynamic Equivalents of Active Distribution Grids for Rotor Angle Transient Stability

In Chapter 4, methods usually used to obtain dynamic equivalents of wide area TPSs are applied to a benchmark ADG with an increased share of small scale hydro units.

The scope is to produce a simulation model suitable for representation of ADGs in transient stability studies of TPSs by taking in consideration the dynamics associated with DG units connected. In order to reduce the ADG network, an Extended Ward equivalent was used, and to aggregate dynamically the DG units a mechanical coherency method based on rotor angle variation was applied.

To validate the algorithm two criteria were proposed. The first looks at the preservation of the voltage magnitude and angle variations at the busbar in the internal area (in this case the MV busbar of the bay transformer where the ADG is connected). These variations are of interest when considering the AVR and load modeling influence on the transient stability study.

The second criterion looks at the preservation of the transient stability margins as an important indication of the rotor angle dynamics associated with the synchronously connected DG units. The study have shown that the dynamic equivalent obtained for ADG preserves the original response, in terms of voltage magnitude and angle variations when a fault emerged at the bay's transformer MV busbar.

Regarding the transient stability margins, a small increase was observed compared to the original one. This small difference is due to the process of aggregation of transient, subtransients and exciter parameters of the synchronous DG units.

In Chapter 4 an investigation regarding the impact of disturbance duration, location and type on the coherency identification of DGs were carried out. It was observed that the composition of clusters is very much influenced by these three factors. Therefore, it can be concluded that these type equivalents are to be obtained and used for each particular study case. Their dynamic content cannot be used for general studies of the main PTS. However, all the disturbances gives a general indication regarding which DG units are coherent for the case when a small signal equivalent is needed.

6.3. Dynamic Equivalents of Active Distribution Grids for Rotor Angle Small Signal Stability

Chapter 5 presented a method to obtain dynamic equivalents of ADGs for small signal stability studies. This method is based on the slow coherency theory developed by Dr. Joe Chow in [62]. In this theory the main idea is that the identification of coherent generators arises in slow inter–area modes due to weak connections between the generators. The main advantage of this method compared with the one described in Chapter 4 is that this method produce the groups of coherent generators independent by the disturbance (location, duration and type). The theory behind this concept used in the singular perturbation method and a tolerance based algorithm developed in the same reference was used to group the small scale hydro units in the test ADG.

In the first part of Chapter 5 it was investigated how the modeling of the synchronous generator impacts the identification of slow coherent generators. In this analysis three models were considered:

- electro–mechanical model
- transient model
- transient model with excitation system

For these models the general equations of synchronizing torques in multi–machine power systems were developed. Using these equations the reduced system matrices to the internal buses of generators were used to compute the eigenvalues and right eigenvectors.

Then by using the tolerance based algorithm described in Section 5.4.1 the coherent groups of generators are obtained. It was observed that by using the electro–mechanical and transient models the same groups of generators were obtained. By including the excitation system a grouping similar to the one produced by running a time domain simulation for a small perturbation in the system was observed.

This similarity is showing that by increasing the generator modeling and including the excitation system a better approximation of the synchronizing torques values are obtained, which is important to have a better image over the similarity or dissimilarity between the generators.

By modeling the excitation system and varying the amplifier gain K_A it was shown that generators from the same coherent group can be excluded from the group for large values of K_A. This is due to decreasing the synchronizing torques.

In the second part of Chapter 5 a new method for clustering DG units in a test ADG is proposed. This method allows the computation of the instantaneous Euclidean Distance in polar coordinates for clustering Distributed Generation units, and is based on modes decomposition and *"free motion time responses"* computation, as presented in [11]. This is done to obtain the instantaneous magnitudes and phases for the state variable used to recognize the coherency between DGs. This method can be applied to off-line studies of power systems and the computation of instantaneous magnitudes and phases is done by running iterative modal analyses of the known ADG, at each time step *t*.

The advantage of this method is that by using the *ED(t)* in polar coordinates, both the coherency of magnitude and phase can be achieved with one tool.

The method produces an accurate clustering of DGs. However, the main drawback is that the topology of the ADG needs to be known, in order to run iterative modal analysis. And a trade–off must be done between the number of equivalent generators to be obtained and the accuracy of the eigenvalues of the equivalent model. This method is a time domain method and the clustering is very dependent of the magnitude of the excitation. Lower magnitude of excitation will give a smaller number of equivalent generators and a smaller degree of dissimilarity between them. Higher magnitude of excitation will give opposite results. However, high excitation can make certain controllers to reach their limits; therefore a thorough investigation must be done to choose the right value of excitation and the right variable to which this excitation have to be applied. Good values of the excitation are 0.01–0.02 p.u. and the recommended signals for which this excitation can be applied are the ones with the highest participation factor in the considered mode. As one is mainly interested in the electromechanical modes it is advisable that the selected signal to be mechanical torque

or reference speed of the governor and respecting the rule that the controllers' do not reach their limits.

Later in Chapter 5, the proposed method is extended so that it can be used to compute equivalent signals from the eigenvectors and participation factors of coherent generators. This equivalent signals are computed for certain eigenvalues which have to be retained. The scope of rebuilding these equivalent signals from the eigenvectors and participation factors of the coherent generators (within certain eigenvalues) is to obtain the parameters of the equivalent generators. This is done by using a parameter identification method and fitting these equivalent generators' parameters on the equivalent signals.

It was observed that by applying the method described above to identify the clusters of DGs for all the electromechanical modes, the inter–area modes can be recognized. It was also observed that for these modes the clusters composition show up the same.

However, it was observed that the aggregation method based on the equivalent signals performs well and retains the modes needed. The higher the number of modes used to compute the equivalent signals, the higher are the retained modes and they are also more accurate. This type of equivalents presents the advantage that can be obtained not only from computed signals (as speed, rotor angle etc) but also from measured signals (voltage, current and power).

Chapter 7

Conclusions and Future Research

This Chapter summarizes the main findings of the research presented in this thesis and presents some suggestions for future work with respect to this work.

7.1. Main Conclusions

Power systems are passing through profound changes, mainly due to the liberalization of electricity markets, the depletion of primary energy resources and the concern about climate change. These premises have created a favorable framework for development of distributed energy resources. As a result, the level of integration of distributed generation (DG) technologies, especially in distribution networks has increased. In order to counteract the impact of DG on the stability and reliability of power systems, the transmission and distribution systems operators have started to reconsider and update their national grid codes.

After surveying different national grid codes related to DG integration, some general conclusions can be drawn:

- The surveyed grid codes were from both transmission and distribution level of the power system, as some of the countries introduce requirements for DG connection in their national transmission grid codes. This was mainly due the fact that DG penetration grade in their national power system is not so high and the need for a distinct distribution grid code has not been necessary. It was observed that the technical connection guidelines in the presented national grid codes are varying between different countries. Sometimes, new requirements (LV–FRT, reactive current injection or absorption) makes the most recent grid codes more stringent than the previous versions where DG units were asked to disconnect during severe perturbations. The main reasons for this are the grade of DG penetration and the robustness of the national power systems.
- The new grid codes are making a clear distinction in the requirements between DG units which presents a power electronic interface and those based on synchronous generators. Also, the trend is to divide these requirements with respect to the specifics of the generation site where DG units are installed e.g. in onshore and offshore requirements (offshore requirements are related to wave energy and offshore wind power plants).
- Some international publications (from IEEE and ENTSO-E) were also found interesting, having a regulatory harmonization approach and presenting some new features for DG connection requirements.

As presented throughout of this thesis the PhD work address grid codes requirements related to DG integration. The research done in this work is divided in two main parts:

i. Investigations related to the LV−FRT requirement
ii. Investigations related to the ADG modelling from a TSO perspective

However, special attention was given to the LV−FRT requirement for DGs during this survey, and some topics which were not covered by this requirement were found. These topics became research topics for this work:

- The adequacy of the representation of the external grid
- The impact of the voltage phase variation on the capabilities of small scale hydro units

With respect to the adequacy of the representation of the external grid the following main conclusions can be drawn:

- By using a Thévenin equivalent, overall inaccurate LV−FRT results are obtained for the main parameters of DG unit (rotor angle, voltage magnitude and angle variation, active and reactive power). This is mainly due to the fact that a Thévenin equivalent does not represent the electromechanical dynamics as a complete model representation of power system would do.
- By using dynamic equivalents of the benchmark power system it was observed that the original response was roughly preserved, mostly by using a dynamic Extended Ward equivalent. This is mainly due to a more accurate representation of reactive power flow. Some errors are introduced by the equivalency process, mainly due to the aggregation method used and the process of power system reduction technique.

By studying the impact of the voltage phase variation on the capabilities of small scale hydro units, the following main results can be presented:

- The transient response of a hydro power DG-unit equipped with a synchronous generator strongly depends both on change in amplitude and phase angle of the terminal voltage, resulting from a fault in the system.
- The type and parameterization of the unit's automatic voltage controller have a significant impact on the unit's CCT. Also, it was observed that by decoupling the magnitude and phase angle of voltage, there will be large differences in rotor angle excursions meaning that the appreciation of the transient stability margin is erroneous.

Regarding the second research topic the main findings can be resumed as follows:

- By using dynamic equivalent for transient stability, it was shown that these equivalents obtained for ADG preserves the original response, in terms of voltage magnitude and angle variations when a fault emerged at the bay's transformer MV busbar. Regarding the transient stability margins, a small increase was observed in comparison with the original one. It was observed that the composition of clusters is very much influenced by the disturbance location, duration and type. Therefore, it can be concluded that these type equivalents are to be obtained and used for particular study case.
- By using dynamic equivalents for small signal stability based on slow coherency theory, disturbance independent equivalents of the ADG can be computed. For this, the impact of the synchronous generator modelling over the slow coherent groups' identification was studied. It was observed that by using the electro−mechanical and

transient models to produce the reduced system matrices, the same groups of generators were obtained. By including the excitation system more accurate coherent groups are obtained. These groups of generators being similar with the one obtained by using a time domain simulation.

- By including the excitation it was observed that the slow coherent groups of generators are dependent by the amplifier gain constant K_A value. High values to the amplifier gain can significantly change the composition of the coherent groups. It was also observed that when including the excitation system the electromechanical eigenvalues computed for this equivalent model are more accurate than by using simple models of the generator.
- It was seen that for ADGs with high penetration of small scale hydro, units the coherency phenomena occurs for DGs at modes with higher damped frequencies, which can be confirm by running a small signal time domain analysis. Normally the magnitude of excitation for a small signal time domain analysis is so small that by observing the time response of some state variables these groups of coherent generators are very difficult to identify. Therefore a new method was proposed for clustering DG units in the test ADG. This method allows the computation of the instantaneous Euclidean Distance in polar coordinates for clustering Distributed Generation units, and is based on modes decomposition and *"free motion time responses"* computation.
- The advantage of this method is that by using the *ED(t)* in polar coordinates, both the coherency of magnitude and phase can be achieved with one tool. However, the main drawback is that the topology of the ADG needs to be known, in order to run iterative modal analysis. And a trade−off must be done between the number of equivalent generators to be obtained and the accuracy of the eigenvalues of the equivalent model.
- Also as this method is a time domain method the clustering is very dependent by the magnitude of the excitation. Lower magnitude of excitation will give a smaller number of generators and a smaller degree of similarity between them. Higher magnitude of excitation will give opposite results. However, it was observed that the aggregation method based on the equivalent signals performs well and retains the modes need it. The higher is the number of modes used to compute the equivalent signals, the higher are the retained modes and more accurate.

7.2. Future Work

Active Distributions Grids are an important topic in the agenda of DSOs and TSOs as the degree of penetration of DG units is expected to increase. Therefore it can be expected that the research related to the integration of such units in the future power systems will be more visible in the next years. Moreover, the grid code requirements will play an important role in ensuring that the security and reliability of supply will not be violated by integrating DG units in the distribution grids. Many aspects of these requirements must be further clarified. For example, in terms of LV−FRT capabilities an investigation is needed related to the adequacy of external grid modelling when integrating non-synchronous generators (as wind and photovoltaic generators) and storage devices. In this regard, an important topic to be

studied is how the dynamics and control strategies for these types of units are affected when increasing the modelling complexity of external grid model.

As presented in Chapter 3 by decoupling the voltage magnitude variation to the variation of the voltage phase angle, erroneous results can be obtained when the LV–FRT is investigated. Aspects related to this assumption were thoroughly investigated in Chapter 3 and the assumption was validated for synchronously based small scale hydro units. But an important question remains related to how the control strategies of non–synchronous generators units must be adapted to comply with the voltage phase angle variation when LV–FRT capabilities are assessed.

In the last years it was observed an increase attention to the development of large HVDC projects.

Therefore it can be expected that future large transmission power systems will be representing a mix of AC and DC electricity transmission technologies. An important aspect to be studied can be related to how the slow coherency theory can be adapted to build dynamic equivalents of the future transmission power systems. Further, an algorithm can be developed based on the slow coherency theory to identify the slow areas consisting of non-synchronous generators (wind, PV). Moreover, new methods used to produce on–line equivalents of large interconnected power systems can be found adequate for reducing the ADGs models.

Reference List

[1] J. B. Ward, "Equivalent Circuits for Power-Flow Studies," *Trans. of the American Institute of Electrical Engineers,* vol. 68, no. 1, pp. 373-382, July 1949.

[2] J. Undrill, J. Casazza, E. Gulachenski and L. Kirchrnayer, "Electromechanical Equivalent for Use in Power System Stability Studies," *EEE Trans. Power Apparatus and Systems,* Vols. PAS-90, no. 5, pp. 2060-2071, Sept. 1971.

[3] H. Taxt, M. Catrinu and D. Nordgård, "Overall challenges and recommendations concerning the integration of small scale hydro in MV distribution networks," in *Electricity Distribution (CIRED 2013), 22nd International Conference and Exhibition on*, Stockholm, 10-13 June 2013.

[4] D. Nordgård, M. Istad, T. Solvang, M. Catrinu, L. Aleixo and G. Kjølle, "Methodology for planning of distributed generation in weak grids," in *PowerTech, 2011 IEEE*, Trondheim, 19-23 June 2011.

[5] CIGRE Working Group 37-23, "Impact of increasing contribution of dispersed generation on the power system".

[6] IEEE Std. 1547/2003, "Standard for Interconnecting Distributed Resources with Electric Power Systems," July 2003.

[7] Eurostat, "Electricity generated from renewable sources," [Online]. Available:http://epp.eurostat.ec.europa.eu/tgm/table.do?tab=table&init=1&language=en &pcode=tsie, 9 June 2010.

[8] L. Scott and W. G. Willis, Distributed Power Generation, Marcel Dekker: New York, 2000.

[9] Norwegian Water Resources and Energy Directorate, "Small power plants potential", Available Online: http://arcus.nve.no/website/potensial_smaakrv/viewer, 2010, 28 October.

[10] V. Knazkins, "Stability of power systems with large amounts of distributed generation," PhD Thesis published at KTH University, Stockholm, 2004.

[11] A. Azmy and I. Erlich, "Identification of dynamic equivalents for distribution power networks using recurrent ANNs,," *Power Systems Conference and Exposition, 2004. IEEE PES,* vol. 1, pp. 348-353, 10-13 Oct. 2004.

[12] A. Ischchenko, J. M. A. Myrzik and W. Kling, "Dynamic equivalencing of distribution networks with dispersed generation," *Power Engineering Society General Meeting, 2006. IEEE,* p. 8, 2006.

[13] T.-N. Preda, K. Uhlen and D. Nordgård, "An overview of the present grid codes for integration of distributed generation," in *Integration of Renewables into the Distribution Grid, CIRED 2012 Workshop*, Lisbon, 2012.

[14] T. Preda, K. Uhlen, D. Nordgård and T. Toftevaag, "External Grid Representation for Assessing Fault Ride Through Capabilities of Distributed Generation Units," *Innovative Smart Grid Technologies (ISGT Europe), 2012 3rd IEEE PES International Conference and Exhibition on,* pp. 1,9, 14-17 Oct. 2012.

[15] T. Preda, K. Uhlen, D. Nordgård and T. Toftevaag, “Dynamic equivalents of active distribution power systems for investigation of transient stability,” in *Electricity Distribution (CIRED 2013), 22nd International Conference and Exhibition on*, Stockholm, 2013.

[16] T. Preda, K. Uhlen and D. Nordgård, “Clustering Distributed Generation Using the Instantaneous Euclidean Distance in Polar Coordinates,” *Innovative Smart Grid Technologies Europe (ISGT EUROPE), 2013 4th IEEE/PES,* no. 6-9 Oct. 2013, pp. 1-5, 6–9 Oct. 2013.

[17] Hydro-Quebec. Distribution, "Requirements for the Interconnection of Distributed Generation to the Hydro-Québec Medium-Voltage Distribution System," Available online: http://www.hydroquebec.com/transenergie/fr/commerce/pdf/e1201_fev09_en.pdf, February 2009.

[18] Manitoba-Hydro, "Interconnection Guideline for Connecting Distributed Resources to the Manitoba Hydro Distribution System," Available online: http://oasis.midwestiso.org/documents/Mheb/Interconnection%20Guideline%20for%20Connecting%20Distributed%20Resources%20to%20Manitoba%20Hydro%20Distribution%20System.pdf, January 2003.

[19] Energinet.dk, "Technical Regulation for Thermal Power Station Units larger than 11 kW and smaller than 1.5MW," Available online: in http://www.energinet.dk/EN/El/Forskrifter/Technical-regulations/Sider/Regulations-for-grid-connection.aspx, October 2008.

[20] BDEW, "Guideline for generating plants’ connection to and parallel operation with the medium-voltage network," Available online: http://www.bdew.de/internet.nsf/id/A2A0475F2FAE8F44C12578300047C92F/$file/BDEW_RL_EA-am-MS-Netz_engl.pdf, June 2008.

[21] The EirGrid, "EirGrid Grid Code, version 3.5," Available online: http://www.eirgrid.com/media/2011%20Mar%2008%20EirGrid%20Grid%20Code%20Clean%20Version%203.5.pdf, March 2011.

[22] SINTEF Energy, "Network Code for Requirements for Grid Connection Applicable to generators with maximum active power production less than 10 MW in (the) distribution grid," October 2006.

[23] Red Electrica, "Technical requirements for wind power and photovoltaic installations and any generating facilities whose technology does not consist on a synchronous generator directly connected to the grid," O.P. 12.2 Restricted to the technical requirements of wind power and photovoltaic facilities (draft), October 2008.

[24] National Grid Electricty Transmission plc, "The Grid Code, Issue 4, revision 7," Available online: http://www.nationalgrid.com/uk/Electricity/Codes/gridcode/gridcodedocs/, August 2011.

[25] Energy Network Association, "The Distribution Code," Available online: http://www.energynetworks.info/the-distribution-code/, August 2011.

[26] ENTSO-E, “ENTSO-E Draft Network Code for Requirements for Grid Connection applicable to all Generators,” 24 January 2012.

[27] IEEE Std., “IEEE Std. 1547/2003, Standard for Interconnecting Distributed Resources with Electric Power Systems,” July 2003.

[28] A. Adamczyk, R. Teodorescu and P. Rodriguez, "Adaptation of 12-bus System for Wind Power Integration Studies," in *Proc. of the 9th International Workshop on Large-Scale Integration of Wind Power into Power systems*, Denmark, Aarhus, 25-26 Oct. 2010.

[29] F. Iov, A. Hansen, P. Sørensen and N. Cutululis, "Mapping of grid faults and grid codes," Risø National Laboratory, Technical University of Denmark, Roskilde, Denmark, Tech. Rep. Risø-R-1617(EN), Roskilde, Denmark, July 2007.

[30] IEC Std. 61400-21, "Wind turbines- Part 21: Measurement and assessment of power quality characteristics of grid connected wind turbines," IEC 61400-21, Edition 2.0, p. 22-23, 2008-08.

[31] J. Shan, U. Annakkage and A. Gole, “A platform for validation of FACTS models,” *IEEE Trans. Power Delivery,* vol. 21, no. 1, pp. 484- 491, Jan. 2006.

[32] S. Chen, "Network reduction in power system analyses," Master project thesis, Department of Electrical Engineering, Technical University of Denmark, Available Online: http://www.dtu.dk/centre/cet/english/education/student_projects/09/sc.aspx, DK-2800 Kgs. Lyngby, Denmark, March 2009.

[33] K. Lo, L. Peng, J. Macqueen, A. Ekwue and N. Dandachi, "Extended Ward equivalent of external system for on-line security analysis," *2nd International Conference on Advances in Power System Control, Operation and Management, 1993, APSCOM-93.,* vol. 1, pp. 54-59, 7-10 Dec 1993.

34] T. L. Baldwin, L. Mili and A. G. Phadke, "Dynamic Ward Equivalent for Transient Stability Analysis," *IEEE Trans. Power Systems,* vol. 9, no. 1, February 1994.

[35] A. Chang and M. Adibi, "Power System Dynamic Equivalents," *IEEE Trans. Power Apparatus and Systems,* Vols. PAS-89, no. 8, pp. 1737-1744, Nov. 1970.

[36] M. L. Ourari and L. A. a. D. V. Q. Dessaint, "Generating Units Aggregation for Dynamic Equivalent of Large IEEE Power System," *IEEE Power Engineering Society General Meeting, 2004,* vol. 2, pp. 1535-1541, June 2004.

[37] M. A. Husby, "Stasjonære analyser i forbindelse med tilkobling av vindmølleparken i Ytre Vikna," Master semester project, Department of Electric Power Engineering , Norwegian University of Science and Technology (NTNU), p. 17-22, Trondheim, Norway, December 2011.

[38] DigSilent GmbH, "DIgSILENT PowerFactory Version 14.0 – User’s Manual," DIgSILENT GmbH, Gomaringen, Germany, July 2010.

[39] M. Poller and S. Achilles, "Aggregated Wind Park Models for Analyzing Power System Dynamics," *DIgSILENT GmbH, Gomaringen, Germany, Available Online:http://digsilent.de/tl_files/digsilent/files/services-references/WindParkModeling.pdf.*

[40] J. Machowski, J. Bialek and J. Bumby, "Power System Dynamics: Stability and Control, Second Edition," John Wiley & Sons, 2008.

[41] P. Kundur, "Power System Stability and Control," New York: Mcgraw-Hill Professional, 1994.

[42] Y. Zhou, Y. Duan, B. Zhang, J. Li and K. Wang, "Study of Coherency-based Dynamic

Equivalent Method for Power System with HVDC," *International Conference on Electrical and Control Engineering (ICECE), 2010,* pp. 2013-2016, 25-27 June 2010.

[43] J. Machowski, A. Cichy, F. Gubina and P. Omahen, "External subsystem equivalent model for steady-state and dynamic security assessment," *IEEE Trans. Power Systems,* vol. 3, no. 4, pp. 1456-1463, Nov 1988.

[44] A. Monticelli, S. Deckmann and A. a. S. B. Garcia, "Real-Time External Equivalents for Static Security Analysis," *IEEE Trans. Power Apparatus and Systems,* Vols. PAS-98, no. 2, pp. 498-508, March 1979.

[45] M. Eremia(coordinator) – "*Electric Power Systems. Volume I. Electric Networks*" (in English), Publishing House of the Romanian Academy , Bucharest , 2005.

[46] H. Alsafih and R. Dunn, "Identification of critical areas for potential wide- area based control in complex power systems based on coherent clusters," *2010 45th International Universities Power Engineering Conference (UPEC),* pp. 1-6, 31 Aug.- 3 Sept. 2010.

[47] N. Senroy, "Generator Coherency Using the Hilbert–Huang Transform," *Power Systems, IEEE Transactions on,* vol. 23, no. 4, pp. 1701-1708, Nov. 2008.

[48] O. Lino, M. Fette and J. Ramirez, "Electromechanical distance and identity recognition in dynamic equivalencing," *Power Tech, 2005 IEEE Russia,* pp. 1-9, 27-30 June 2005.

[49] M., Eremia, N. Crisciu, B. Ungureanu and C. Bulac, in *Computer Aided Analysis of the Electric Power Systems*, Bucharest, Romania, Technical Publisher, 1983.

[50] A. Zin, B. Kok, M. Mustafa, K. Lo and A. A.E., "Time domain dynamic aggregation of generating unit based on structure preserving approach," *Proc. 2003 PECon, Power Engineering Conference,* pp. 154- 160, 15-16 Dec. 2003.

[51] J. Slootweg and W. Kling, "Aggregated modelling of wind parks in power system dynamics simulations," *Proc. 2003 IEEE PowerTech Conference, Bologna,* vol. 3, p. 6, 23-26 June 2003.

[52] T. Toftevaag, J. I. Marvik and T. N. Preda, "Impact of voltage phase angle changes on low-voltage ride-through performance of DG-units," *Integration of Renewables into the Distribution Grid, CIRED 2012 Workshop,* pp. 1,4, 29–30 May 2012.

[53] T. Toftevaag, T. N. Preda and K. Uhlen, "Impact of voltage phase angle changes on low-voltage ride-through performance of small scale hydro DG units," *Electricity Distribution (CIRED 2013), 22nd International Conference and Exhibition on,* pp. 1,4, 10–13 June 2013.

[54] IEEE, "IEEE Std 421.5, 2005, IEEE Recommended practice for Excitation System Models for Power System Stability Studies," New York, USA.

[55] AB STRI, "SIMPOW User Manual 11.0," STRI AB, Västerås, Sweden, 2010-09-24.

[56] M. Ribens-Pavella, "Transient stability of power systems: theory and practice," Chichester, West Sussex, UK, John Wiley & Sons, p. 8.

[57] M. Eremia and M. Shahidehpour, in *Handbook of electrical power system dynamics: modeling, stability and control*, New Jersey, The Institute of Electrical and Electronics Engineers, Johen Wiley & Sons, 2014.

[58] J. Winkelman, J. Chow, B. Bowler and B. K. P. Avramovic, "An Analysis of Interarea

Dynamics of Multi-Machine Systems," *Power Apparatus and Systems, IEEE Transactions on ,,* Vols. PAS-100, no. 2, pp. 754-763, Feb. 1981.

[59] J. Chow, in *Power System Coherency and Model Reduction*, New York, Springer, 2013.

[60] J. Chow, J. Winkelman, M. Pai and P. Sauer, "Singular perturbation analysis of large-scale power systems," *Electrical Power and Energy Systems,* vol. 12, no. 2, April 1990.

[61] P. Anderson and A. Fouad, "Power System Control and Stability", New York:, Wiley-IEEE Press, 2002.

[62] J. Chow and P. Kokotovic, "Time Scale Modeling of Sparse Dynamic," *IEEE Transactions on Automatic Control,* vol. 30, no. 8, pp. 714-722, Aug. 1985.

[63] L. Vanfretti, "Phasor measurement-based state estimation of electric power systems and linearized analysis of power system network oscillations," Rensselaer Polytechnic Institute, Troy, New York, Troy, New York, December 2009.

[64] M., Pai, "Small Signal Analysis of Power Systems", New Delhi: Norsa Publishing House, 2004.

[65] P. W. Sauer and M. Pai, "Power System Dynamics and Stability", Upper Saddle River: New Jersey: Prentice Hall, 1998.

[66] J. Chow and K. Cheung, "A Toolbox for Power System Dynamics and Control Engineering Education and Research," *IEEE Transactions on Power Systems,* vol. 7, no. 4, p. 1559–1564, Nov. 1992.

[67] R. Singh, M. Elizondo and S. Lu, "A review of dynamic generator reduction methods for transient stability studies," *Power and Energy Society General Meeting, 2011 IEEE,* pp. 1,8, 24-29 July 2011.

[68] S.-K. Joo, L. Chen-Ching, J. L.E. and J.-W. Choe, "Coherency and aggregation techniques incorporating rotor and voltage dynamics," *Power Systems, IEEE Transactions on,* vol. 19, no. 2, pp. 1068,1075, May 2004.

[69] A. Bruns, "Fourier-,Hilbert- and wavelet-based signal analysis: are they really different approaches?," *Journal of Neuroscience Methods,* vol. 137, no. 2, pp. 321-332, March 2004.

[70] D. Bowman, "A List of Analytic Expressions for Instantaneous Frequency Determined via the Hilbert Transform," The University of North Carolina at Chapel Hill, Chapel Hill, 2013.

[71] Y. Phulpin, M. Begovic and M. Petit, "External Network Modeling for MVAr Scheduling in Multi Area Power Systems," *IEEE Power Tech Conf., Lausanne, 2007,* pp. 1039-1043, 1-5 July 2007.

Appendix 1

APPENDIX 1
Test Transmission Power System

In this Appendix are presented the single line diagram (SLD) and the data of electrical components of the test transmission power system used in Chapter 3, as in [37].

In Figure A1.1 the SLD of the test transmission power system is depicted.

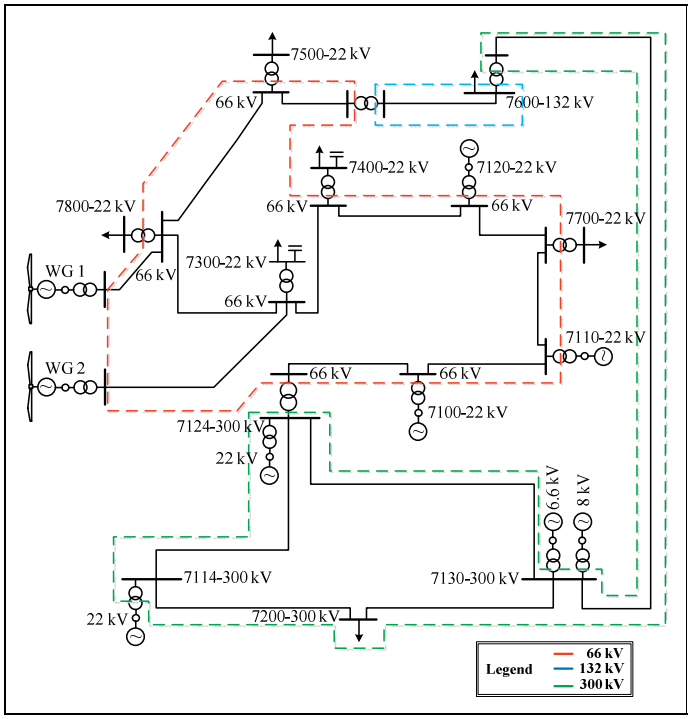

Figure A1.1. SLD of the test transmission power system [37]

In the next tables the data of electrical components of the test transmission power system are given. In Table A1.1 the line parameters are presented:

Table A1.1. Line data

Name	**Bus From**	**Bus To**	**R** [Ω/km]	**X** [Ω/km]	**B** [μS/km]	**Length** [km]	**Number of Circuits**
L1	7100–66	7110–66	0.151	0.386	6.63	22.	1
L2	7110–66	7700–66	0.1	0.373	6.81	15	1
L3	7700–66	7120–66	0.1	0.373	6.81	22	1
L4	7120–66	7400–66	0.1	0.373	6.81	15.7	1
L5	7400–66	7300–66	0.1	0.373	6.81	17.	1
L6	7300–66	7800–66	0.257	0.405	6.42	15.5	1
L7	7300–66	WG2–66	0.191	0.394	6.54	9	1
L8	7800–66	WG1–66	0.151	0.386	6.63	20	1
L9	7800–66	7500–66	0.061	0.358	7.02	24	1
L10	7500–66	7900–66	0.151	0.386	6.63	22.7	1
L11	7900–132	7600–132	0.098	0.398	6.64	37.2	1
L12	7600–300	7130–300	0.019	0.238	10.	42	1
L13	7130–300	7200–300	5.085	53.865	295.65	1	1
L14	7200–300	7114–300	0.801	10.035	95.94	1	1
L15	7114–300	7124–300	0.9	11.205	107.91	1	1
L16	7124–300	7130–300	1.503	18.792	179.73	1	1

In Table A1.2 the dynamic data of generators are presented:

Table A1.2. Generators data

Name	X_d [p.u]	X_q [p.u]	X'_d [p.u]	X''_d [p.u]	X''_q [p.u]	$T'_{d,0}$ [sec]	$T'_{q,0}$ [sec]	$T''_{d,0}$ [sec]	$T''_{q,0}$ [sec]	H [MVA/sec]
G–7130_6.6	0.9659	0.5814	0.2982	0.1734	0.1734	4.6686	–	0.05	0.15	6.18
G–7130_8	1.01	0.62	0.26	0.17	0.17	5.3	–	0.05	0.15	6.18
G–7114	1.17	0.68	0.167	0.1073	0.1073	7.3	–	0.05	0.15	6.5
G–7124	1.0556	0.6213	0.2754	0.1956	0.1956	6.5087	–	0.05	0.15	6.5
G–7100	1.5	1.	0.21	0.2	0.2	1.428	–	0.0105	0.1	0.45
G–7110	1.5	5.	0.4	0.3	0.4	3.	–	0.02667	0.75	2.
G–7120	1.5	2.5	0.3	0.2	0.25	2.	–	0.03	0.2	1.683

In Table A1.3 the load flow data of generators are presented:

Table A1.3. Generators data

	S_{gen} [MVA]	P_{gen} [MW]	$Q_{lim,max}$ [MVAr]	$Q_{lim,min}$ [MVAr]	$U_{g,nom}$ [kV	Bus
G–7130_66	74	53	–40	20	66	7130_6.6
G–7130_8	180	149	–180	180	8	7130_8
G–7114	900	78.911	–20	20	66	7114
G–7124	100	66.047	–100	100	66	7124
G–7100	1.6	0.8	–1.6	1.6	22	7100
G–7110	50	42	–50	50	22	7110
G–7120	10	9	–10	25	22	7120

In Table A1.4 the dynamic data of the wind power plants are presented:

Table A1.4. Wind power plant data

Name	U_n [kV]	S_n [kVA]	f_n [Hz]	P_n [MW]	No. of Pole Pairs	R_S [p.u.]	X_S [p.u.]	X_m [p.u.]	H [kgm^2]	Rotor Type	No. of generators
WPP−1	0.69	2222.	50.	2	2	0.01	0.1	3.5	75.	Single Cage	20
WPP−2	0.69	2222.	50.	2	2	0.01	0.1	3.5	75.	Single Cage	20

In Table A1.5 the data of the transformers are presented:

Table A1.5. Transformers data

Name	**Bus From**	**Bus To**	S_n [MVA]	$U_{n,HV}$ [kV]	$U_{n,LV}$ [kV]	X_1 (Sbase=St) [p.u.]
T1	7100−22	7100−66	15	66	22	0.03
T2	7110−22	7110−66	10	66	22	0.03
T3	7114−22	7114−300	80	300	66	0.03
T4	7120−22	7120−66	15	66	22	0.03
T5	7124−22	7124−300	100	300	66	0.03
T6	7130−6.6	7130−300	56	300	66	0.03
T7	7130−8	7130−300	600	300	8	0.03
T8	7300−22	7300−66	30	66	22	0.03
T9	7400−22	7400−66	30	66	22	0.03
T10	7500−22	7500−66	15	66	22	0.03
T11	7600−132	7600−300	100	300	132	0.03
T12	7700−22	7700−66	20	66	22	0.03
T13	7800−22	7800−66	45	66	22	0.03
T14	7900−66	7900−132	70	66	132	0.03
T15	WG1−0.69	WG1−66	50	66	0.69	0.05
T16	WG2−0.69	WG2−66	50	66	0.69	0.05

In Table A1.6 the data of the loads are presented:

Table A1.6. Loads data

	P [MW]	Q [MVAr]	Bus
L1	400	−	7200_300
L2	4.669	0.948	7300_22
L3	10.962	2.226	7400_22
L4	6.395	1.299	7500_22
L5	−31.7	4	7600_22
L6	4.568	0.92	7700_22
L7	14.313	2.906	7800_22

In Table A1.7 the data of the shunt elements are presented:

Table A1.7. Shunt elements data

	Q [MVAr]	Bus
C1	+7.2	7300_22
C2	+7.2	7400_22

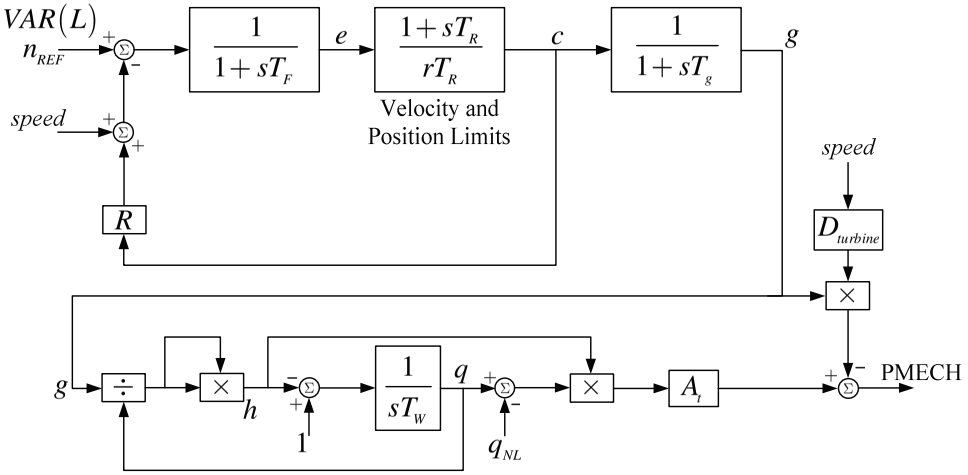

Figure A1.2. Governor model HYGOV [38]

Table A1.8. HYGOV governor data [38]

Parameter	Value			
	G–7130_66	G–7130_8	G–7114	G–7124
Permanent Droop R [p.u.]	0.05	0.05	0.05	0.05
Temporary Droop r [p.u.]	0.4	0.4	0.4	0.4
Governor Time Constant T_r [s]	8	8	8	8
Filter Time Constant T_f [s]	0.05	0.05	0.05	0.05
Servo Time Constant T_g [s]	0.2	0.2	0.2	0.2
Gate Velocity Limit V_{elm} [p.u.]	0.2	0.2	0.2	0.2
Maximum Gate Limit G_{MIN}	0	0	0	0
Minimum Gate Limit G_{MAX}	1	1	1	1
Water Starting Time T_w [s]	1.2	1.2	1.2	1.2
Turbine Gain A_t [p.u.]	1.1	1.1	1.1	1.1
Frictional losses factor pu D_{turb} [p.u.]	0.3	0.3	0.3	0.3
No Load Flow q_{nl} [p.u.]	0.1	0.1	0.1	0.1
Turbine Rated Power(=0–>PN=Pgn)	0	0	0	0

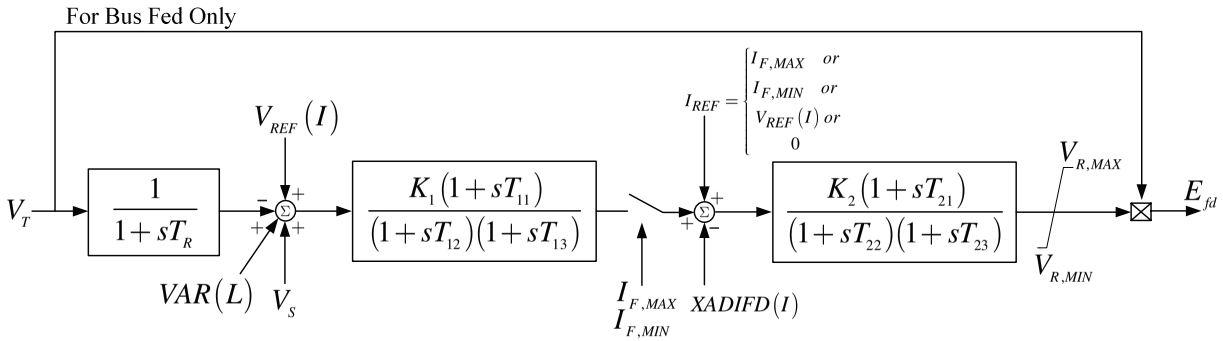

Figure A1.3. Excitation system model EXNEBB [38]

Table A1.9. AVR EXNEBB data [38]

Parameter	Value	
	G−7130_66	G−7114
Measurement Delay T_R	0	0
Voltage Controller Gain K_1	300	300
Controller 1th Delay Time Constant T_{12}	15	15
Controller 1th Derivative Time Constant T_{11}	1	1
Controller 2th Delay Time Constant T_{13}	0.03	0.03
Field Current Controller Gain K_2	4.8	4.8
Controller 1th Delay Time Constant T_{22}	0.03	0.03
Controller 1th Derivative Time Constant T_{21}	0.2	0.2
Controller 2th Delay Time Constant T_{23}	0.09	0.09
Minimum Field Current $I_{F,MIN}$	0	0
Maximum Field Current $I_{F,MAX}$	−4	−4
Controller Minimum Output $E_{FD,\ MIN}$	0	0
Controller Maximum Output $E_{FD,\ MAX}$	4	4
Selector for Solid(=1) or Bus (=0) Fed	0	0

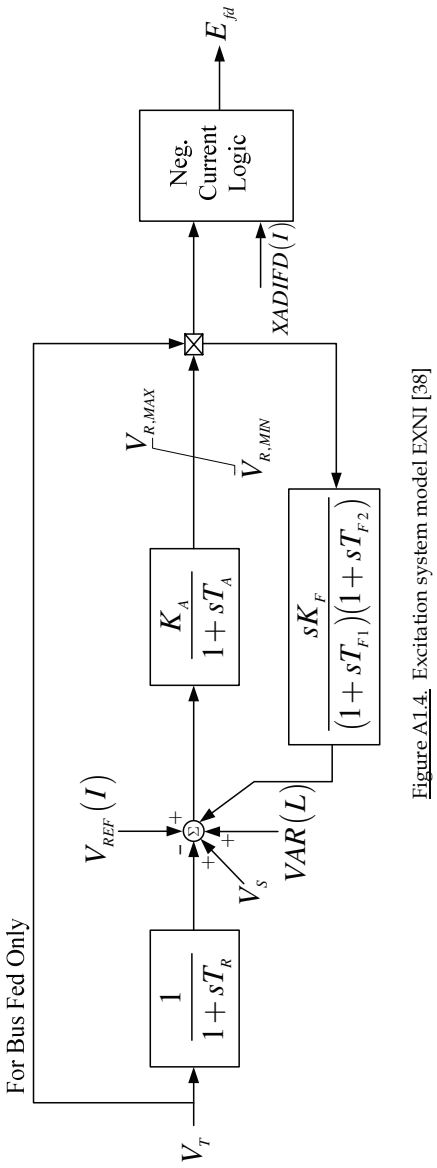

Figure A1.4. Excitation system model EXNI [38]

Table A1.10. AVR EXNI data [38]

Parameter	Value	
	G−7130_8	G−7124
Filter Time Constant T_R	0.06	0.06
Controller Gain K_A	150	150
Controller Time Constant T_A	0	0
Stabilizer Gain K_F	0.018	0.018
Stabilizer Time Constant 1 T_{f1}	0.64	0.64
Stabilizer Time Constant 2 T_{f2}	0.32	0.32
Controller Minimum Output $V_{R, MIN}$	−4	−4
Controller Maximum Output $V_{R, MAX}$	4	4
Selector for Solid(=1) or Bus (=0) Fed $(\text{switch})_3$	0	0
Crowbar resistor factor R	10	10

Appendix 2

APPENDIX 2
Test Radial Distribution Grid

In this Appendix are presented the single line diagram (SLD) and the data of electrical components of the radial distribution grid used in Chapter 3 to investigate the impact of the voltage phase angle variation on the LV–FRT requirement.

In Figure A2.1 the SLD of the test transmission power system is depicted.

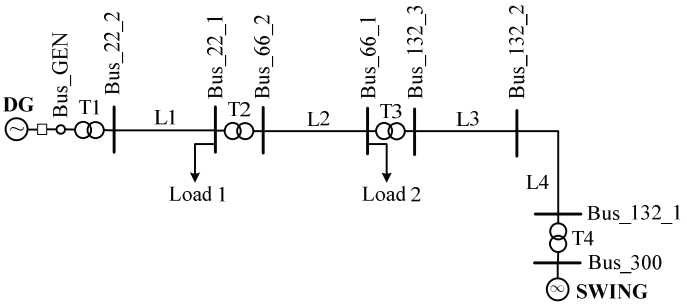

Figure A2.1. SLD of the radial distribution grid [52]

In the next tables the data of electrical components of the test transmission power system are given [52].

In Table A2.1 the line parameters are presented:

Table A2.1. Line parameters

NAME	R [Ω/km]	X [Ω/km]	B [μS/km]	Length [km]
L1	0.359	0.373	3.0756	25
L2	0.395	0.415	1.98	30
L3	0.098	0.398	2.8934	55.2
L4	0.098	0.398	2.8934	36.5

In Table A2.2 the dynamic parameters of the DG unit are presented:

Table A2.2. DG parameters

Parameter		DG model
X_d	[pu]	2.04
X'_d	[pu]	0.238
X''_d	[pu]	0.143
X_q	[pu]	1.16
X''_q	[pu]	0.137
r_a	[pu]	0.00219
X_l	[pu]	0.13
$T'_{d,0}$	[s]	2.38
$T''_{d,0}$	[s]	0.0117
$T''_{q,0}$	[s]	0.11
H	[s]	1.0
V1D	[pu]	1.0
SE1D	[pu]	0.1
V2D	[pu]	1.2
SE2D	[pu]	0.3

In Table A2.3 the parameters of the transformers are given:

Table A2.3. Transformers parameters

NAME	S_n [MVA]	$U_{n,1}$ [kV]	$U_{n,2}$ [kV]	ER12 [pu]	EX12 [pu]
T1	5	0.69	22.0	0.005	0.100
T2	50	129.0	67.0	0.005	0.125
T3	20	62.0	23.0	0.005	0.100
T4	70	290.0	135.0	0.005	0.125

In Table A2.4 the loads data is presented:

Table A2.4. Loads data

NAME	P_{load} [MW]	Q_{load} [MVAr]
Load 1	20	7.5
Load 2	16	4

Next are presented the two models of excitation systems used for the investigation in the Chapter 3, Sub−Section 3.3.

Voltage regulator Model 1: IEEE AC8B Type

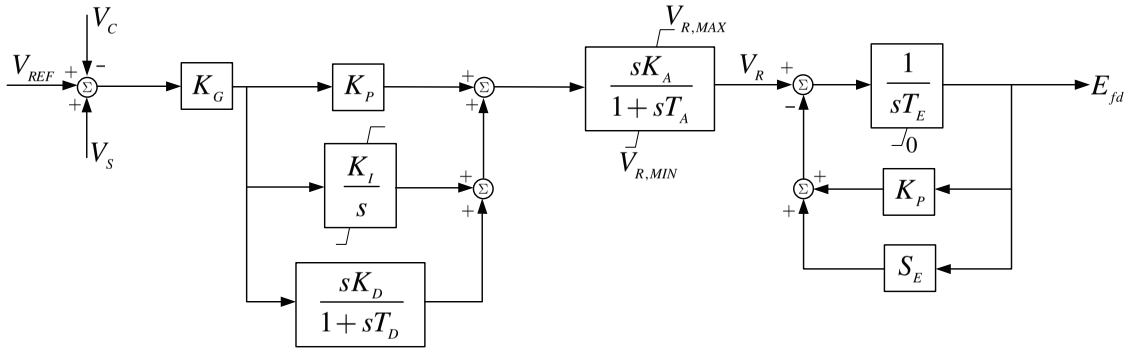

Figure A2.2. Voltage regulator Model 1: IEEE AC8B Type [54]

Table A2.5. Voltage regulator Model 1: IEEE AC8B Type [54]

Parameter			Description
K_P	[pu]	120.5	PID proportional gain
K_I	[pu]	165.5	PID integral gain
K_D	[pu]	24	PID derivative gain
T_D	[s]	0.01	PID derivative time constant
K_A	[pu]	1.0	Voltage regulator gain
T_A	[s]	0	Regulator time constant
V_{Rmax}	[pu]	35	Maximum regulator output
V_{Rmin}	[pu]	0	Minimum regulator output
K_E	[pu]	1.0	Exciter constant
T_E	[s]	0.5	Exciter time constant
S_{E1}	[pu]	1.346	Saturation curve value at point 1
E_1	[pu]	2.222	Voltage value at point 1
S_{E2}	[pu]	1.9	Saturation curve value at point 2
E_2	[pu]	2.962	Voltage value at point 2

Voltage regulator Model 2

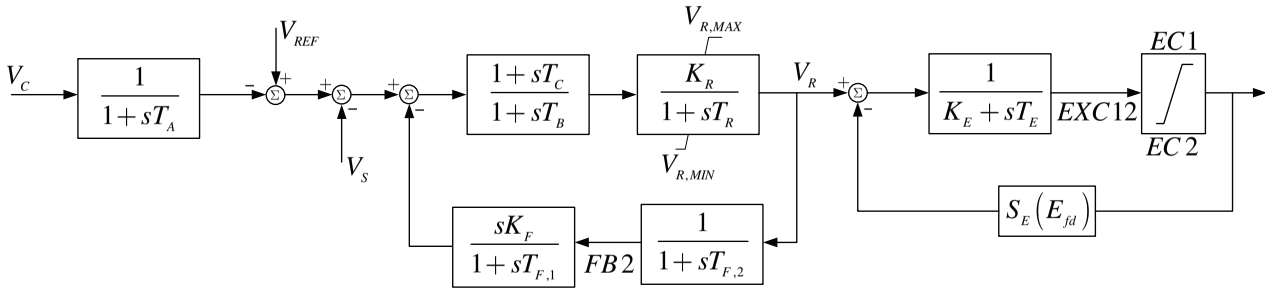

Figure A2.3. Voltage regulator Model 2 [55]

Table A2.6. Voltage regulator Model 2 [55]

Parameter			Description
T_A	[s]	0.05	Regulator amplifier time constant
T_B	[s]	0.01	Time constant
T_C	[s]	0.01	Time constant
K_R	[pu]	500.0	Voltage transducer filter gain
T_R	[s]	0.10	Voltage transducer filter time constant
K_F	[pu]	0.04	Regulator stabilizing circuit gain
$T_{F,1}$	[s]	0.7	Regulator time constant 1
$T_{F,2}$	[s]	0.05	Regulator time constant 2
V_{Rmax}	[pu]	35	Maximum regulator output
V_{Rmin}	[pu]	0	Minimum regulator output
K_E	[pu]	0.8	Exciter constant
T_E	[s]	0.4	Exciter time constant
S_{E1}	[pu]	0.0	Saturation curve value at point 1
E_1	[pu]	1.59	Voltage value at point 1
S_{E2}	[pu]	0.0	Saturation curve value at point 2
E_2	[pu]	2.12	Voltage value at point 2
EC_1	[pu]	6.2	Limit-parameter for saturation 1
EC_2	[pu]	0.01	Limit-parameter for saturation 2

Appendix 3

Appendix 3
Test Active Distribution Grid

In this Appendix the data of the test active distribution grid is presented. The test ADG is a common Norwegian distribution grid and it was provided by one of the DSOs participating in the OiDG project. This grid was first introduced in investigation [den] conducted within the same project (OiDG) as the PhD work. The grid comes from Mid−Norway part, namely from the Namsskogan area where circa 40 MW are planned to be built. [4] *The excerpt from the map is presented in Figure A3.1. Information regarding this grid was obtained from the local DSO and the grid was used further as a benchmark grid for the research produced in this PhD work.*

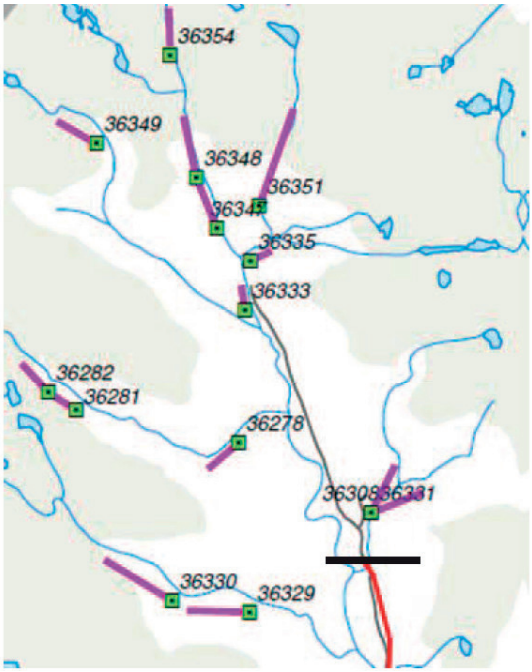

Figure A3.1. Excerpt from the map of the Namsskogan distribution grid [4]

The SLD of this test system is presented in Figure A3.2

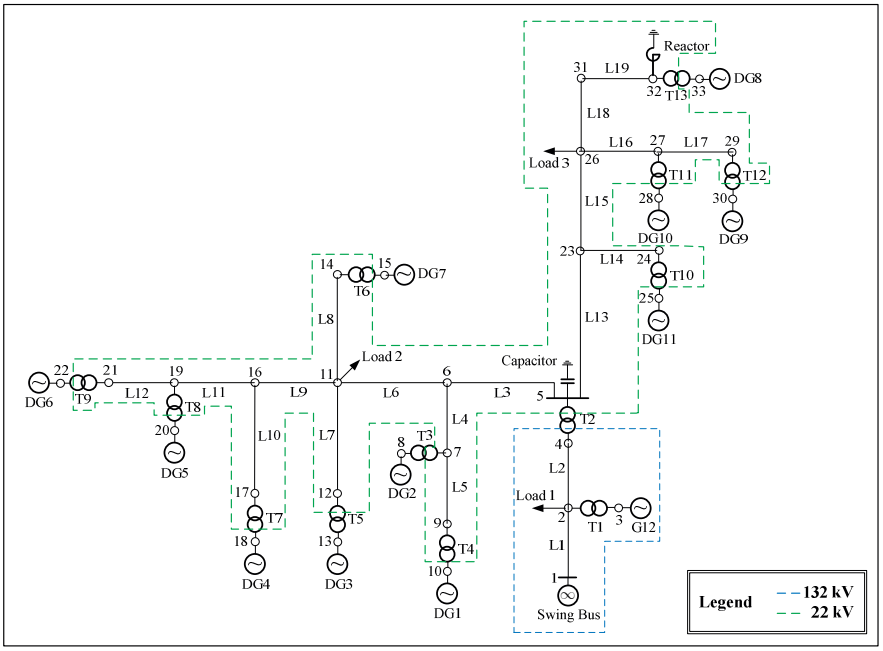

Figure A3.2. Namsskogan distribution grid

In the next lines the data of the electrical equipments are presented in the next Tables:

Table A3.1. Line parameters (physical units).

	Bus From	**Bus To**	**R** [Ω/km]	**X** [Ω/km]	**B** [μS/km]	**Length** [km]	**Number of Circuits**
L1	1	2	0.076	0.365	3.173008	7.7	1
L2	2	4	0.076	0.365	3.173008	7.7	1
L3	5	6	0.141	0.32	2.965663	0.9	2
L4	6	7	0.141	0.32	2.965663	2.2	1
L5	7	9	0.359	0.373	3.074099	1.8	1
L6	6	11	0.141	0.32	2.965663	0.9	1
L7	11	12	0.359	0.373	3.074099	1.3	1
L8	11	14	0.721	0.395	2.895	0.3	1
L9	11	16	0.19	0.35	3.2694	2.5	1
L10	16	17	0.721	0.395	2.895	1.3	1
L11	16	19	0.19	0.35	3.2694	2.5	1
L12	19	21	0.721	0.395	2.895	0.9	1
L13	5	23	0.19	0.35	3.2694	4	1
L14	23	24	0.721	0.395	2.895	0.9	1
L15	23	26	0.359	0.373	3.074099	13.7	2
L16	26	27	0.359	0.373	3.074099	1.5	1
L17	27	29	0.721	0.395	2.895	1.5	1
L18	26	31	0.359	0.373	3.074099	10	1
L19	31	32	0.721	0.395	2.895	1	1

Table A3.2. Generator dynamic parameters (per unit values $S_{base} = S_{gen}$).

	X_d [p.u]	X_q [p.u]	X'_d [p.u]	X'_q [p.u]	X''_d [p.u]	X''_q [p.u]	$T'_{d,0}$ [sec]	$T'_{q,0}$ [sec]	$T''_{d,0}$ [sec]	$T''_{q,0}$ [sec]	H [MVA/sec]
G1	2	1.5	0.2	0.3	0.15	0.25	4	–	0.026667	0.18	2.5
G2	1.5	1	0.3	0.3	0.2	0.15	3	–	0.015	0.2	2.5
G3	2	1.5	0.2	0.3	0.15	0.25	4	–	0.026667	0.18	2.5
G4	2	1.5	0.2	0.3	0.1	0.15	3	–	0.02	0.2	0.7
G5	2	1.5	0.2	0.3	0.1	0.2	4	–	0.02	0.225	1
G6	2	1.5	0.2	0.3	0.1	0.2	4	–	0.04	0.225	1.5
G7	1.5	1	0.15	0.3	0.1	0.1	2	–	0.015	0.1	0.5
G8	2	1.5	0.2	0.3	0.1	0.15	3	–	0.02	0.2	0.7
G9	2	1.5	0.2	0.3	0.1	0.2	4	–	0.02	0.225	1
G10	1.5	1	0.15	0.3	0.1	0.1	2	–	0.015	0.1	0.5
G11	2	1.5	0.2	0.3	0.1	0.1	3	–	0.02	0.15	0.5
G12	1.05	0.8	0.3	0.3	0.2	0.2	2.8	–	0.03	0.12	2.5

Table A3.3. Generator load flow parameters (physical units).

	S_{gen} [MVA]	P_{gen} [MW]	Q_{gen} [MVAr]	$Q_{lim,max}$ [MVAr]	$Q_{lim,min}$ [MVAr]	$U_{g,nom}$ [kV]	Bus
G1	8	5.2	–	2.518474	−1.709157	6.6	10
G2	15	10	–	4.84322	−3.28684	6.6	8
G3	8	6	–	2.905932	−1.972104	6.6	13
G4	4	2.6	–	1.259237	−0.8545784	6.6	18
G5	5	3.4	–	1.646695	−1.117526	6.6	20
G6	6	3.9	–	1.888856	−1.281868	6.6	22
G7	1.6	1.3	–	0.6296186	−0.4272892	0.69	15
G8	4	2.6	–	1.259237	−0.8545784	6.6	33
G9	5	3.6	–	1.743559	−1.183262	6.6	30
G10	1.6	1	–	0.484322	−0.328684	0.69	28
G11	2	1.5	–	0.726483	−0.493026	0.69	25
G12	45	35	–	16.95127	−11.50394	6.6	3

Table A3.4. Transformer Parameters (per unit values $S_{base} = S_{nom}$).

	Bus From	**Bus To**	S_{nom} [MVAr]	$U_{n,HV}$ [kV]	$U_{n,LV}$ [kV]	X_1 [p.u.]
T1	2	3	50	132	6.6	0.1
T2	4	5	50	132	22	0.1
T3	7	8	14	22	6.6	0.09
T4	9	10	14	22	6.6	0.09
T5	12	13	14	22	6.6	0.09
T6	14	15	2	22	0.69	0.06
T7	17	18	5	22	6.6	0.07
T8	19	20	5	22	6.6	0.07
T9	21	22	8	22	6.6	0.08
T10	24	25	2	22	0.69	0.06
T11	27	28	2	22	0.69	0.06
T12	29	30	8	22	6.6	0.08
T13	32	33	5	22	6.6	0.07

Table A3.5. Load Data

	P [MW]	Q [MVAr]
L1	0.702	0.143
L2	0.2116	0.043
L3	0.0074	0.0018

Table A3.6. Shunt elements data

	Q [MVAr]	Bus
C1	+8	5
B2	−2	32

Voltage regulator Model 1: IEEE AC8B Type

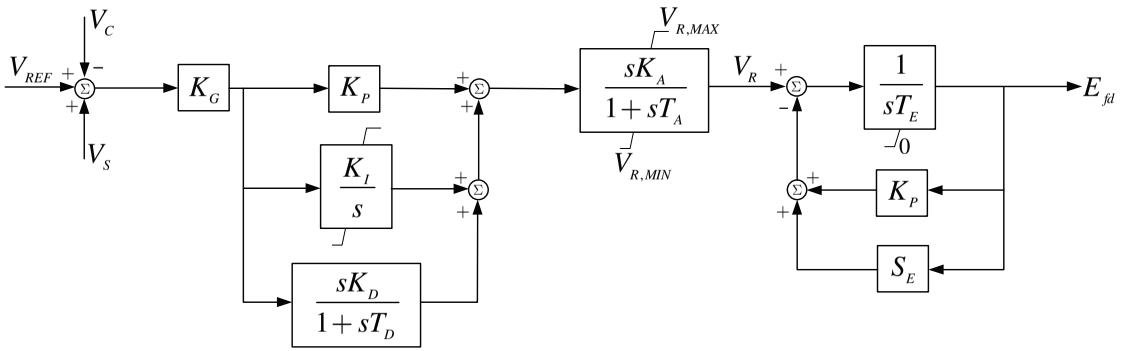

Figure A3.3. Voltage regulator Model 1: IEEE AC8B Type [54]

Table A3.7. Voltage regulator Model 1: IEEE AC8B Type

Parameter		G1	G2	G3	G4	G5	G6	G7	G8	G9	G10	G11	G12
K_P	[pu]	30	30	30	25	40	40	20	25	40	20	20	50
K_I	[pu]	3	5	3	5	5	5	5	5	5	5	5	15
K_D	[pu]	10	10	10	10	10	10	5	10	10	5	5	5
T_D	[s]	0.1	0.1	0.1	0.1	0.1	0.1	0.1	0.1	0.1	0.1	0.1	0.1
K_A	[pu]	1	1	1	1	1	1	1	1	1	1	1	1
T_A	[s]	0	0	0	0	0	0	0	0	0	0	0	0
V_{Rmax}	[pu]	15	15	15	15	15	15	15	15	15	15	15	15
V_{Rmin}	[pu]	0	0	0	0	0	0	0	0	0	0	0	0
K_E	[pu]	1	1	1	1	2	1	1	1	1	1	1	1
T_E	[s]	1.2	1.2	1.2	1.2	1.2	1.2	1.2	1.2	1.2	0.12	0.12	0.5
S_{E1}	[pu]	0.3	0.3	0.3	0.3	0.3	0.3	0.3	0.3	0.3	0.3	0.3	0
E_1	[pu]	6.5	6.5	6.5	6.5	6.5	6.5	6.5	6.5	6.5	6.5	6.5	0
S_{E2}	[pu]	3	3	3	3	3	3	3	3	3	3	3	0
E_2	[pu]	9	9	9	9	9	9	9	9	9	9	9	0

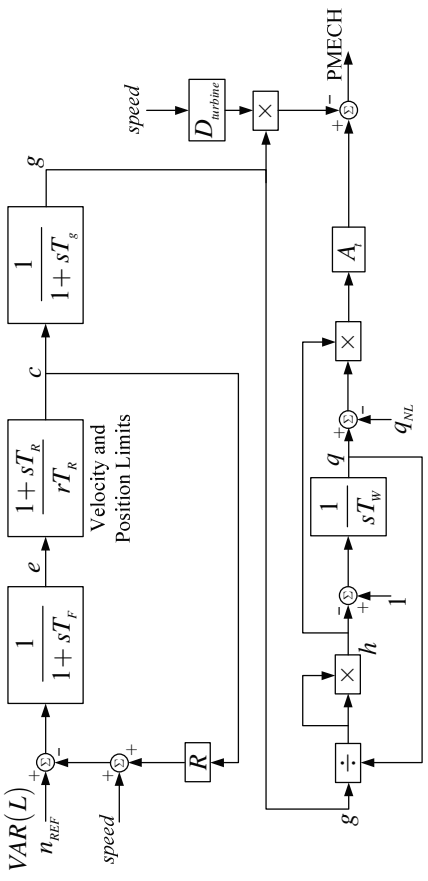

Figure A3.4. Governor model HYGOV [38]

Table A3.8. HYGOV governor data [38]

Parameter	Value
Permanent Droop R [p.u.]	0.04
Temporary Droop r [p.u.]	0.1
Governor Time Constant T_r [s]	10
Filter Time Constant T_f [s]	0.05
Servo Time Constant T_g [s]	0.3
Gate Velocity Limit V_{elm} [p.u.]	0.29
Maximum Gate Limit G_{MIN}	0
Minimum Gate Limit G_{MAX}	1
Water Starting Time T_w [s]	1
Turbine Gain A_t [p.u.]	1.15
Frictional losses factor pu D_{turb} [p.u.]	0.01
No Load Flow q_{nl} [p.u.]	0.08
Turbine Rated Power(=0->PN=Pgnn)	0

Appendix 4

APPENDIX 4

The Impact of Generator and Excitation System Modeling on the Slow Coherency Identification– Computed Eigenvalues

In this Appendix the eigenvalues computed for the equivalent models of the ADG are presented in the next Tables. The equivalent models are produced as in Sub–Section 5.1 from Chapter 5 with the scope of observing how the modeling of the generators and excitation system impacts the slow coherency grouping. In the end of this investigation the computed electromechanical modes were compared for

Table A4.1. Complex Conjugate Eigenvalues of the Original Model

Electromechanical Modes	**Real Part**	**Imaginary Part**	**Damped Frequency**	**Damping Ratio**
–	**[1/s]**	**[rad/s]**	**[Hz]**	**[%]**
Mode 1	−12.631	±33.876	5.391	34.938
Mode 2	−16.006	±31.575	5.025	45.213
Mode 3	−12.493	±30.870	4.913	37.514
Mode 4	−6.622	±22.514	3.583	28.218
Mode 5	−4.270	±19.588	3.117	21.299
Mode 6	−5.606	±18.064	2.875	29.642
Mode 7	−5.886	±16.068	2.557	34.396
Mode 8	−3.854	±14.954	2.380	24.956
Mode 9	−2.374	±12.283	1.954	18.982
Mode 10	−2.412	±11.546	1.837	20.455
Mode 11	−2.223	±10.069	1.602	21.561
Mode 12	−1.916	±9.834	1.565	19.126
Mode 13	−3.730	±3.423	0.544	73.678
Mode 14	−9.476	±3.171	0.504	94.828
Mode 15	−1.687	±2.612	0.415	54.256
Mode 16	−9.517	±2.569	0.408	96.544
Mode 17	−11.626	±2.546	0.405	97.685
Mode 18	−1.168	±1.183	0.188	70.264
Mode 19	−11.120	±0.913	0.145	99.664
Mode 20	−0.891	±0.908	0.144	70.042
Mode 21	−0.832	±0.676	0.107	77.570
Mode 22	−0.880	±0.666	0.106	79.745
Mode 23	−0.855	±0.642	0.102	79.947
Mode 24	−0.796	±0.641	0.102	77.885
Mode 25	−0.752	±0.621	0.098	77.103
Mode 26	−1.309	±0.526	0.083	92.774
Mode 27	−3.332	±0.185	0.029	99.845
Mode 28	−0.203	±0.022	0.003	99.385

each of the equivalent models in order to observe if the damped frequencies and damping ratios are preserved. Next are presented the complete list of the computed eigenvalues for each equivalent of the ADG.

Table A4.2. Complex Conjugate Eigenvalues of the Electromechanical and Transient Models

Electromechanical Modes	**Real Part**	**Imaginary Part**	**Damped Frequency**	**Damping Ratio**
–	**[1/s]**	**[rad/s]**	**[Hz]**	**[%]**
Mode 1	−5.226	±22.801	3.628	22.343
Mode 2	−2.968	±15.855	2.523	18.402
Mode 3	−2.302	±12.236	1.947	18.493
Mode 4	−2.323	±11.668	1.857	19.529
Mode 5	−2.252	±10.034	1.597	21.898
Mode 6	−1.955	±9.827	1.564	19.518
Mode 7	−1.684	±2.615	0.416	54.146
Mode 8	−1.144	±1.184	0.188	69.501
Mode 9	−10.827	±1.005	0.160	99.571
Mode 10	−0.751	±0.729	0.116	71.740
Mode 11	−0.750	±0.630	0.100	76.573
Mode 12	−0.028	±0.0000004	0.00000006	100

Table A4.3. Complex Conjugate Eigenvalues of the Transient Model with Excitation System

Electromechanical Modes	**Real Part**	**Imaginary Part**	**Damped Frequency**	**Damping Ratio**
–	**[1/s]**	**[rad/s]**	**[Hz]**	**[%]**
Mode 1	−13.674	± 34.491	5.489	36.855
Mode 2	−1.141	± 22.949	3.652	4.966
Mode 3	−2.930	± 18.381	2.925	15.744
Mode 4	−2.290	± 12.265	1.952	18.359
Mode 5	−2.387	± 11.771	1.873	19.881
Mode 6	−2.303	± 10.058	1.600	22.327
Mode 7	−1.988	± 9.855	1.568	19.782
Mode 8	−1.683	± 2.614	0.416	54.131
Mode 9	−1.139	± 1.191	0.189	69.101
Mode 10	−10.925	± 0.986	0.156	99.595
Mode 11	−0.754	± 0.736	0.117	71.579
Mode 12	−0.752	± 0.631	0.100	76.591
Mode 13	−0.086	± 0.0152	0.002	98.497

Appendix 5

APPENDIX 5

Dynamic Equivalents of Active Distribution Grids using a Model Parameter Identification Method

In the first part of this Appendix the complete list of eigenvalues computed for the dynamic equivalents produced using method proposed in Sub−Section 5.6 of the Chapter 5 are presented. In the second part the standard parameters of the equivalent generators produced using this method are given.

Table A5.1 presents the complete list of eigenvalues of the dynamic equivalent produced using the dominant modes.

Table A5.1. Complex Conjugate Eigenvalues of the Dominant Modes Dynamic Equivalent Model

Electromechanical Modes	**Real Part**	**Imaginary Part**	**Damped Frequency**	**Damping Ratio**
−	**[1/s]**	**[rad/s]**	**[Hz]**	**[%]**
Mode 1	−2.331	±10.005	1.592	22.690
Mode 2	−2.115	±9.964	1.585	20.763
Mode 3	−1.448	±8.162	1.299	17.467
Mode 4	−49.636	±8.147	1.296	98.679
Mode 5	−2.345	±5.238	0.833	40.861
Mode 6	−0.451	±5.129	0.816	8.759
Mode 7	−1.861	±4.021	0.640	42.001
Mode 8	−2.103	±3.827	0.609	48.159
Mode 9	−1.671	±2.534	0.403	55.051
Mode 10	−0.705	±1.204	0.191	50.524
Mode 11	−0.738	±1.183	0.188	52.926
Mode 12	−0.823	±1.079	0.171	60.637

Table A5.2 presents the complete list of eigenvalues of the dynamic equivalent produced using multi−modes.

Table A5.2. Complex Conjugate Eigenvalues of the Multi−Modes Dynamic Equivalent Model

Electromechanical Modes	**Real Part**	**Imaginary Part**	**Damped Frequency**	**Damping Ratio**
–	**[1/s]**	**[rad/s]**	**[Hz]**	**[%]**
Mode 1	−11.105	±18.348	2.920	51.779
Mode 2	−-4.811	±17.540	2.791	26.450
Mode 3	−13.568	±16.969	2.700	62.450
Mode 4	−5.154	±13.371	2.128	35.971
Mode 5	−2.083	±9.880	1.572	20.633
Mode 6	−2.393	±9.785	1.557	23.757
Mode 7	0.417	±6.792	1.081	−6.138
Mode 8	−1.680	±2.616	0.416	54.030
Mode 9	−3.081	±2.241	0.356	80.869
Mode 10	−1.598	±1.942	0.309	63.532
Mode 11	−2.079	±1.912	0.304	73.611
Mode 12	−25.933	±1.689	0.268	99.788
Mode 13	0.582	±1.458	0.232	−37.090
Mode 14	−1.141	±1.125	0.179	71.192
Mode 15	−0.380	±1.071	0.170	33.473
Mode 16	0.055	±0.881	0.140	−6.251
Mode 17	−27.131	±0.841	0.133	99.951
Mode 18	−0.793	±0.8052	0.128	70.192
Mode 19	−1.557	±0.714	0.113	90.893
Mode 20	−11.138	±0.580	0.092	99.864
Mode 21	−0.563	±0.550	0.087	71.532

Table A5.3. Equivalent Generators and AVRs Parameters
(Dominant Modes)

Parameters	Equivalent Generator 1	Equivalent Generator 2	Equivalent Generator 3
$H\ [s]$	7.5	4	3
$X_d\ [p.u.]$	2.109	2.404	2.44
$X_q\ [p.u.]$	1.388	1.612	1.301
$X'_d\ [p.u.]$	0.5474	0.438	0.316
$X''_d\ [p.u.]$	0.08	0.04	0.05
$X''_q\ [p.u.]$	0.1519	0.327	0.203
$T'_{d,0}\ [p.u.]$	2.9842	3.8891	3.973
$T''_{d,0}\ [p.u.]$	0.0151	0.0413	0.0201
$T''_{q,0}\ [p.u.]$	0.203	0.226	0.2254
Parameters	**AVR 1**	**AVR 2**	**AVR 3**
$K_a\ [p.u.]$	197.47	199.85	200.016
$T_a\ [s]$	0.02	0.02	0.019
$K_e\ [p.u.]$	0.5003	0.5	0.5
$T_e\ [s]$	0.3537	0.35	0.349

Table A5.4. Equivalent Generators and AVRs Parameters (Multi-Modes)

Parameters	Equivalent Generator 1	Equivalent Generator 2	Equivalent Generator 3	Equivalent Generator 4
$H\ [s]$	2,5	1,5	0,5	1,
$X_d\ [p.u.]$	2,714211	2,719104	2,001728	3,830842
$X_q\ [p.u.]$	2,219677	2,1765	0,901892	2,873131
$X'_d\ [p.u.]$	1,211266	1,877289	0,500058	0,383084
$X''_d\ [p.u.]$	0,15	0,1	0,1	0,1
$X''_q\ [p.u.]$	0,981541	0,30868	0,12613	0,383084
$T'_{d,0}\ [p.u.]$	4,711583	6,885344	0,942531	7,661684
$T''_{d,0}\ [p.u.]$	0,46245	0,340882	0,056278	0,038308
$T''_{q,0}\ [p.u.]$	0,892286	0,3047	0,042744	0,43097
Parameters	**AVR 1**	**AVR 2**	**AVR 3**	**AVR 4**
$K_a\ [p.u.]$	200,7127	143,7795	459,1889	383,0841
$T_a\ [s]$	0,732607	0,027474	0,045522	0,038308
$K_e\ [p.u.]$	1,211268	0,818316	0,715221	0,95771
$T_e\ [s]$	1,062633	0,602576	0,828648	0,670397

Appendix 6

APPENDIX 6

Magnitude and Phase Calculation Using the Time Decomposition of the State Variables

With j represent the imaginary unit and t representing the time vector

Considering the right eigenvector $\Phi_{i,k}$ of the i^{th} state variable corresponding to the k^{th} eigenvalue λ_k defined as:

$$\Phi_{i,k} = \phi_{i,k} e^{j\varphi_{i,k}} = \phi_{i,k}\left(\cos\left(\varphi_{i,k}\right) + j\cos\left(\varphi_{i,k}\right)\right) = a + jb \tag{A6.1}$$

In the same manner the left eigenvector $\Psi_{i,k}$ of the i^{th} state variable corresponding to the k^{th} eigenvalue λ_k defined as:

$$\Psi_{i,k} = \psi_{i,k} e^{j\chi_{i,k}} = \psi_{i,k}\left(\cos\left(\chi_{i,k}\right) + j\sin\left(\chi_{i,k}\right)\right) = x + jy \tag{A6.2}$$

With the eigenvalue λ_k defined as:

$$\lambda_k = \alpha_k + j\Omega_k \tag{A6.3}$$

The following time response of the i^{th} state variable can be written

$$\Delta x_i(t) = \Phi_{i,1} c_{i,1} e^{\lambda_1 t} + \Phi_{i,2} c_{i,2} e^{\lambda_2 t} + \cdots + \Phi_{i,k} c_{i,k} e^{\lambda_k t} \tag{A6.4}$$

For a particular eigenvalue k this time response become:

$$\Delta x_i(t) = \Phi_{i,k} c_{i,k} e^{\lambda_k t} = \Phi_{i,k} \Psi_{i,k} \Delta x(0) e^{\lambda_k t} \tag{A6.5}$$

With (1), (2) and (3), then (5) can be rewritten as:

$$\Delta x_{i,k}(t) = \Phi_{i,k} \Psi_{i,k} \Delta x(0) e^{\lambda_k t} = (a + jb)(x + jy)\Delta x(0) e^{(\alpha_k + j\Omega_k)t} \tag{A6.6}$$

Or

$$\Delta x_{i,k}(t) = (a + jb)(x + jy)\Delta x(0)e^{(\alpha_k + j\Omega_k)t} = \\ \left[(ax - by) + j(ay + bx)\right]\Delta x(0)e^{\alpha_k t}\left[\cos(\Omega_k t) + j\sin(\Omega_k t)\right] \tag{A6.7}$$

With:

$$\begin{aligned} A &= (ax - by) \\ B &= (ay + bx) \\ \mathrm{M}(t) &= \cos(\Omega_k t) \\ \mathrm{N}(t) &= \sin(\Omega_k t) \end{aligned} \tag{A6.8}$$

$$\Delta x_{i,k}(t) = \Delta x(0)e^{\alpha_k t}(A + jB)\left(\mathrm{M}(t) + j\mathrm{N}(t)\right) \tag{A6.9}$$

$$= \Delta x(0)e^{\alpha_k t}\left[\left(A\mathrm{M}(t) - B\mathrm{N}(t)\right) + j\left(A\mathrm{N}(t) + B\mathrm{M}(t)\right)\right]$$

$$\begin{aligned} \Delta x_{i,k}(t) = &\left\{\Delta x(0)e^{\alpha_k t}\left(A\mathrm{M}(t) - B\mathrm{N}(t)\right)\right\} + \\ &j\left\{\Delta x(0)e^{\alpha_k t}\left(A\mathrm{N}(t) + B\mathrm{M}(t)\right)\right\} \end{aligned} \tag{A6.10}$$

Then the real and imaginary parts are:

$$\begin{aligned} \mathrm{Re}\left\{\Delta x_{i,k}(t)\right\} &= \left\{\Delta x(0)e^{\alpha_k t}\left(A\mathrm{M}(t) - B\mathrm{N}(t)\right)\right\} \\ \mathrm{Im}\left\{\Delta x_{i,k}(t)\right\} &= \left\{\Delta x(0)e^{\alpha_k t}\left(A\mathrm{N}(t) + B\mathrm{M}(t)\right)\right\} \end{aligned} \tag{A6.11}$$

With (11) the magnitude and phase can be computed as:

$$\begin{aligned} X_{i,k}(t) &= 2\sqrt{\left(\mathrm{Re}\left\{\Delta x_i(t)\right\}\right)^2 + \left(\mathrm{Im}\left\{\Delta x_i(t)\right\}\right)^2} \\ \mathrm{P}_{i,k}(t) &= \arctan\left(\frac{\mathrm{Im}\left\{\Delta x_i(t)\right\}}{\mathrm{Re}\left\{\Delta x_i(t)\right\}}\right) \end{aligned} \tag{A6.12}$$

The real and imaginary parts are computed at each time instant t_i and further the magnitude and phase are calculated.